



University of **HUDDERSFIELD**

University of Huddersfield Repository

Huang, Yuxiang

Open Area Concealed Weapon Detection (CWD) Sensor System Development

Original Citation

Huang, Yuxiang (2021) Open Area Concealed Weapon Detection (CWD) Sensor System Development. Doctoral thesis, University of Huddersfield.

This version is available at <http://eprints.hud.ac.uk/id/eprint/35629/>

The University Repository is a digital collection of the research output of the University, available on Open Access. Copyright and Moral Rights for the items on this site are retained by the individual author and/or other copyright owners. Users may access full items free of charge; copies of full text items generally can be reproduced, displayed or performed and given to third parties in any format or medium for personal research or study, educational or not-for-profit purposes without prior permission or charge, provided:

- The authors, title and full bibliographic details is credited in any copy;
- A hyperlink and/or URL is included for the original metadata page; and
- The content is not changed in any way.

For more information, including our policy and submission procedure, please contact the Repository Team at: E.mailbox@hud.ac.uk.

<http://eprints.hud.ac.uk/>

Open Area Concealed Weapon Detection (CWD) Sensor System Development

Yuxiang Huang

Submitted in accordance with the requirements for the degree
of PhD. Electronics Engineering

University of Huddersfield
School of Computing and Engineering

May 2021

Abstract

The detection of concealed weapons is a key requirement when considering the personal security of individuals in a public environment, such as a sporting event, airports, festivals, schools or universities etc. Hence, being able to efficiently discover any illicit items hidden within luggage or underneath the clothes of an individual, for example, is essential. The development of a concealed weapon detection (CWD) system, which efficiently addresses the issue of accurate identification and classification of dangerous objects, will aid in minimising the potential danger for a high volume of individuals in open area environments.

Searching all visitors who pass through security points is normally an inefficient process, comprising of individual manual inspection, which often leads to congestion at the entrance of the event. Conversely, highly sophisticated systems with minimal manual intervention, utilising image scanning, are typically claimed to be a high risk to personal privacy and the possible leakage of confidential information, such as identification of belongings, where carried items underneath clothes are displayed on the screen, even if no weapon is detected.

The traditional weapon detection process depends upon the manual recognition of a threat with currently available commercial systems generally being unable to achieve the accurate recognition of potential threat objects from other non-threat items, often resulting in what ‘the generation of false alarms’. Therefore, the development of a CWD system to accurately determine and categorise different illicit targets, such as knives and guns etc, in real time and efficiently monitor the public security in an open area environment, is increasingly becoming an essential requirement. Hence an innovative CWD solution that uses the pulse-induction (PI) technique to recognise and classify threat objects, through the novel characterisation of the induced electromagnetic signal utilising a sigma delta ($\Sigma\Delta$) analogue to digital modulation device to yield an analysable signature is proposed.

In comparison, to typical digital conversion processes, with excessive data samples required to provide distinguishable object signal characteristic information, the system features a single bit data flow from a $\Sigma\Delta$, to simplify the analogue sampling measurement. The $\Sigma\Delta$ modulating approach facilitated a novel algorithm development to accurately identify potential weapons, enabling features (shape, size and material) of a target object to be identifiable within the signature. The weapon detection scheme delivers the signature evaluation based on marked points of the single bit stream facilitating the specific threat characteristics of the detected target to be identified in real-time.

A practical, FPGA based implementation of the object identification procedure proved the concept of an algorithm to identify object characteristics of threat objects, principally that of a typical hand-held weapon (knife) through the identification of weapon characteristics, e.g. edge sharpness, thus efficiently differentiating between potential threats from other objects of similar shape, mass, etc. All the key aspects of an open area weapon detection system, operating in real-time, have been proven, thus future development and implementation of the proposed algorithm for an individual sensor could be expanded to form a multi-detection system to track a weapon trajectory, contributing to the development of an accurate and efficient identification of weapons in an open area environment.

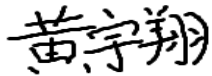
Intellectual Property

The candidate confirms that the work submitted is his/her own and that appropriate credit has been given where reference has been made to the work of others.

This copy has been supplied on the understanding that it is copyright material and that no quotation from the thesis may be published without proper acknowledgement.

© 2021 The University of Huddersfield, Yuxiang Huang

Signed

A handwritten signature in black ink, appearing to read '黄宇翔' (Huang Yuxiang).

Acknowledgements

I am eternally grateful to my supervisor, Dr Peter Mather, who devoted his time and energy to academic guidance, effective encouragement, valuable suggestion and beneficial discussion over the past three years. I sincerely appreciate his constructive supervision and positive guidance throughout my PhD time as his student. I still remember what he taught me, the research has its ups and downs, but the patience can tide over the difficulties. I truly have no idea when I was stuck if he hadn't provided the constructive feedback and motivated me. He always offered the extraordinary support to attend the international conferences and critical comments for my presented papers. I also would also like to show my gratitude to my co-supervisor Dr Martin Sibley for his expertise that greatly assisted the research. I would like to thank the School of Computing and Engineering for offering me a great opportunity to undertake this program with the fee waiver scholarship. My thanks go out to the financial support I received from the University of Huddersfield, funding the travel grants for conferences etc. Completing this work would be harder than I thought and have been impossible without the continued support from the staff of electronics laboratory. I gratefully acknowledge their assistance. Finally, I would like to express my sincere gratitude to my parents, who have supported me to explore my potential and pursue my doctoral degree. I am indebted to my sister, brother-in-law for their immeasurable care, kindness and encouragement during this challenging period. And to lovely nephew Kyle for spreading the happiness and bring me luck.

List of Publications

- Y. Huang, P. J. Mather and M. J. N. Sibley, "Open Area Concealed Weapon Detection Sensor System Development," Progress in Electromagnetics Research Symposium, Toyama, Japan, 2018, pp. 611-620.

Contribution: Developed the concealed weapon detection scheme based on the induced electromagnetic energy, identifying the potential threat in the open area. The signal analysis defined and classified the characteristics of targets in terms of material, size, shape and detection distance. The innovative architecture was established to acquire and process the induced response, revealing the target characterizes.

- Y. Huang, P. Mather and M. Sibley, "Open Area Concealed Weapon Detection (CWD) Sensor System and Algorithm Development," 2019 Photonics Electromagnetics Research Symposium, Rome, Italy, 2019, pp. 4078-4085.

Contribution: The main contribution of this publication, is based on this research work, covering the design and build of a detection architecture to efficiently distinguish the threat and no threat objects from the pulse-induction (PI) signature. The publication includes the implementation of the sigma-delta modulation method to simplify the data conversion for the single bit digital outcome. A novel algorithm is proposed to evaluate the samples at the time points of object signature, which can reflect the feature for identification.

Contents

| | | |
|----------|---|-----------|
| 1 | Introduction | 1 |
| 1.1 | Background | 1 |
| 1.2 | Project scope | 3 |
| 1.3 | System objectives | 4 |
| 1.4 | Object specification | 6 |
| 1.4.1 | Shape experiment | 6 |
| 1.4.2 | Size experiment | 7 |
| 1.4.3 | Distance experiment | 7 |
| 1.4.4 | Sharpness experiment | 8 |
| 1.5 | Thesis structure | 8 |
| 2 | Literature Review | 10 |
| 2.1 | Imaging detection | 12 |
| 2.1.1 | Terahertz (THz) imaging | 13 |
| 2.1.2 | Millimetre wave imaging | 13 |
| 2.1.3 | X-ray imaging | 13 |
| 2.1.4 | Microwave imaging | 14 |
| 2.1.5 | Infrared imaging | 14 |
| 2.2 | Electromagnetic (EM) detection | 15 |
| 2.2.1 | Walk through metal detector | 15 |
| 2.2.2 | Hand-held metal detection | 16 |
| 2.2.3 | Electromagnetic imaging detection | 16 |
| 2.2.4 | Magnetic induction tomography | 17 |
| 2.3 | Signal capture platform | 17 |
| 2.3.1 | Analogue signal acquisition | 17 |
| 2.3.2 | Digital signal acquisition | 18 |

| | | |
|----------|---|-----------|
| 2.4 | Weapon detection algorithms | 20 |
| 2.4.1 | Image-based identification | 21 |
| 2.4.2 | Signal-based identification | 24 |
| 2.5 | Summary | 25 |
| 3 | Theory | 28 |
| 3.1 | Architecture and methodology | 29 |
| 3.1.1 | Sensor structure | 29 |
| 3.1.2 | Pulse induction approach | 31 |
| 3.1.3 | Electromagnetic induction equations | 33 |
| 3.2 | Simulation analysis | 35 |
| 3.3 | Sigma-Delta modulation | 39 |
| 3.4 | Summary | 41 |
| 4 | Weapon Detection System Development | 43 |
| 4.1 | Overall structure | 43 |
| 4.2 | Detection device scheme | 46 |
| 4.2.1 | Search coil | 47 |
| 4.2.2 | Circuit scheme | 48 |
| 4.3 | Response configuration | 53 |
| 4.4 | Program design | 55 |
| 4.4.1 | ADC conversion | 56 |
| 4.4.2 | Section division | 56 |
| 4.4.3 | Data simplification | 57 |
| 4.4.4 | Decay monitoring | 59 |
| 4.5 | Process simulation | 61 |
| 4.5.1 | Two variable parameters | 62 |
| 4.5.2 | Edge variable | 63 |
| 4.6 | Summary | 64 |
| 5 | Results and Discussion | 66 |
| 5.1 | Experimental configuration | 66 |
| 5.2 | Experimental processing | 67 |

| | | |
|----------|---------------------------------------|------------|
| 5.3 | Experimental verification | 69 |
| 5.3.1 | Edge demonstration | 69 |
| 5.3.2 | Cylinder demonstration | 73 |
| 5.4 | Algorithm development | 76 |
| 5.4.1 | Mark points evaluation | 76 |
| 5.5 | Discussion | 88 |
| 5.5.1 | Delay phase analysis | 88 |
| 5.5.2 | Decay phase analysis | 90 |
| 5.5.3 | Comprehensive analysis | 95 |
| 5.6 | Summary | 96 |
| 6 | Conclusions and Future Work | 98 |
| 6.1 | Conclusions | 98 |
| 6.2 | Future work | 101 |
| | References | 103 |
| | A SCHEMATIC BLOCK DIAGRAM | 116 |
| | B VHDL PROGRAM FILES | 118 |
| B.1 | Pulse Generation | 118 |
| B.2 | Digital Sampling Conversion | 119 |
| B.3 | Signal Monitoring | 120 |
| B.4 | Modulation Processing | 123 |
| B.5 | Data Identification | 126 |
| | C MATLAB FILES | 129 |
| C.1 | Sample Collection | 129 |
| C.2 | Date Modification | 130 |
| C.3 | Decay Analysis | 130 |
| | D COMSOL SIMULATION | 132 |
| D.1 | Shape model simulation | 132 |
| D.2 | Size model simulation | 133 |
| D.3 | Distance model simulation | 134 |

| | |
|-------------------------------------|-----|
| D.4 Sharp edge simulation | 135 |
|-------------------------------------|-----|

List of Figures

| | | |
|------|---|----|
| 1.1 | System objectives chart | 5 |
| 2.1 | Concealed weapon detection technologies. | 11 |
| 2.2 | Concealed weapon detection methods. | 11 |
| 2.3 | Single Shot Detector model. | 21 |
| 2.4 | Convolutional Neural Network architecture. | 23 |
| 2.5 | Digital data acquisition system. | 24 |
| 3.1 | System theory structure. | 29 |
| 3.2 | Basic architecture for sensor system. | 30 |
| 3.3 | Pulse induction process.Reproduced from [Yuxiang, 2018][121]. | 33 |
| 3.4 | COMSOL based model simulation for a knife | 36 |
| 3.5 | Response simulation with variable parameter of material | 36 |
| 3.6 | Response simulation with variable parameter of shape | 37 |
| 3.7 | Response simulation with variable parameter of distance | 38 |
| 3.8 | Response simulation with variable parameter of size | 38 |
| 3.9 | Sigma-Delta modulation | 39 |
| 3.10 | Oversampling and sigma-delta conversion. Redrawn based on [Fujcik, 2016][120] | 40 |
| 4.1 | Detection system structure for practical processing | 44 |
| 4.2 | Detection system structure for simulation processing | 45 |
| 4.3 | Fundamental structure of detection scheme | 46 |
| 4.4 | Analog circuit design | 48 |
| 4.5 | MOSFET conversion 3.3 V and 5 V | 49 |
| 4.6 | Pulse generation block | 49 |
| 4.7 | Improved pulse generation block | 50 |
| 4.8 | Differential amplifier building block | 52 |

| | | |
|------|--|----|
| 4.9 | Results for amplification and adjustment | 53 |
| 4.10 | Record and division via MATLAB. Reproduced from [Yuxiang, 2018][129]. | 54 |
| 4.11 | Distinction between targets and background in 200 Hz, 400 Hz and 800 Hz | 55 |
| 4.12 | ADC conversion for object detection. Reproduced from [Yuxiang, 2018][129]. | 56 |
| 4.13 | Difference monitor for the section division | 57 |
| 4.14 | Sigma-Delta processing | 58 |
| 4.15 | Binary sequence between background and targets after the $\Sigma\Delta$ module | 58 |
| 4.16 | Range of slopes for the decay signal | 60 |
| 4.17 | Measurement simulation procedure.Reproduced from [Yuxiang, 2019][130]. | 62 |
| 4.18 | Analysis for two variable parameters | 63 |
| 4.19 | Analysis for shape edge | 64 |
| 5.1 | Practical signature procedure. | 68 |
| 5.2 | Modulation simulation procedure. | 69 |
| 5.3 | Experimental result of variable edge | 70 |
| 5.4 | Verification procedure for variable edge | 71 |
| 5.5 | Practical and simulated variable edge comparison | 72 |
| 5.6 | Experimental result of variable cylinder | 73 |
| 5.7 | Response simulation and signal conditioning for variable cylinder. | 74 |
| 5.8 | Practical and simulated cylinder comparison | 75 |
| 5.9 | Voltage analysis for material. | 78 |
| 5.10 | Mark points identification for material. | 78 |
| 5.11 | Voltage analysis for shape. | 80 |
| 5.12 | Mark points identification for shape. | 81 |
| 5.13 | Voltage analysis for size. | 82 |
| 5.14 | Mark points identification for size. | 83 |
| 5.15 | Voltage analysis for distance. | 84 |
| 5.16 | Mark points identification for distance. | 85 |
| 5.17 | Detection distance assessment. | 85 |
| 5.18 | Voltage analysis for sharpness 5° | 87 |
| 5.19 | Mark points identification for sharpness 5° | 87 |
| 5.20 | Size and distance relationship | 89 |

| | | |
|------|--|-----|
| 5.21 | Trigonometric expression for object distinction. | 92 |
| A.1 | Block diagram layout | 117 |
| D.1 | Shape model simulation. | 133 |
| D.2 | Size model simulation. | 134 |
| D.3 | Distance model simulation. | 135 |
| D.4 | Sharp edge model simulation. | 136 |

List of Tables

| | | |
|-----|--|----|
| 1.1 | Variable shape object specification | 7 |
| 1.2 | Variable size object specification (unit: mm) | 7 |
| 1.3 | Variable distance object specification (unit: mm) | 8 |
| 1.4 | Variable sharpness object specification | 8 |
| 2.1 | Comparison of different imaging sensors. Reproduced from [Haynes, 2011]. | 12 |
| 2.2 | Bounding boxes for convolution layer. Reprinted from [Tsang, 2018][123] | 22 |
| 3.1 | BFO, VLF and PI comparison. Reproduced from [Tyson, 2001][93]. | 32 |
| 4.1 | Search coil parameters | 48 |
| 4.2 | Marked points record from rise section (unit: μs). Reprinted from [Yuxiang, 2019] | 59 |
| 4.3 | The statistics for the range of slopes (unit: μs) | 60 |
| 4.4 | Mark points around the maximal slope (unit: μs) | 61 |
| 4.5 | Mark points around the minimal slope (unit: μs) | 61 |
| 4.6 | Record time for variable size and distance (unit: μs). Reprinted from [Yuxiang, 2019][130] | 63 |
| 4.7 | Record time for sharpness (unit: μs). Reprinted from [Yuxiang, 2019][130] | 64 |
| 5.1 | Practical and simulated edge comparison | 72 |
| 5.2 | Practical and simulated variable cylinder comparison | 75 |
| 5.3 | Sampling-domain mark points evaluation for material | 77 |
| 5.4 | Voltage-domain mark points evaluation for material | 77 |
| 5.5 | Sampling-domain mark points evaluation for shape | 79 |
| 5.6 | Voltage-domain mark points evaluation for shape | 80 |
| 5.7 | Sampling-domain mark points evaluation for size | 81 |
| 5.8 | Voltage-domain mark points evaluation for size | 82 |
| 5.9 | Sampling-domain mark points evaluation for distance | 83 |

| | |
|---|----|
| 5.10 Voltage-domain mark points evaluation for distance | 84 |
| 5.11 Sampling-domain mark points evaluation for sharpness 5° | 86 |
| 5.12 Voltage-domain mark points evaluation for sharpness 5° | 86 |
| 5.13 Cube, triangle and cylinder coefficients | 89 |
| 5.14 Fourier coefficients for cylinder and sharpness | 93 |
| 5.15 Polynomial parameters for cylinder and sharpness | 95 |

List of Equations

| | | |
|-----|---|----|
| 3.1 | Biot–Savart Law | 33 |
| 3.2 | Magnetic Flux Density Integration | 34 |
| 3.3 | Ampere’s Law | 34 |
| 3.4 | Dynamic Magnetic Field | 34 |
| 3.5 | Faraday’s Law | 34 |
| 3.6 | Maxwell’s Equation | 34 |
| 3.7 | Resistor-Inductor (RL) Circuit Model | 35 |
| 4.1 | Wheeler Approximation | 47 |
| 4.2 | Inverting Operational Amplifier Model | 50 |
| 4.3 | Feedback Voltage Model | 51 |
| 4.4 | Gain Amplifier | 51 |
| 4.5 | Gain Model | 51 |
| 4.6 | Superposition Theorem | 52 |
| 5.1 | Delay Exponential Function | 89 |
| 5.3 | Fourier Series | 92 |
| 5.4 | Fourier Series in Term 2 | 93 |
| 5.5 | Least Squares Model | 94 |
| 5.6 | Matrix Expression Model | 94 |

Chapter 1

Introduction

Weapon detection technology is considered to be a critical attribute in the process of monitoring public security and safeguarding open places which have high levels of human traffic, such as transport interchanges, educational establishments and entertainment venues etc. In recent decades, there has been a significant requirement to increase security applications in order to detect weapons and thus attempt to mitigate the risk and reduce the threat to the public.

The basic action is individually searching the figure of a target for an inspector to discriminate between threat and no threat items. The typical manual procedure, in current use, identifies a concealed metal object dependent on the conductivity. The metal detection applications identify the conductive components which may deliver the threat, and weapon identification still requires manual judgment to locate the targets. In addition, the imaging classification by the scanning technique requires a considerable amount of and manpower for weapon tracking. The traditional detection techniques, dependant on the personal scanning procedure, sacrifice time and precision for threat defining and locating. In order to achieve high efficiency and accuracy, an advanced detection system is increasingly required to significantly reduce the imminent threat posed by the carrying weapons hidden under human clothing.

1.1 Background

Due to the more frequent violence and terrorism events, the security inspection department has an ongoing interest in reliably identifying prohibited items which present a threat to public security. The illicit objects typically present harm to individual health or damage to public

assets and are commonly hidden and carried through a range of security inspections as they are challenging to detect [2]. An intelligent detection system features the accurate recognition of weapons, specifically guns and knives, concealed beneath clothing or in carried luggage, and is regarded as an important safeguard for an open area. The classical security procedure commonly used, involving individual inspection, imaging surveillance and electromagnetic monitors, exhibits unsatisfactory results for the detection of concealed threat items in an open area.

The conventional techniques of manual inspection, such as hand-held and walk-through detection, usually deployed at the security entrance, can process the inspection on the individual basis. The classic walk-through metal detector, commonly implemented at the airport entrance, features the sequential detection to provide the maximal throughput of a single visitor per second [3]. The gateway detection providing contraband warning requires the manual supervision to investigate any alarm indicating potential threats from the metallic item indications [4].

Accordingly, their execution is inefficient and time consuming for an open area under surveillance, particularly if a high volume of people access it in an uncontrolled sequence. The individual surveillance procedure based on an arranged queue occupies human resources and consumes time, which increasingly becomes an obstacle to high efficiency.

The existing manual inspection technology shows the limitation that the threat objects cannot be automatically classified and considered as weapons separate from other authorised components, when they are detected at the same time. Hence, the security procedure still requires experienced personnel to recognise the threat items manually, and the obtained weapon recognition knowledge influences the accuracy rate, resulting in the occurrence of false alarms. The traditional imaging detection technique illustrates the concealed items in the pocket or luggage of individual targets, including personal and confidential information [5]. In terms of respecting human privacy, the inspection procedure is supposed to identify a weapon rather than screen the personal and confidential information that is allowed and no harm through check points [6]. In addition, the emerging techniques, like analysing thermal infrared images by temperature distribution to form a figure of the hidden object from the background, are susceptible to environmental influences [7].

The commercial imaging detection solution technology specialises in the autonomous weapons recognition to photograph the suspicious items by scanning the portal space (6 ft wide)[8]. However, the typical intelligent system requires the potentially costly application deployment

for the supporting device instalment, and the surrounding environment influence commonly restricts the stable threat assessment. The increasing false alerts also confuses the intelligent identification between the weapons and common objects [9].

Increased imaging monitor applications, installed in open spaces, are unable to facilitate threat protection completely because a weapon hidden on the body is seldom captured and noticed. Moreover, the imaging surveillance system, a reliable method of threat detection, requires costly infrastructural developments and is difficult to implement in a public area.

For electromagnetic detection techniques, the induced response analysis can learn the specified characteristics of a signature that provide the target information for identification. The behaviour of electromagnetic response delivers a unique reaction which defines the detail regarding the material, shape, volume and distance. Hence, the response study provides the identification of characteristics, such as the sharp edge of a knife and steel of guns, which determines the potential threat objects.

Obviously, the analogue signature processing demands a high sampling rate and resolution to capture the responses which are accurately converted to digital data for feature analysis. The conversion and classification requirements are a high volume of data and speedy processing performance to investigate the digital characteristics for threat identification.

The complex detection techniques reach the acceptable identification but only on investigating the sharp point of a knife threat by commonly 1500 positive and negative sampling analysis [10]. The intensive processors are subject to real-time processing, due to highly used samples. The available data requirement and processing speed limits the traditional weapon detection and results in the challenge of the high computational cost.

Therefore, the project investigates an innovative approach to minimize the data volume required for object identification, effectively solving the computation and space consumption. Meanwhile, the proposed system contributes to optimize the embedded signal processing and address the local data from sensors, achieving an accurate and synchronous identification for threat identification.

1.2 Project scope

The increased demand for a valuable technological solution is coming to recognize and alarm the concealed weapons with high accuracy and efficiency is coming to the fore, advancing the

security of open areas. A non-obtrusive weapon detection system with a low false alarm rate is deployed to penetrate the clothing and bodies of humans and reveal the concealed threat objects without leaking personal information. The development of technology with high success and low cost is required to detect potential threat objects for the uncontrolled flow of people to help prevent crime in real time [11]. Furthermore, the economical testing applications should be equipped with weapon identification which can filter out no threat items, and process at a high data rate to enable effective classification, to characterise threat targets.

This project proposes an innovative weapon detection system to accurately identify the potential threat objects among the concealed items moving across the surveillance area. The dynamic monitoring depends on signature processing while avoiding the risk of imaging and exposing personal information. The signature-based technique for weapon detection is known as non-destructive testing to human health. to address the high volume of people, the innovative solution achieves synchronous monitoring for the entire open zone, rather than the arranged pass-through sequence. Hence, there is a noticeable increase in time saving to inspect the several visitors at the same time once entering the area under surveillance, replacing the single person detection sequentially.

In contract to the excessive information analysis conducted , like targets imaging technologies the system developed in this thesis simplified signature data to process based on the low-cost and portable Field Programmable Gate Array (FPGA) platform. In addition, the FPGA based system is cost effective and flexible to deploy in open areas for continuous inspection, compared with the costly intensive processors for the specific applications. Therefore, the high performance synchronised weapon detection system handles the identification and real-time alerts for potential threat objects.

1.3 System objectives

The system detection procedure aims to develop the signature recording and data processing by the individual functional modules, proposing a novel algorithm for weapon recognition.

The objectives of the CWD project are essentially specified as the characterization of induced response, the definition of digital results, the application of the proposed algorithm, and the distinction of threat targets as the implemented procedure in Figure 1.1.

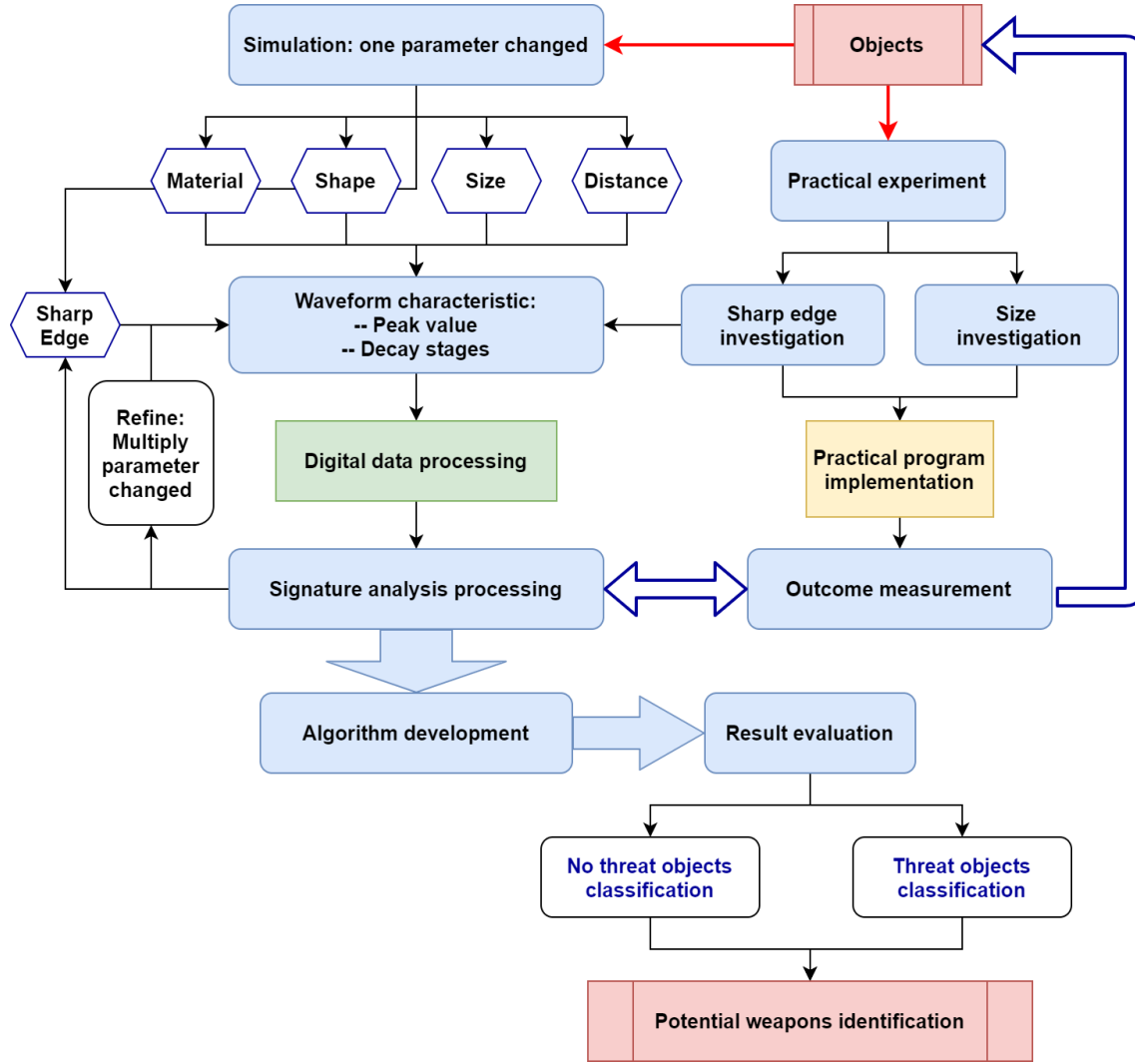


Figure 1.1: System objectives chart

To equip the primary device to process the analogue signature, the parameters of the coil are configured to transmit pulses and receive responses, and components in the analogue circuit are demonstrated to adjust the signature.

To definite the feature of induced results from conductive objects via the simulation of individual factors like material, shape, size and distance from the coil. By comparing one-parameter variation, the evident differences indicate the waveform characteristic, which is used to distinguish between individual cases efficiently.

To define the system transmitting frequency to clarify the distinction for accurate observation. The frequency of generated pulse becomes suitable to produce effective discrimination for specific cases, benefiting system performance.

To convert the analogue received signature into the digital data, which characterizes the

variation of induction from an object. Thus, weapon identification depends on the analysis of simplified data, which effectively reduces sample size.

To develop an algorithm using digital data to differentiate targets with varied parameters. From the data analysis, the featured samples are measured to determine the unique induced response, further reflecting the characterizes of a target.

To refine the object distinction with multiple parameters alteration. Thereby, the identification of induced response from a target is required to accomplish by the proposed procedure, despite simultaneous adjustment of two parameters.

To design and implement the practical experiment for systematic variation of sharpness. The onboard solution provides the identical result for identification to demonstrate and verify the feasibility of the simulation procedure.

To classify threat components according to the sharpness on edge. The developed algorithm should recognize simulation of a sharp edge to define the illicitness of a detected target.

To identify the object characteristics and detect the threat of the sharp components in the practical detection distance for the feasible weapon detection applications.

To acknowledge the characteristics of a target by the collection of mark points from the induced response. Thereby, the OWD system can display the feature and safety of objects (sharpness), analysing the digital data from the inductance signature.

1.4 Object specification

The project aims to develops the weapon identification system to classify the potential threat and no threat objects. In this work, the objects are specified regarding the testing experiment for the sharp, size, detection distance and sharpness.

1.4.1 Shape experiment

The different object shapes considered for detection are the of sphere, torus, block and knife with the specific dimensions, while other parameters were fixed. The typical size of a knife is decided as the common contraband to compare with the regular shape of allowed components, assisting the response distinction for the threat and no threat analysis. The model development defines the system results for the shape changes independently.

Table 1.1: Variable shape object specification

| Name | Block | Torus | Sphere | Knife |
|-------------------|------------------------------------|-----------------------------------|-------------|--|
| Material | Basic, free machining iron (Fe) | | | |
| Volume | $20 \times 10^3 \text{ mm}^3$ | | | |
| Distance | 300 mm | | | |
| Dimension (mm) | Length=50 Width=20 Height=20 | Major radius=20 Minor radius=7 | Radius=16.8 | Thickness=5 length= 130 Blade= 80 Handle=50 Width=30 |

1.4.2 Size experiment

The variable sizes of a cubic object are defined to test the system signal changes due to the parameter variation of size, while other parameters are identical. The normal cube as the typical shape for the varying dimension presents the clear response comparison for the variable parameter of size.

Table 1.2: Variable size object specification (unit: mm)

| Name | Size_1 | Size_2 | Size_3 | Size_4 |
|-----------|---------------------------------|-------------------------------|-------------------------------|--------------------------------|
| Shape | Cube | | | |
| Material | Basic, free machining iron (Fe) | | | |
| Distance | 300 mm | | | |
| Dimension | 20×20×20 | 30×30×30 | 40×40×40 | 50×50×50 |
| Volume | $8 \times 10^3 \text{ mm}^3$ | $27 \times 10^3 \text{ mm}^3$ | $64 \times 10^3 \text{ mm}^3$ | $125 \times 10^3 \text{ mm}^3$ |

1.4.3 Distance experiment

The distance detection allocates the same object at the specific distance to the coil for measuring the induction strength. . The project tests the detection distance around 30 cm based on the strength of received induced response based on the experimental design. Obviously, the basic model of a conductive block object placed in the different location enables the induced result study regarding the distance parameter examination.

Table 1.3: Variable distance object specification (unit: mm)

| Name | Distance_1 | Distance_2 | Distance_3 | Distance_4 | Distance_5 |
|-----------|---------------------------------|------------|------------|------------|------------|
| Shape | Block | | | | |
| Material | Basic, free machining iron (Fe) | | | | |
| Dimension | 20×20×60 | | | | |
| Volume | $24 \times 10^3 \text{ mm}^3$ | | | | |
| Distance | 200 mm | 220 mm | 240 mm | 270 mm | 300 mm |

1.4.4 Sharpness experiment

The variable volume of the detected targets with a specific sharp edge is determined to assess the system performance for the threat identification. It is known that the sharp edge as a critical judgement, mainly determines a potential of danger to safety, thus providing the sharp degree modelling for the varying volume to investigate the threat object response of the detection system.

Table 1.4: Variable sharpness object specification

| Name | Sharpness_1 | Sharpness_2 | Sharpness_3 | Sharpness_4 |
|--------------|---------------------------------|-------------------------------|-------------------------------|-------------------------------|
| Material | Basic, free machining iron (Fe) | | | |
| Sharp degree | 5° | | | |
| Distance | 300 mm | | | |
| Length | 50 mm | 100 mm | 150 mm | 200 mm |
| Volume | $10 \times 10^3 \text{ mm}^3$ | $20 \times 10^3 \text{ mm}^3$ | $30 \times 10^3 \text{ mm}^3$ | $40 \times 10^3 \text{ mm}^3$ |

1.5 Thesis structure

This thesis contains the following sections:

Chapter 2 includes the literature review of electromagnetic detection techniques currently in use to access for potential threat components carried by visitors. A range of the concealed weapon detectors are introduced in terms of imaging and electromagnetic detection practices. The benefits of the individual detection technique are discussed, as well as the drawbacks and limitations for weapon surveillance. It also explains the detection methods of the signal capture processing and weapon identification algorithms.

Chapter 3 introduces the basic theory to support the foundation of the CWD system and principal methodology applied to analyse the characteristics of weapons. The mathematical equations for pulse-induction technology are provided to explain the waveform energy alteration in the electromagnetic field. A mathematical model for decay response is derived to describe the electromagnetic changes resulting from a conductive object. In addition, the primary methodologies are provided to theoretically underpin the application of the detection system.

Chapter 4 presents the fundamental design of the detection system scheme including the practical and simulated analysis procedure. The elementary equipment includes the transducer, analogue circuit and digital conversion module, in conjunction with the on-board program for data analysis. The evaluation method based on FPGA processing determines the features of a detected target.

Subsequently, the chapter explains the elemental modules of the experimental detection system involving the analogue device of the sensor and circuitry, and the digital program of data conversion and processing. The analogue induced response is translated into a binary digital sequence to simplify the system. The system optimises the feature recognition of targets depending on the simplified digital data, and further identifies the potential illicit items by the collected mark points. Furthermore, the measurement process simulation of mark points from the digital sequence effectively shows the distinction between variable targets.

Chapter 5 performs the process result to explain the practicability of proposed weapon identification solution. Compared with the practical evidence, the simulation procedure produces the verification of target distinction for variable edge and cylinder analysis. It facilitates the algorithm's development based on the mark points evaluation, consequently, the comprehensive assessment method characterises the changes of induced responses and identifying the threat objects.

This chapter also gives the results of the investigation into the proposed weapon detection method including the delay duration analysis and mark points evaluation for the decay phase. An extensive discussion of digital signature analysis primarily concerns the coefficients of mathematical expressions and features the induced signal from a detected target.

Chapter 6 presents the future work about data processing and system optimisation in the further development and summarises the CWD system proposed in this work.

Chapter 2

Literature Review

In this chapter, the major concealed weapon detection technologies currently in use are introduced in terms of primary detecting technologies and principal methods for object identification. The fundamental systems employ the imaging detection and electromagnetic detection structure to distinguish the different weapons from the targets. The principal methods of object detection techniques generally capture and recognise the signal from sensors for data classification and analysis, based on the proper processing platforms. Subsequently, the weapon identification approaches deliver the effective characteristics of detection according to the signal processing practices, which defines and discriminates the threat targets, as seen in Figure 2.1.

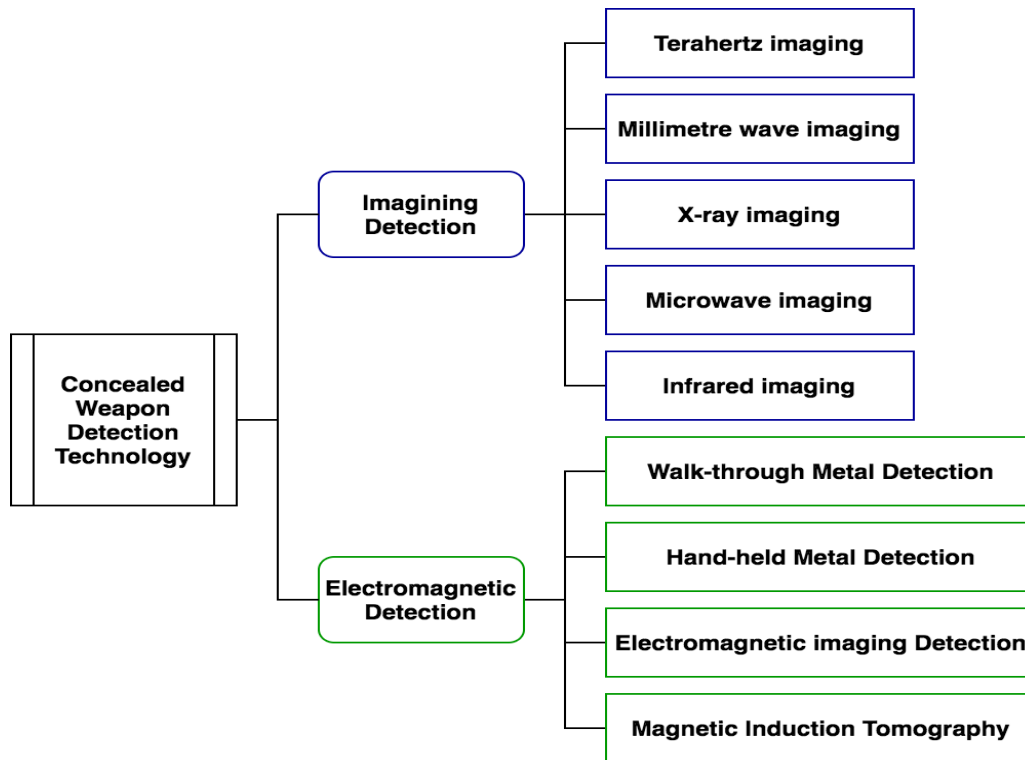


Figure 2.1: Concealed weapon detection technologies.

In recent years, the basic imaging techniques of illicit components, applied in open areas, scan the bodies and luggage in the controlled access environment, as seen in Figure 2.1 [12]. The screening procedure applied at the checkpoints images individuals in order to pinpoint the position of a weapon on the body or inside the luggage [13]. Alternatively, the technologies used to detect concealed weapons primarily apply a form of electromagnetic detection to recognise the conductive objects. The characterisation of metallic objects which have been identified by electromagnetic based metal detection primarily relies on manual operation to define the potential of threat on an individual basis.

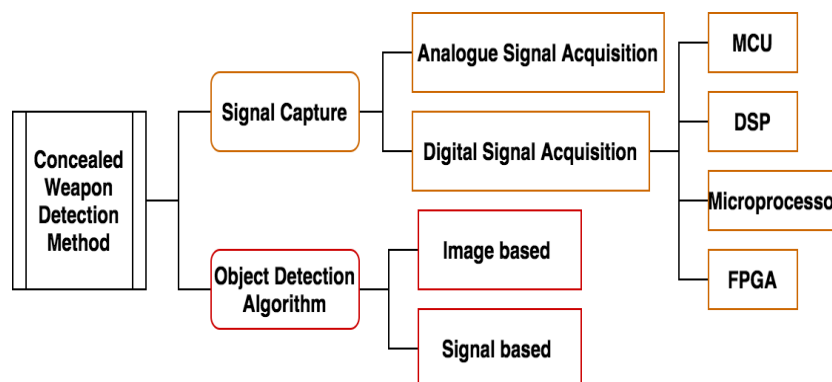


Figure 2.2: Concealed weapon detection methods.

The detection applications typically acquire the analogue signal and handles the digital data for the target's study and recognition, based on the processing platforms in Figure 2.2 [14]. The platform aims to capture the sensory input from the transducers, and then modify the signal for amplification and conditioning stages. As the analogue signal converted, the data processing procedure manages and analyses the digital information for effective identification and classification. The required platform addresses the digital data processing and management to define the characterises of physical changes which are used to describe the object.

The detection practices recently in use gave rise to the advancement of weapon identification methods and algorithms regarding image and signal analysis. A wide range of image recognition approaches examine and discriminate the screening pictures to identify the danger. Meanwhile, the signal-dependent detection methods normally translate the physical signals to the digital code, characterising the investigated targets. The developed surveillance systems use weapon recognition methods to attempt to identify suspicious items, ensuring public security without any physical contact.

2.1 Imaging detection

In order to address the issue of concealed weapon recognition, the imaging detection applications screen carried items, identifying danger individually at major transportation hubs. The screening procedure has been developed to visually display the optical patterns of a suspected object for security surveillance. The major imaging approaches are principally dependent on the radiation waves over a range of frequencies, as mentioned in Table 2.1 [15].

Table 2.1: Comparison of different imaging sensors. Reproduced from [Haynes, 2011].

| Imaging sensors type | Illumination | Proximity | Portability | Frequency Range |
|-------------------------|--------------|-----------|-------------|-------------------|
| Terahertz imaging | P | F | T | 100 GHz ~ 10 THz |
| Millimetre wave imaging | A/P | F | H/T | 30 GHz ~ 300 GHz |
| X-ray imaging | A | N | T | 30 PHz ~ 30 EHz |
| Microwave imaging | A | N/F | T | 300 MHz ~ 30 GHz |
| Infrared imaging | P | F | T | 300 GHz ~ 430 THz |

Note. A means active and P is passive, F represents far and N is near, H means handheld and T represents transportable.

2.1.1 Terahertz (THz) imaging

The terahertz (THz) imaging technique usually evaluates the radiometric temperature of a detected object compared with the background [16]. It employs electromagnetic waves with a frequency in the range of $0.1 \sim 10$ THz (wavelength $3000 \sim 30 \mu\text{m}$), so that less energy is generated in the results of biological entities [17][18]. It also penetrates clothing and different types of covers and enclosures for high-quality photographing of concealed targets.

Nevertheless, the passive performance of imaging is restricted due to the low signal-to-noise ratio and poor contrast [19]. THz detectors using THz frequencies are typically limited to be sensitive to dynamic objects, and the restricted number of pixels makes it difficult to physically scan a target [20]. Due to the dedicated material for varied frequencies, the optical lenses are typically not manufactured for THz imaging construction [21].

2.1.2 Millimetre wave imaging

A millimetre-wave (MMW) scanner is capable of full-body photographing a passenger and concealed objects using radio waves in the millimetre range ($30 \sim 300$ GHz) [22]. The scanning application realizes the penetration through clothing because conductive targets feature low emissivity and high reflectivity, compared with the background radiation [23].

The current MMW detectors employed for security screening are conceptually classified as either active or passive. For the active method, the energy reflected off the physical passenger and concealed items helps form the scanned photograph [24]. A passive MMW detector usually measures the natural millimetre wave from the radiation of a human body in order to monitor abnormal temperatures due to the emergence of a subject [25]. As a result, it is safe to identify the differences in emitted waves, protecting privacy without screening the anatomical details of a traveller [26].

However, the external environment and coherent interference results in inaccurate measurements and weakens the detectability of accessed objects. Due to glints and specular reflection, the probability of a false alarm considerably increases even in the absence of real danger [27].

2.1.3 X-ray imaging

A number of applications with X-ray imaging have been advanced over the decades, supplying high-energy in the X-radiation region (3×10^{16} Hz to 3×10^{19} Hz) which has considerable sensitivity to concealed items [28]. It offers the benefit of fast and highly efficient process

performance, as well as compositional analysis of a target with significantly enhanced quality due to the high transmitting flux [29].

The adverse effect is the potential harm to the physical body from an X-ray demonstration [30]. Due to the relatively high radiation dose, a long environmental exposure time increases the risk of tissue effects, e.g., hair loss and skin damage, and even the more serious problem of cancer [31]. Despite high-resolution visual measurement, there is a high possibility for scanned people to physically suffer from the wide use of conventional X-ray imaging devices.

2.1.4 Microwave imaging

Microwave imaging detectors provide satisfactory diagnostic capability and typically visualise the scene for security inspection using harmless microwaves within the frequency range $0.3 \sim 30$ GHz [32]. It normally relies on near-field imaging probes to evaluate the electric field polarisation to structurally photograph the targets. Based on the frequency, an estimation of the external scattered field through the radiated object reconstructs the distribution showing dielectric properties, and thus shapes the image [33].

The active incoherent imaging offers the advantage of cost savings and implementation simplicity, as well as positive propagation characteristics, such as negligible attenuation through clothing materials [34]. Nevertheless, less sensitivity in inspection scenarios is an obstacle to characterising polarised objects with cracks and sharp edges. The orientation of a detected component highly influences the incident electric field vector, consequently, the polarisation evaluation by the established probes is not always feasible [35].

2.1.5 Infrared imaging

Infrared imaging relies on the thermal distribution of the object to produce detailed photographs of infrared radiation in the spectrum range of $300 \text{ GHz} \sim 430 \text{ THz}$, even in low visibility environments. In general, the heat sensor, which is capable of capturing subtle variations of temperature from a radiation sample in the background environment, formulates a thermal picture [36].

This non-contact temperature sensing detector features an efficient and intuitive evaluation of infrared energy to help recognise distinct components clearly [37]. It is considerably sensitive to thermal emissions from concealed targets, and thus creates high-resolution thermographic patterns for monitoring abnormalities [38]. However, infrared thermography techniques have

their own limitations in concealed items' recognition in the absence of clothing penetration. When external covers are loosened or their thickness increases, the infrared radiation is unable to extend over the interior space, thus degrading photographing performance [39].

2.2 Electromagnetic (EM) detection

Electromagnetic propagation is the basis of transmission solutions. Electromagnetic waves travel in the form of a radio wave and are widely applied for weapon detection [40]. An electromagnetic field is commonly produced to distribute power and broadcast signals and reflects the presence of conductive targets [41]. Therefore, the detection applications evaluate the radiant energy through the magnetic field, coupled with electric waves, to identify a metallic weapon.

2.2.1 Walk through metal detector

Walk through detectors are commonly arranged to recognise metal inclusions concealed within luggage when accessing security checkpoints. The detector is setup to operate with security personnel for a controlled flow of traffic, as metallic components as potential threats are prohibited from being carried through secured facilities such as ports and government offices [42].

The principle used to identify metallic objects in walk through detection electromagnetic inductance through metallic objects coupled with the coil array. The transmitter produces a time-varying magnetic field while the receiver on the opposite side of the device senses the secondary induction from the presence of conductive items [43]. Multi zone detection arrayed zone detectors are normally deployed in this type of application for indicating the weapons in real-time [44].

The benefit of zone-based walk-through detectors is that they identify metallic items whilst also pinpointing a location on a person according to the position of individual sensors. However, the sensitivity of detection is limited which makes it unsuitable for open application with a high throughput of candidates, as electronic noise interferes with the receiver circuitry, which is termed as the body effect [45]. In addition, the metallic items generate the result and the distinction between threat and no threat is generally limited, resulting in a false positive, which is also referred to as a false alarm.

2.2.2 Hand-held metal detection

Handheld metal detection devices are used for active body search scanning and individually conducting a non-invasive inspection of visitors. For a metal detector, the basic electronic oscillator generates a periodic radio wave that transmits through a coil to supply a magnetic field [46]. Once a conductive metal is presented within the indication range, another coil as the receiver is capable of estimating the change of magnetic field and raising the audio alarm.

The hand-held detection device offers a portable and convenient alternative for security at indoor/outdoor events, which can be freely arranged and set up at the checkpoints without requiring the implementation of any significant adjustments. It also features an uncomplicated operation, requiring a sweep across an individual's body or containers to locate where metal objects are potentially concealed.

While the high sensitivity was recently developed to detect small metal items and wide application has become low cost, the manual procedure on the individual basis is not time efficient and the efficiency heavily relies on personnel experience. The technique is also subject to a high possibility of interference, limited range and proximity distance for a single detector. The ineffective distinction of a threat objects is an obvious drawback as all metallic items, even those that are not a threat to security, trigger an alarm.

2.2.3 Electromagnetic imaging detection

The major task for an electromagnetic imaging system is extracting the induced response signature and constructing a two-dimensional picture for weapon validation. The solution is to set up a vibrating magnetic field associated with the electric wave source, to probe the environment. Unlike the normal detection of electromagnetic signal, the EM imaging procedure collects the information from the sensor arrays to build up a pattern, reflecting the induction value for each pixel [47].

For image processing purposes, this approach addresses the response signature from the standoff sensors. Hence, the human body does not suffer from any obstruction and coercion [48]. Based on the picture provided on the screen, the size, shape, and physical composition of the scanned objects can be visually recognized, which helps alert the security personnel to contraband items. Nonetheless, the EM imaging detector faces the significant challenge of prohibitive cost for the basic equipment and arrayed sensors. In addition, the image has a high spatial resolution and obviously requires an advanced processor to calculate a great mass of data. The accuracy is

heavily based on the skill of the operators to determine the threat of a target based on the scanned image.

2.2.4 Magnetic induction tomography

Magnetic induction tomography (MIT), known as an emerging imaging modality, uses the interaction of altering magnetic field with conductive media, with a view to screening the properties of an object concealed in parcels [49]. According to the fundamental principles of the MIT approach, an excitation coil registers the oscillating magnetic field which is perturbed by eddy current in the material and then measured by sensing coils [50]. In essence, the solution uses electromagnetic resonance to explore injecting and sensing electrodes in order to visualize the distribution of electrical impedance inside a conductive weapon [51].

The automated MIT technique provides a magnetic field with an adjustable frequency, thereby achieving the optimal imaging for the variable parameters (permittivity, permeability and conductivity) of the target under investigation [52]. It also has the advantage of contact-less and non-invasive operation for real-time image reconstruction [53]. However, the drawback of MIT is its instability and imprecision due to the low conductivity contrast between the object and background [54]. This difficulty was recently found in employing the computational approach to deal with the corresponding inverse problems, as intensive calculations are required to reconstruct an image [55].

2.3 Signal capture platform

The fundamental architecture of signal collection and transmission depends on using the proper platform to acquire the information and execute the operation. The basic requirement is to capture and manipulate the analogue signal on the practical circuit. Furthermore, the conversion and processing modules implemented on the feasible platforms collect and transform the analogue signal to the digital data for target detection recognition.

2.3.1 Analogue signal acquisition

The analogue signal capture technique traditionally uses electronic circuitry to collect and monitor the electromagnetic signal, such as the hand-held metal detector. Fundamentally, the electronic devices perform the signal amplification, filtration, modulation and transformation

for analogue processing, estimating the analogue variable for signal detection.

The analogue signal processors feature an uncomplicated structure, so that the applications become economical for the rectification and replacement of faulty components in the circuit. However, the non-programmable framework suffers the limitation of single functionality, which barely addresses the changeable environment for a complicated and systematic project.

2.3.2 Digital signal acquisition

As analogue samples are obtained, the analogue-to-digital conversion is an indispensable procedure for the digital input acquisition of detection devices. The signal digitisation facilitates the digital data processing and analysis on the platforms, describing the features of sensing changes. The digital data processors typically operate the data conversion and transformation depending upon the programmable structure of a central processing unit (CPU). The programmable processors present the flexible adaptation and high performance of instruction execution and program design for digital study. They efficiently deliver the digital code acquisition, processing and investigation to characterise the sensing signal of a detected target.

Microcontroller unit (MCU)

A microcontroller commonly employs a single integrated circuit chip to logically perform the digital signal conversion and data transformation arithmetic. The von Neumann architecture of MCUs classically facilitates the interaction of the central chip with the built-in memory that stores both instructions and data located at the system address [56]. The behavioural structure conducts the implanted program by internal buses, controlling and recording the digital input signal for data communication.

The stored-program design of MCUs allows for coding to reconfigure and update the changeable hardware and device components. The direct interface of the microcontroller and sensors can automatically operate the collection, transmission and conversion of a detected signal, according to the specified program.

Nonetheless, the MCU instruments lack flexibility regarding program modifications because the single chip is assigned to control a singular function in a device for a specific scenario [57]. In addition, the basic arrangement to register the instruction execution or data record separately, share a common bus which increases the communication congestion and reduces computation

speed [58].

Digital signal processor (DSP)

The DSP instruments realise multiple operations to perform the commands and transfer the data simultaneously based on the Harvard architecture. The structure mainly divides the processing space into the program memory and data storage according to different bit widths [59]. It also has separate buses dedicated to fetching and executions respectively, therefore, the built-in random access memory (RAM) synchronously calls the instructions and data to process the signal [60].

The outstanding mathematical calculations of DSPs derive from the parallel computation of a separate arithmetic logic unit (ALU), embedded inside of a signal processing module [61]. The pipelined execution units dramatically improve the effectiveness to read the subsequent word during the operation, due to the concurrent data access independent from program execution [62].

As an instruction-based technique, the DSP features a single cycle of multiple instructions that can conduct the numeric operation at each instruction cycle. Thus, the achievement of synchronous communication generates unanticipated latencies due to instructions' execution in multiple steps. Moreover, the resources shared by tasks for the DSP arrangement typically give a restriction of addressing signals when requiring a high data sampling rate [63].

Microprocessors

The development of microprocessors incorporates the multifunctional units on a universal implanted chip as an integrated circuit (IC) for general-purpose performance [64]. A microprocessor, as the central engine of computers, can accomplish arithmetic and logical tasks to control the complex signal and transport the massive data [65]. The sequential actions from control units directly fetch the information and execute the instructions in the register array for computational operations.

The ubiquity of microprocessors in the computer world reveals the broad functionality to speedily perform the sophisticated signal operation and information analysis [66]. The highly integrated chip benefits a small-scale framework, and the versatile computational behaviour increases the design simplicity for complicated applications.

To maximise the computer power of the chip, the architecture density and complexity inevitably

increase the power consumption [67]. The embedded system employs the microprocessor chip in conjunction with the supporting apparatus like extensive memory, input and output terminals.

Field programmable gate arrays (FPGA)

An integrated FPGA circuitry applies the essential architecture of logic cell array, principally referred to multiple programmable logic blocks interconnected for changeable configurations [68]. The logic modules prebuilt in arrays can structure the digital implementation to perform multitask functions according to the hierarchy of reconfigurability [69]. The programmable connection gates wire the elementary logic units to change the electrical functionality for multi-purpose applications. As a result, the clock-based solution of FPGAs provides the customizable logic and interface functions by programming the logic arrays [70].

The distinguishing feature of FPGA technology shows the immense flexibility to reconfigure and modify the implemented control circuitry, achieving updated functionality requirements. The efficient programmability is feasible to accelerate the data computing performance for rapid prototyping and complex combinational functions, based on the reliable hardware solution. The expansive parallelism capabilities facilitate the optimization of embedded system design, presenting the dynamical adaptability for massive information processing [71].

Furthermore, a FPGA-based approach offers the real-time behavior for signal manipulation, which reacts to stimuli from the environment within the negligible lag. Considering the engineering cost, FPGAs become attractive as low-cost and power-efficient alternatives for equipment manufacturing and system development, designed by a very high-speed hardware description language (VHDL) [72].

2.4 Weapon detection algorithms

The approach to potential weapon recognition primarily depends on the signal and data analysis algorithms, correspondent to the provided platform. The investigation practice applies the shape image recognition method to examine and identify the object under analysis. Alternatively, the data analysis algorithm models a behaviour of the detected signal to study the distinction between the target cases.

2.4.1 Image-based identification

The imaging detection approach primarily acquires the elemental information of pixels according to positional recognition and takes a digital photograph to illustrate the potential objects. When an imaging signal is accepted, the basic procedure segments the elemental regions for imaging reconstruction and extracts the required pixels of an object from the background [73]. The feasible practices assign the class labels to an image for classification and analysis, so that the image fusion synthesises the complementary information of each class to display a composite assessment [74]. Meanwhile, the identification analysis delivers the features description and object localisation, which predicts the identity of a suspicious component within an image [75]. The image-based recognition mainly involves a single shot detector (SSD), histogram of oriented gradients (HOG) and convolutional neural network (CNN), where the algorithms explore the maximum likelihood to evaluate the behaviour of an illicit target in an image.

Single Shot Detector (SSD)

The SSD model establishes a single-forward convolutional network, which primarily collect the scores through the layers to understand the saliency target data [76]. The training practice principally applies the structural discretisation of classes of default boxes at multiple aspect ratios, and then predicts the feature maps for the resolution examination in Figure 2.3 [77].

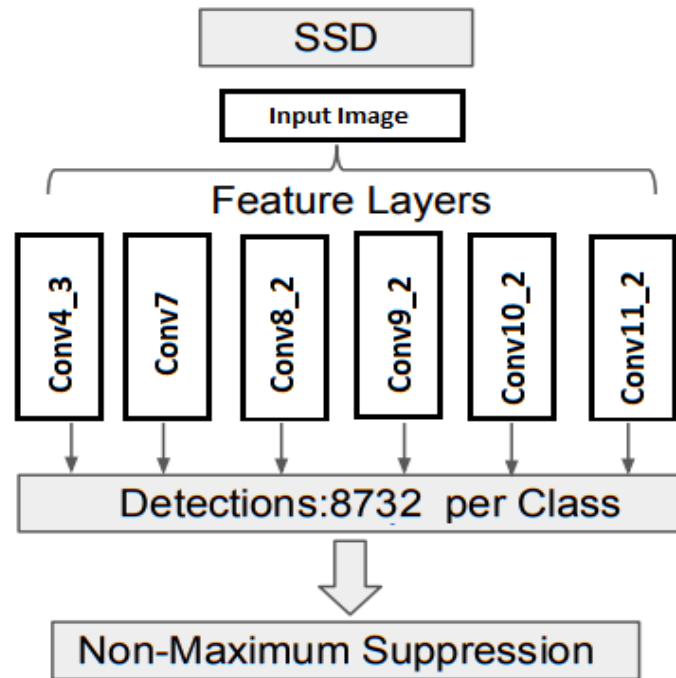


Figure 2.3: Single Shot Detector model.

The base network is located at an early stage and performs the convolutional filtering to classify the input image within the bounding box [78]. The extra functional layers combine the multi-scale feature maps and convolutional predictors of default boxes for each location cell, as shown in Table 2.2. Therefore, the SSD achievements of object detection solves the feature resampling of various sizes, omitting the step of the proposal.

Table 2.2: Bounding boxes for convolution layer. Reprinted from [Tsang, 2018][123]

| | CONVOLUTION | BOUNDING BOXES |
|-----------|-------------|--------------------------------|
| 1ST LAYER | conv4_3 | $38 \times 38 \times 4 = 5776$ |
| 2ND LAYER | conv7 | $19 \times 19 \times 6 = 2166$ |
| 3RD LAYER | conv8_2 | $10 \times 10 \times 6 = 600$ |
| 4TH LAYER | conv9_2 | $5 \times 5 \times 6 = 150$ |
| 5TH LAYER | conv10_2 | $3 \times 3 \times 4 = 36$ |
| 6TH LAYER | conv11_2 | $1 \times 1 \times 4 = 4$ |
| TOTAL | | 8732 |

As a single stage detection method, the SSD framework features a feed-forward convolutional network for speedy processing and achieves the comparable advantage of precision. The convenience of algorithm training and system implementation creates considerable competitiveness for detection components and steps that delivers a unified processing architecture.

Histogram of Oriented Gradients (HOG)

The fundamental method of this representative model trains a feature classifier to extract and process behavioural information for object detection. It evaluates the network of gradient orientations from the histogram demonstration to represent the target figure in an image [79]. For a grid of elemental blocks, the computing procedure calculates the pixel value of the intensity gradient and edge directions in a histogram assessment. In order to eliminate the background, value normalisation efficiently describes the appearance of the major object, avoiding block overlapping. The classifier extracts the major information, evaluating the distribution of gradient vectors, to learn the distinct classification for characteristics' study.

The efficient and controllable computing of the HOG algorithm is dependent on the data representation of gradient measurement within the located blocks of an image, usually defined as the region of interest (ROI). It also benefits the intelligent learning and understanding for geometric transformations and classifying the primary data collection [80].

Convolutional Neural Network (CNN)

The typical neural networks of visual image recognition feature the multilayer perception that each neuron, connected in a sequence of layers, which respond to stimuli within the receptive region through convolution processing. The architecture extracts and classifies object proposals for region division after capturing an input image [81]. The solution computes the features of each neuron over the pooling classes, as seen in Figure 2.4. The network structure identifies the target and predicts the bounds using convolution through the functional layers [82].

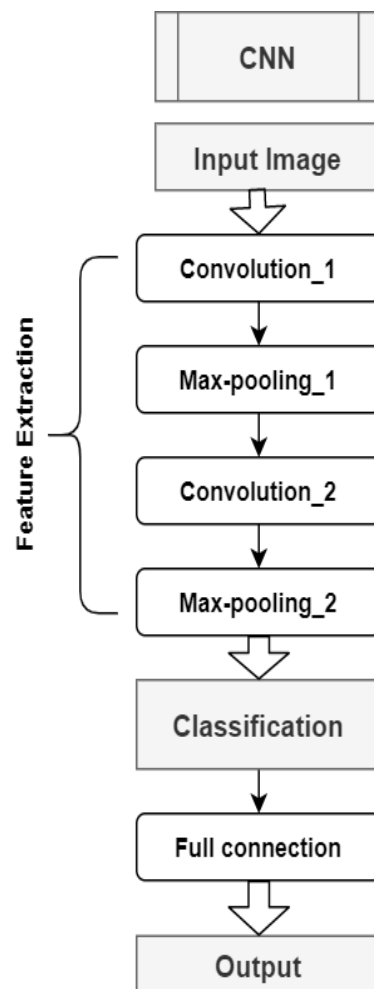


Figure 2.4: Convolutional Neural Network architecture.

The class pattern minimises the computation for the imaging scenario and simplifies the object identification without the data loss. The computing models gives an accurate response for features classification for locating the object. Nevertheless, the algorithm requires massive computing power and memory to process the analysis and prediction for a single image capture [83]. The technique exposes the limitations of the process speed as it extracts the multi-layer

information based on the region detection.

In general, region-based identification faces a challenge of limited sensitivity to separate an object from the background information, due to the colour contrast and shape similarity. The technique spends massive computation time on integrating the pixel-level detection to fetch the combined imaging description. Hence, the imaging method achieves the object's visualization by sacrificing efficiency and economies as a high computational cost is required.

2.4.2 Signal-based identification

The data acquisition system (DAQ) typically measures, transforms and stores the resulting samples to the digital data used to document the scenes. The signal identification procedure measures and analyses the electromagnetic quantity of the interaction through the calculation models, investigating the physical pattern of a target. The data transformation and computation processes a set of signals in the time or frequency domain to output the numerical representation of a reference [84].

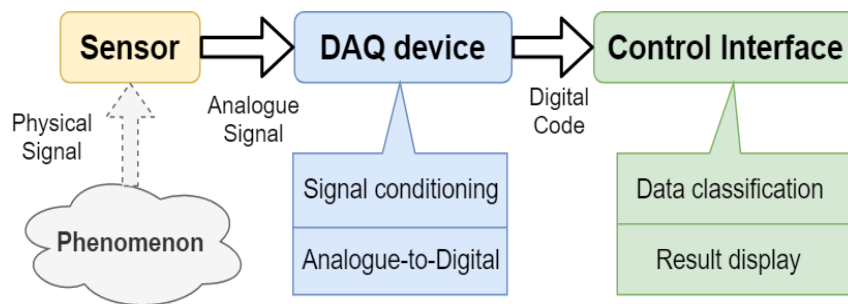


Figure 2.5: Digital data acquisition system.

In essence, the transducer component acquires the raw analogue input from physical parameters of the phenomenon in Figure 2.5. At the next stage, the signal conditioning procedure of DAQ hardware filters the wave amplitude for the desired range. The conversion technique translates the analogue features into the digital values afterwards, which performs the digitisation of practical measurement continuously. Eventually the display and analysis interface, based on the quantised code, and defines and classifies the physical models showing readable and meaningful results [85].

Serial communication data acquisition

The basic techniques of data acquisition propose that serial communication converts the physical electromagnetic waveform to digital signal detection. The principle is that the data receives and monitors that the sampling procedure and is investigated to measure the analogue changes from the sensing response. The conversion processes the consecutive digital transform to deliver the binary codes for signal identification, which represents the characteristics of the induced response.

High speed data acquisition

Signal identification using the high-speed approach encodes the transmitting waves to characterise the target at high frequencies, typically reaching the GHz frequency response [86]. The conversion analysis evaluates the sensing signature based on high frequency sampling, delivering the features of an analogue response. Through speedy transformation, the model can realise the digital identification and classification for feature description.

The high frequency modulating solution demonstrates the merits of a swift response and effective identification, while the performance requires high-frequency configuration [87]. In addition, the high frequency sampling hinders the accurate measurement of the minor practical changes due to errors that occur.

Signal-based identification is becoming the prevailing method to describe the dynamic behaviour of an object because of its convenience and feasibility. On the other hand, the difficulty with this approach occurs in real-time detection, where the sophisticated transformation and calculation steps postpone the response time. Moreover, the signal processing applications meet the challenges of large-scale data computation resulting from the limitation of storage space and operating speed. In the practice of weapon detection, the discrimination capabilities expose the shortcomings of accuracy and efficiency when automatically identifying the threat and non-threat components [88].

2.5 Summary

Based on the review of current detection techniques, it was concluded that an eligible detection approach that satisfied the intelligent threat decision without manual investigation for the real-time concealed targets detection in an open area was difficult to find. The primary technical

issue focused on the real-time inspection of hidden objects for the volume of visitors in open area. Meanwhile, the contraband targets determination was the challenge to intelligently excludes non-threat items that passed through the surveillance zone.

After the evaluation of the advanced imaging-based detection techniques for concealed weapons currently in wide use, it was determined that they are able to provide photographic evidence of illicit objects after scanning visitors. The shortcomings are that the verification exercise requires time to visually monitor the delicate items even they are actually innocuous. However, the screening techniques inevitably visualize all personal information, even if it presents no threat to safety. Consequently, the disadvantage is the invasion of privacy. In addition, it is impractical to apply the imaging surveillance to a high density of crowd flow as it is designed for individual screening in sequenced access.

For different types of electromagnetic signature-based detection devices, the main advantage is that the recognition method depends on the measurement of the received signal of inductance, avoiding any risk of information leaking. Although they feature a contact-free and non-destructive evaluation, the manual procedure is inefficient and has a limited capability to process uncontrolled crowds in open area. Moreover, the EM applications are vulnerable to false alarms as conductive components are assumed to be weapons.

The analogue signal acquisition is limited for the analogue circuitry design to potentially result in the distortion and interference of data sampling. The digitisation of microcontrollers and DSPs facilitates signal capture and conversion while the limited data collection and computation hinder synchronous communication. Moreover, the microprocessors of a computer scheme provide the powerful capabilities for complex tasks, however, the engineering cost and power consumption are considerable. The low-cost of FPGA is an appropriate alternative to efficiently develop a real-time acquisition and transition design.

The weapon identification algorithms of imaging investigation depend on the high performance of calculations to illustrates and locate a threat object. The image-based approach extracts and reconstructs the shape information through large-scale data computation to estimate the potential to inflict harm. Similarly, the signal recognition methods are primarily restricted to the data storage space and processing volume to accomplish speedy and effective detection. In general, the threat detection algorithms require high levels of computational resources, which is unavoidable due to the levels of data and complexity. Moreover, these approaches are disadvantageous when attempting to efficiently distinguish between the concealment of potential

weapons from non-threatening items when monitoring uncontrolled passenger flow.

The advanced weapon detection technique is seriously considered to predict the potential danger by identifying concealed threat objects, avoiding the personal information leakage. The requirement of the developed surveillance system can realize the real-time characteristics analysing and distinguishing of the threatening target to neutralise imminent threats in an open area. Therefore, the automatic threat recognition sensors mounted at checkpoint sites can track a carried weapon.

In this thesis, the basic structure based on electromagnetic interaction produces the electrical analogue signal for weapon recognition, rather than visualising the information. A signature-based solution is applied to address the identification and classification for concealed weapons, because an induced response is dependent on the characteristics of an object, such as material, shape and size.

However, unlike the normal procedure to extract and evaluate the analogue signal, the new approach must be converted into digital data, providing the efficient computation on the FPGA platform. In addition, in order to avoid excessive data, the detection system with a novel algorithm tends to simplify the information to reduce the calculation and processing time, achieving synchronous verification for public security.

Chapter 3

Theory

In response to the continuous security monitor requirement in public spaces, the concealed weapon detection system is suggested to accurately and effectively recognize and locate an illicit object travelled across the assigned zone. The project primarily demands a reliable surveillance framework to discover a moving potential threat object within an open environment. The multi-sensor arrangement achieves the capacity of real-time detection, searching and investigating a concealed weapon based on the single detector. The identification of a weapon at different sensing spots can reveal the trajectories to lock on the target within the surveillance range.

The basic design for each specific single detector applies the pulse induction technique, measuring a received response from the detected objects. The individual sensor captures the induced response to reflect the conductive target interacted with the oscillating magnetic field supplied from a pulsed excitation. The detection system can measure and analyse a unique responded signature to provide the main characteristic of an object instead of imaging the figure.

For analysing the pulsed inductance, the specific targets with variable factors, such as material, size, shape and distance, are simulated to differentiate the received signature. In principle, the variation of one parameter of a target affects the magnetic field excited by a vibrating electronic pulse, resulting in the corresponding fluctuation of the induced response. The simulated evaluation of specific varied parameters points out the featured change of the received signature from pulse induction. Conversely, according to the simulation testing, the detection system focuses on the analysis of characteristics of an induced signature, thereby distinguishing

and classifying the variation of a detected target.

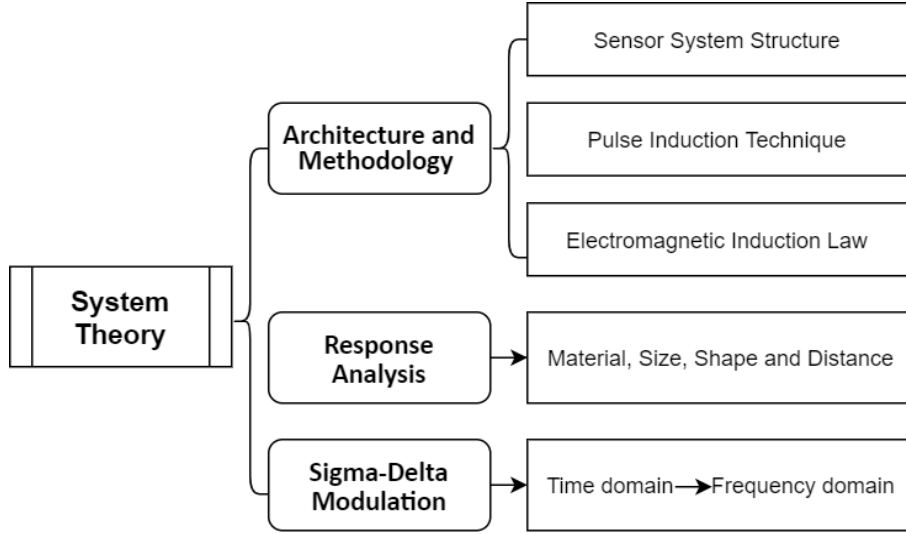


Figure 3.1: System theory structure.

This chapter introduces the fundamental principles of the detection system, arraying the sensors for real-time weapon monitoring for the open space in Figure 3.1. For individual detector, the principal scheme with the pulse induction method uses the response signature to characterize the target investigation. Furthermore, the simulation of induced response demonstrates the influence of variable parameters of a conductive object. The signal conversion procedure applies the sigma-delta modulation technique to translates the sampling data.

3.1 Architecture and methodology

The fundamental framework of this detection system is constructed to monitor the security of an open area environment, to recognize and locate a suspected weapon in real-time effectively. The signature-based scheme applies the pulsed excitation principle to characterize the induction response for a specific target.

3.1.1 Sensor structure

The sensor networks commonly process and act upon high amounts of environmental data from heterogeneous distributed sensors, aggregated as an entity, especially for geospatial solutions [89]. As equipped with sensor nodes, the sensor structure significantly improves connectivity-based localization by determining the coordinate information [90]. The ubiquity of integrated sensors typically benefits the communication platform from remarkable

performance and reliability, ensuring evaluation of environmental monitoring, which intended for measurement and security applications [91]. The detection system applies the multiple sensors structure in an open zone by exploiting the single detection base to effectively explore a threat target dedicated to the locating-based weapon monitoring solution. Another motivation is that the sensor network helps broaden the facilities of real-time weapons tracing within an open area under surveillance.

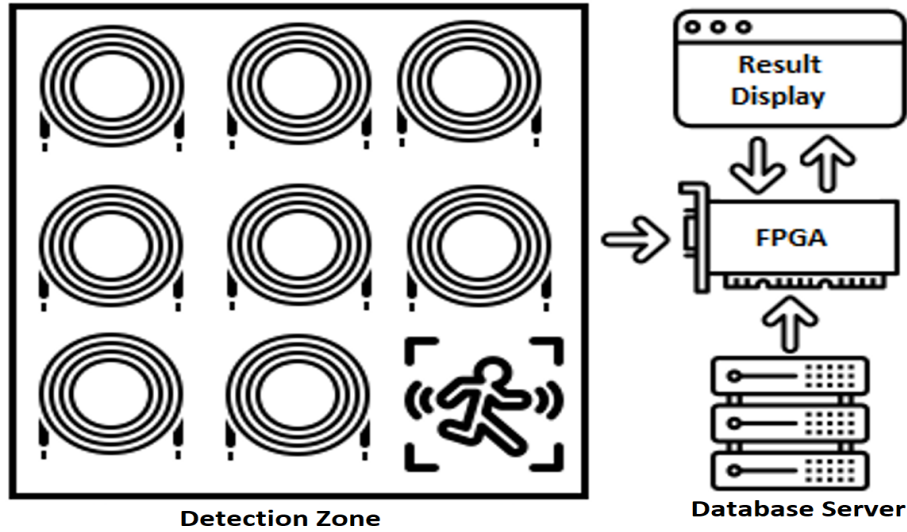


Figure 3.2: Basic architecture for sensor system.

The weapon detection system with multi-sensor structure arrays adequate elemental sensors for alarm at the individual spot to monitor the surveillance space, as seen in Figure 3.2 [92]. A single electromagnetic sensor can non-contact alarming once the passengers carry a potential threat object across the checkpoint [93]. The distribution of multiple sensors arranged in the surveillance zone becomes sensitive to a weapon travelling at any access routes. Simultaneously, a detection area, composed of the assembled sensors, investigates the location of an indicated node and neighbouring nodes to pursue the trajectories of a suspected visitors.

The array sensor structure typically depends on the detecting nodes to dynamically collect the environmental information, enabling early detection and response to a potential threat target travelling across the open zone. There is a matrix of sensors distributed in the surveillance area monitoring and alarming a pass-through weapon and tracking the moving path of a suspected visitor. However, a single detector demands the reliability to accurately identify an illicit object by high-speed processing the analogue response [94]. Consequently, the performance of a single sensor to process the received signature essentially determines the capacity of the detection

system, discovering a threat target passed through an open area.

3.1.2 Pulse induction approach

A single electromagnetic detector is used to identify conductive items based on the mutual energy transmission between the electric radiation and magnetic field. The detection structure principle is that a travelling electric wave produced at the transmitter produces an oscillating magnetic field, transferring the electromagnetic radiant energy [95]. Secondly, the receiver antennas collect the induced electric current resulting from the alteration of the magnetic field once a new conductive target is placed [96]. Therefore, the individual detector propagates electromagnetic energy through a surveillance space to monitor the varied radiant energy due to the emergence of a metallic object.

The classic approaches of electromagnetic detection structure are Beat-frequency oscillator (BFO), Very low frequency (VLF) and Pulse induction (PI). As the simple and basic method, BFO technology equips with two coils that both oscillates the same radiofrequency. The deviation from the reference oscillator decides the types of metallic components.

For the construction of VLF, a vibrating electric wave, such as a sinusoidal wave, supplies the peripheral transmitter coil to generate the magnetic field while the inner hoop acts as the receiver coil to acquire the electric signal [97]. The alternating direction of transmitting electric waves changes the polarity of the magnetic field at the same frequency. A conductive object interacts with the oscillating magnetic field, resulting in the direction opposite magnetic flux. The amplitude and phase demodulators discriminate the detected target, compared with the introduced sin-wave signal.

As a single coil, the PI approach employs the repeated electrical pulse as a transmitting source to produce a pulsating magnetic field. On the other hand, the variation of magnetic flux induces the answering pulse through the same coil for investigation. When a metallic object disturbs the initial magnetic field, the new-emerged magnetic field causes a decayed electrical spike, determining the feature of conductive objects [98].

Table 3.1: BFO, VLF and PI comparison. Reproduced from [Tyson, 2001][93].

| | Beat-frequency oscillator (BFO) | Very low frequency (VLF) | Pulse induction (PI) |
|--------------|--|---|--|
| Advantage | <ul style="list-style-type: none"> ➤ Simply structure to acquire ➤ Low cost to manufacture | <ul style="list-style-type: none"> ➤ Electrical interference resistance ➤ High speed response ➤ Wide range propagation | <ul style="list-style-type: none"> ➤ Considerable detection distance ➤ High accuracy, reliability, stability and sensitivity ➤ Portability and adaptability ➤ Non-conductive penetration |
| Disadvantage | <ul style="list-style-type: none"> ➤ Low quality and performance ➤ Inaccuracy for detection ➤ Advanced technology replacement | <ul style="list-style-type: none"> ➤ Limited detection distance ➤ Less penetration performance ➤ Environmental noise interference ➤ Topographic restriction | <ul style="list-style-type: none"> ➤ Restricted propagation rang ➤ Electrical and electromagnetic interference and noise |

As Table 3.1 lists the advantages and drawbacks of target identification technologies of three main methods, BFO becomes outdated and restricted by accuracy and performance while VLF mainly incurs the limited penetration for clothes and detection distance regarding body inspection [99]. Hence, an alternative of the PI method is applied in the weapon detection system to efficiently inspect the visitors and discover the concealed targets underneath the cloth/bags.

In contrast with the VLF applications that require the transmitters and receivers within the detectable range, the PI technologies typically apply the single search coil as the transceiver. Due to the uncontrolled passenger flow in the open area, the single-coil setup is feasible to construct the transducer buried underground, composing the sensor system for open area surveillance.

According to the PI approach principle for weapon detection, the frequent pulse of the electronic source firstly supplies a vibrating magnetic field around the coil, as shown in Figure 3.3. Then the eddy current flows inside the conductive target due to the oscillating magnetic flux [100].

Finally, the opposite polarity of the secondary magnetic field induces the reflected spike that lasts an extremely short time in the coil. Consequently, the induced response in the opposite direction after a supplying pulse reflects the types of metallic objects [101].

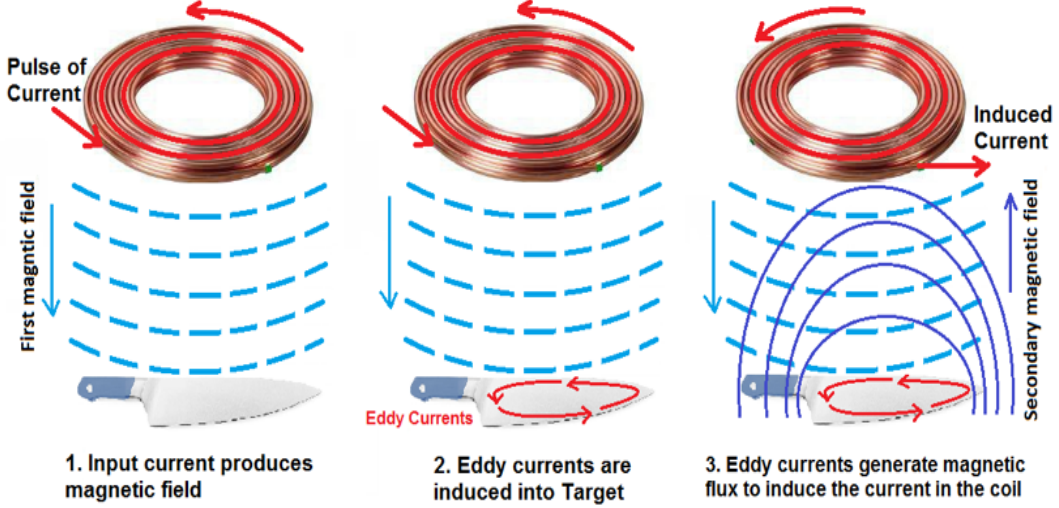


Figure 3.3: Pulse induction process. Reproduced from [Yuxiang, 2018][121].

3.1.3 Electromagnetic induction equations

The detection system employs the PI approach to identify a definite target dependent upon the unique reflected response. That is mainly because the variation of induced electrical signature corresponds to the specific feature of a conductive object and the location in the detection zone. Therefore, the theoretical explanation and mathematical equations validate the practicability of the target recognition scheme using the electromagnetic induction method.

The electric current-carrying source typically charges the constant magnetic flux in the vicinity. The magnitude of the flowing current element at a point inherently affects the surrounding magnetic field, and magnetic flux density B can be described by the Biot–Savart Law [102]:

$$dB = \frac{\mu_0}{4\pi} \cdot \frac{Idl \times r'}{r^3} \quad (3.1)$$

where μ_0 is the permeability of free space, I is source current, l is the integration path, r is the distance from wire element and r' is a unit vector.

Hence, the value of B becomes $\mu_0 \cdot I/2\pi r$, assuming the length of element is infinite. Then the

integration of B for the single loop of current circuit is derived [103]:

$$\int B dl = \mu_0 \cdot I \quad (3.2)$$

According to Stokes' theorem to integrate B of differential forms, the static magnetic field is introduced by the supplied current density J , known as Ampere's Law [104]:

$$\nabla \cdot B = \mu_0 \cdot J \quad (3.3)$$

At the same time, the time-varying current in the conductor certainly induces the fluctuating magnetic flux. Following the same procedure, the dynamic magnetic field is given [105]:

$$\nabla \cdot B = \varepsilon_0 \cdot \mu_0 \frac{\partial E}{\partial t} \quad (3.4)$$

where ε_0 is the dielectric constant of permittivity in the media and E is the electric field vector. The pulsing source supplies the initial magnetic field in the transmitter structure, thus motivating the eddy current within a conductor. Subsequently, the eddy current produces a secondary magnetic field surrounding the coil. Therefore, it is suggested that the eddy current as the electrical source that changes with time determines the density of a new-emerged magnetic field.

It is known that the measurement of magnetic flux ϕ is basically the product of the perpendicular magnetic vector B and pass-through area S . Then the electromotive force EMF is defined in conjunction with the Faraday's law of induction:

$$EMF = -\frac{d\phi}{dt} = -\frac{d}{dt} \int B dS \quad (3.5)$$

In principle, the induced electromotive force is the line integral of the electric field strength in the closed circuit. For the similar purpose, Stokes' theorem integrates the line of the electric field strength into the surface area, which is described by Maxwell's equation:

$$\nabla \cdot E = -\frac{\partial B}{\partial t} \quad (3.6)$$

From these fundamental equations, the magnitude of induced current primarily depends upon the external environment of a time-varying magnetic field [106]. For the receiving circuit, the

variation rate of a secondary magnetic field, developed by the eddy current, decides the strength of induced electric current in the coil. Overall, the value of eddy current within a conductive object decides the strength of nearby magnetic flux, eventually determining the induced current electrical force that charges the coil.

As the induced response appears at the coil, the reflected current increases rapidly for the instantaneous charging then it decays gradually to release the electromagnetic field. As a matter of fact, reflected electrical current successively charge and discharge the coil, which is equivalent to the coupling of an inductor and a resistor. The induced current as the only source supplies the coil initially, while the decay begins at the peak of inductance without any power input. The mode of resistor-inductor (RL) circuit with a zero input defines the decay duration of the induced response [107]:

$$\begin{aligned} i(t) &= I \times e^{-\frac{t}{\tau}} \\ \tau &= \frac{L}{R} \end{aligned} \tag{3.7}$$

where I is the initial value of current and τ is the time constant that is quotient of the inductance L and resistance R .

The characteristic of a target regarding resistance and inductance, coupled with the coil, mainly decides the time constant to reflect the steepness of exponential decay [108]. In brief, the feature of a specific object determines the inductivity and resistivity, resulting in a unique declined signature during the discharge of induced current.

3.2 Simulation analysis

As stated in section 3.1, the characteristics of different conductive objects determine the pattern of a reflected signature of inductance. The COMSOL simulation software delivers the Integrated development environment and workflow for engineering and manufacturing model design and process analysis [109]. The electromagnetic functionality module addresses the signature result analysis for the electromagnetic induction regarding the variable conductive targets.

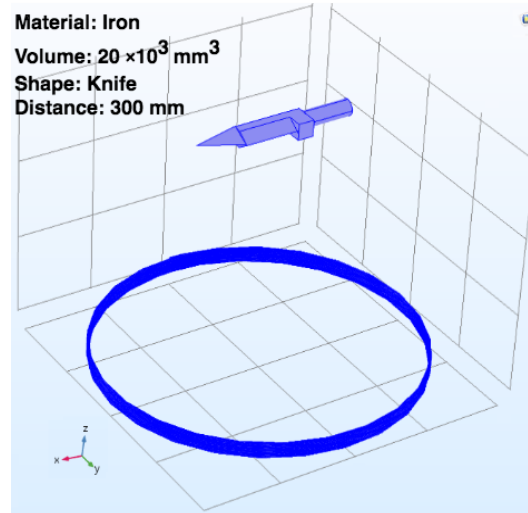


Figure 3.4: COMSOL based model simulation for a knife

To evaluate the features of induced signal response, the COMSOL software simulation are conducted with one target parameter change per series (material, shape, size and distance), ensuring the other parameters constant in Figure 3.4. Hence, the simulation is used to measure the electromagnetic force of induced response when evaluating the change of the specific parameters individually.

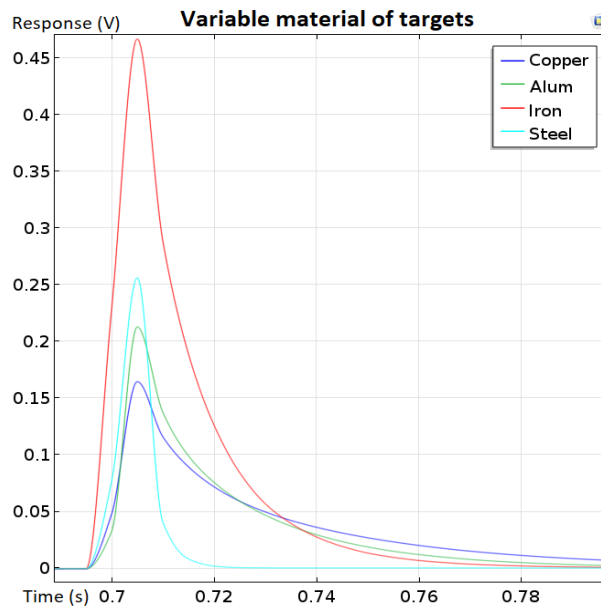


Figure 3.5: Response simulation with variable parameter of material

First of all, the respective materials of targets are simulated to differentiate the induced signature shown, while other parameters of size, shape and distance, are constant in Figure 3.5 [130]. The inductance of iron is evidently identified with the prominent peak point, indicating the high

strength of response. In contrast to copper with an extended decay duration, the induced signature of steel target reduced promptly due to the relative permittivity and permeability of material [110].

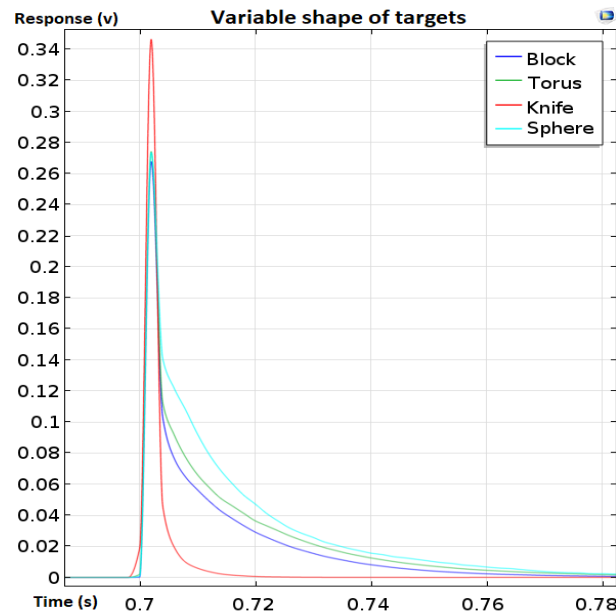


Figure 3.6: Response simulation with variable parameter of shape

The variable object simulation distinguishes the induced results from the regular shapes of a block, a sphere and torus, compared with a knife, where the material is iron, and the volume is fixed in Figure 3.6. The reflected signature of a knife gives a considerable peak value for the irregular figure while the other items remain at the same point at peak. Besides, the sphere or torus shape of the component, by contrast, declines at a slower rate for the larger surface.

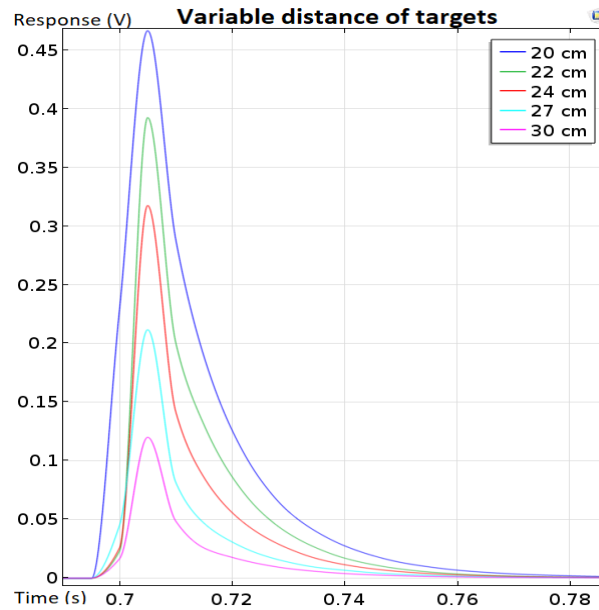


Figure 3.7: Response simulation with variable parameter of distance

Figure 3.7 shows the following comparison of a target (fixed parameter values used) located at a different distance to the sensor coil [130]. As the distance varied, the decay stage remains at the same pace of decline. Whereas the closer distance results in the enhancement of inductance, presenting the significant peak change. The final step operates the altered sizes of a cube-shaped object; as seen in Figure 3.8, the large volume of a target produces a strengthened inductance, increasing the peak value and prolonging the decay duration.

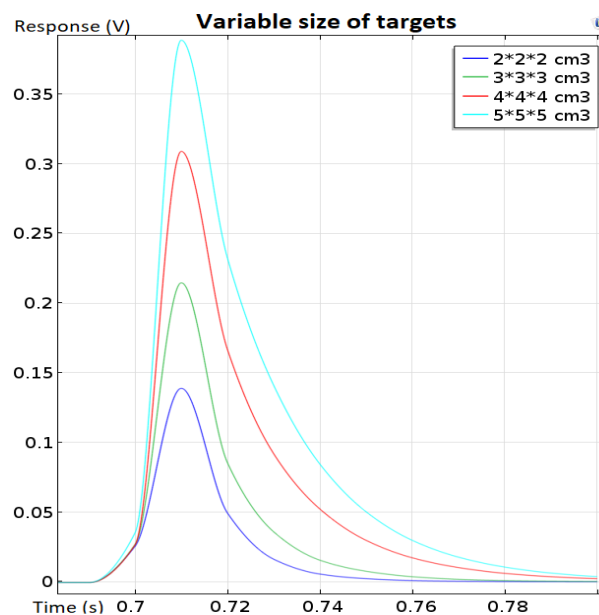


Figure 3.8: Response simulation with variable parameter of size

In general, the classification of simulated targets defines the peak value and decay stage as the significant features between different events of induced response. Consequently, the characteristic of a target can decide the peak and decay duration of induced response and vice versa.

To conclude, the induced response signature realizes the specific features description for a detected object in terms of material, shape, size and distance. The peak value reflects the induced strength from a conductive object, and the decline change of a decaying signature determines the parameter characteristics. Therefore, the response analysis based on the peak and decay periods requires the signal modulation processing to significantly identify the target characteristics.

3.3 Sigma-Delta modulation

The digitalization of the analogue signature over a wide range of frequencies typically adopts the sigma-delta ($\Sigma\Delta$) modulation technique. At the same time, it effectively generates a high-resolution digital data sequence with low bits instead of high-bit words [111].

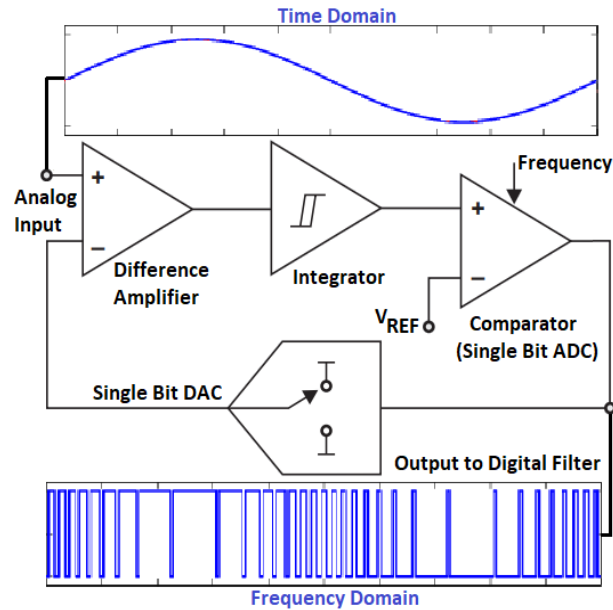


Figure 3.9: Sigma-Delta modulation

As illustrated in Figure 3.9 [112], the negative feedback provides the synchronous adjustment of quantization error, which benefits data conversion by reducing noise for high-speed operation [113] [114]. A subsequent decimation filter eliminates the undesired information, enabling data translation precision [115]. As the conversion completed, the distribution of signal 1 in the

binary waveform identifies the feature of introduced analogue input [116].

When the continuous variable is sampling and transformed into the discrete digital domain, the signal quantization inevitably encounters the undesirable errors derived from the analogue-to-digital conversion. The high-speed digital output with quantization noise requires the filtering function for data acquisition, avoiding noise interference. Therefore, the data modulation requires high integration and low consumption while challenges the signal-to-noise conversion by the high resolution.

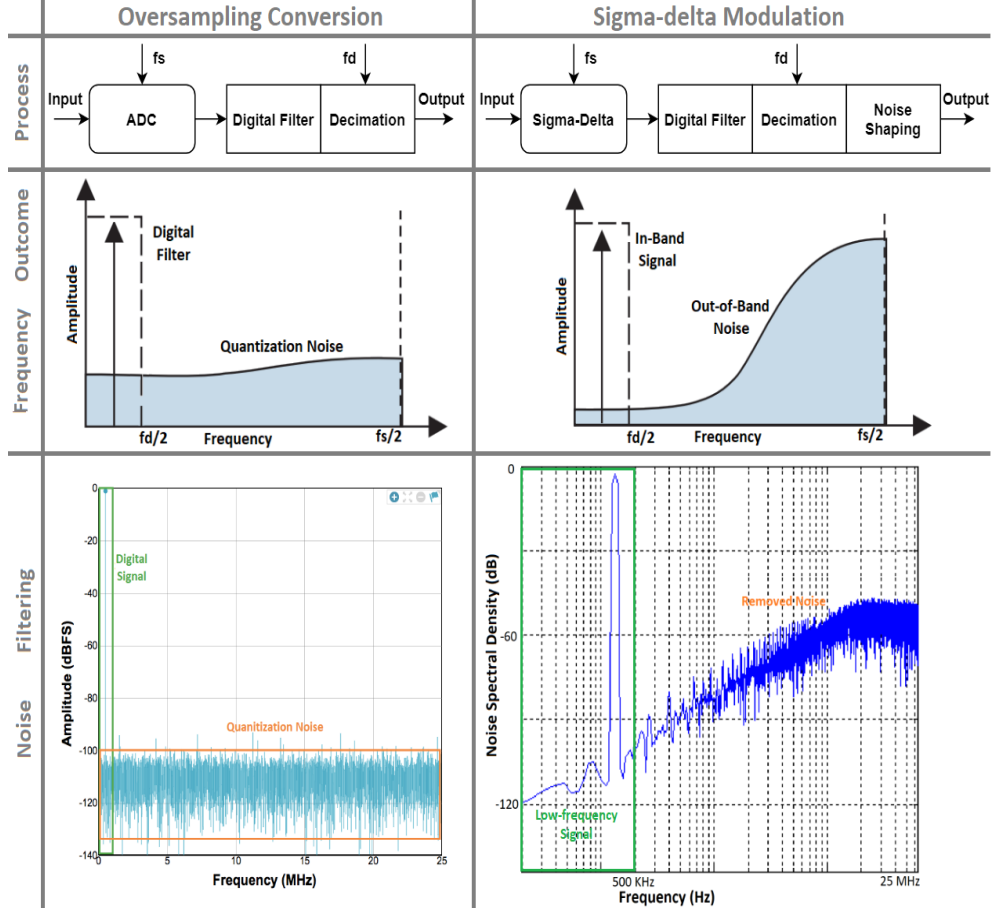


Figure 3.10: Oversampling and sigma-delta conversion. Redrawn based on [Fujcik, 2016][120]

The functions of digital and decimation filters offer the oversampling to the digital samples from ADC in Figure 3.10. The scenario extracts the signal information while the quantization noise affects the data reading and identification. Hence, the quantization process distributes the noise over the spectrum of f_s (sampling frequency) $/2$, term as Nyquist band, as the finite discrete states sampled. For the digital result sampling, the oversampling model faces the difficulty to decrease the impact of the quantization noise within the reading range of digital filtering data, regarded as f_d (out-data rate) $/2$. The rapid fluctuations in the low-frequency conversion

interfere with the digital sampling in an undesirable manner. Therefore, identifying signal characteristics is vulnerable to noise disturbances, resulting in information loss and resultant deviation.

The sigma-delta modulator provides the noise shaping function to remove the quantization noise based on the traditional analogue-to-digital conversion. The digital signal, required to read, is generated within the in-band frequency. Meanwhile, the quantization noise is transformed to migrate at the high-frequency range so that the low-pass filter extracts the digital signal with the noise-free mode. Therefore, the sigma-delta model reaches the low noise rate for data acquisition at low frequency.

3.4 Summary

The multi-sensor structure facilitates a simultaneous detection system to identify and locate a threat target transferred in an uncontrolled sequence of visitors. The arrangement of arrayed sensors, deployed under the foundation of the surveillance zone, benefits the weapon alarm without the limitation of sequenced access. The cooperation of individual sensor also contributes to the dynamic display of the moving path of a passenger who carries the weapons. To sum up, the sensor network addresses real-time weapon detection to monitor the security of an open area.

The PI approach applied in the single detector contributes to a practical weapon detection technique to characterize the induced response rather than contact or image a target. Unlike the conventional methods susceptible to environmental change, the PI technique with high-performance recognition provides a considerable detection distance and range for human inspection at an open area. Hence, the PI solution benefits the signature-based detection scheme due to the contact-free and accuracy-control procedure.

The electromagnetic induction equations explain the interaction of electric waves and magnetic fields based on the detection structure. For the charging process, the eddy current of a conductive target determines the strength of the magnetic flux, resulting in the induced current quantity. The discharge procedure demonstrates a unique decaying signature for a specific object. Therefore, the mathematical formula can clarify the principle of electromagnetic inductance charge and discharge.

The simulated analysis of specific parameters of targets illustrates the featured changes of

induced signal response, associated with the peak point and decay stage. By comparing different cases of detections, it is suggested that the description of peak value and a decaying curve is feasible to characterize the material, size, shape and distance of a target. In summary, the peak point and decaying figure serve as the decisive criterion to discriminate the characteristics of a detected target.

In the following chapter, the project gives the overall organization and primary frame of the detection system according to the response signal processing and analysis. As the characteristics of the sensing signal defined, the following section specifies the basic structure of the system design scheme to address the sampling data and investigate the result.

The system applies the sigma-delta modulation to digitalize the analogue induced response, providing the simplified sequential outcome for data sampling and processing. It also reduces the quantization noise at the system frequency to filter the digital results, describing the analogue signature for the target features recognition. However, the sigma-delta modulating application advances the data conversion and simplification for the digital result analysis in the object identification stage.

The experimental procedures are defined to acquire the analogue signal, process the digital data and optimize the object identification based on the scheme arrangement. Simultaneously, the project applies the verification method to demonstrate the functional modules for practical applications. For the comprehensive functions, the achievements of modules are identified to solve the signal processing and analysis at the individual stage. The next chapter gives the definite objectives for functional components to realize systematic functionality.

Chapter 4

Weapon Detection System Development

The basic architecture of the weapon detection system based on data analysis of the electromagnetic response on the FPGA platform is introduced. The design structure involves the practical experiment and simulation investigation to identify the characteristics of concealed targets.

4.1 Overall structure

The CWD scheme is designed to analyse the characteristic of analogue received signature, simplified as the noted digital samples, to identify the hidden threatening objects, replacing the manual imaging procedure. In order to develop and verify the system design, the overall framework is scheduled as a practical operation to accomplish the identification and classification depending on the serial digital outputs and simulation procedure to confirm the feasibility and effectiveness of the method applied in the CWD system.

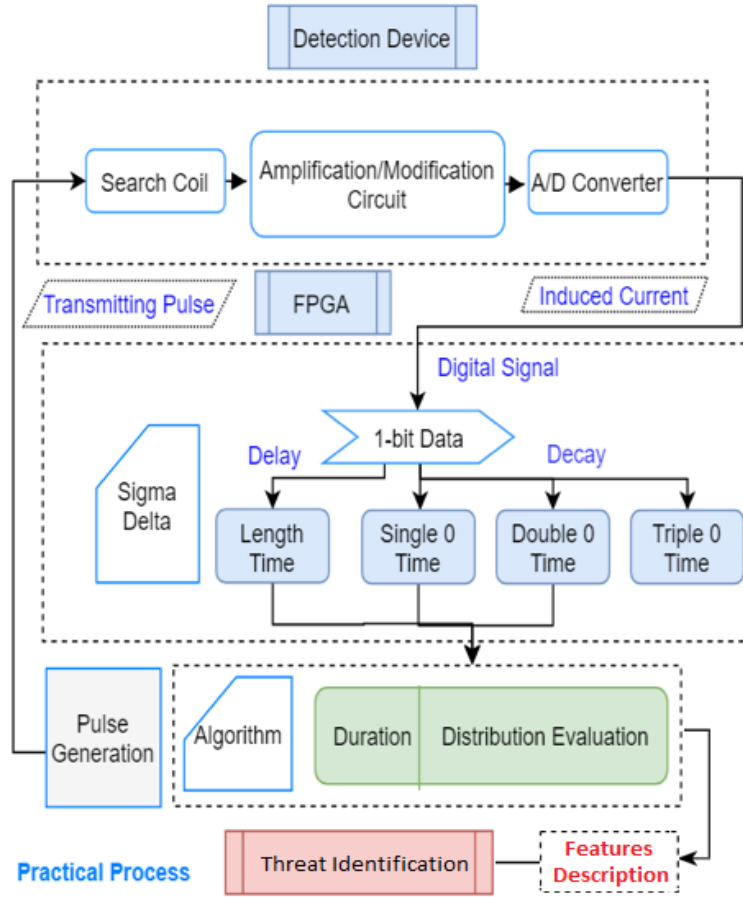


Figure 4.1: Detection system structure for practical processing

The practical structure schemes based on the experimental device include sensing coil, circuit, and the processing programme on the FPGA in Figure 4.1. The onboard programme firstly generates the repeated electronic pulse into the search coil for transmitting. Once the received signature reaches the analogue circuit, the device conducts amplification and modification, then prepares for conversion to digital data. For FPGA processing, the sigma-delta modulation is implemented to simplify the output into a single bit digital flow. The time recorded at the different points is collected to reflect the characteristics of the induced signature, and thus the features of threat targets are distinguished and considered as the potential weapons.

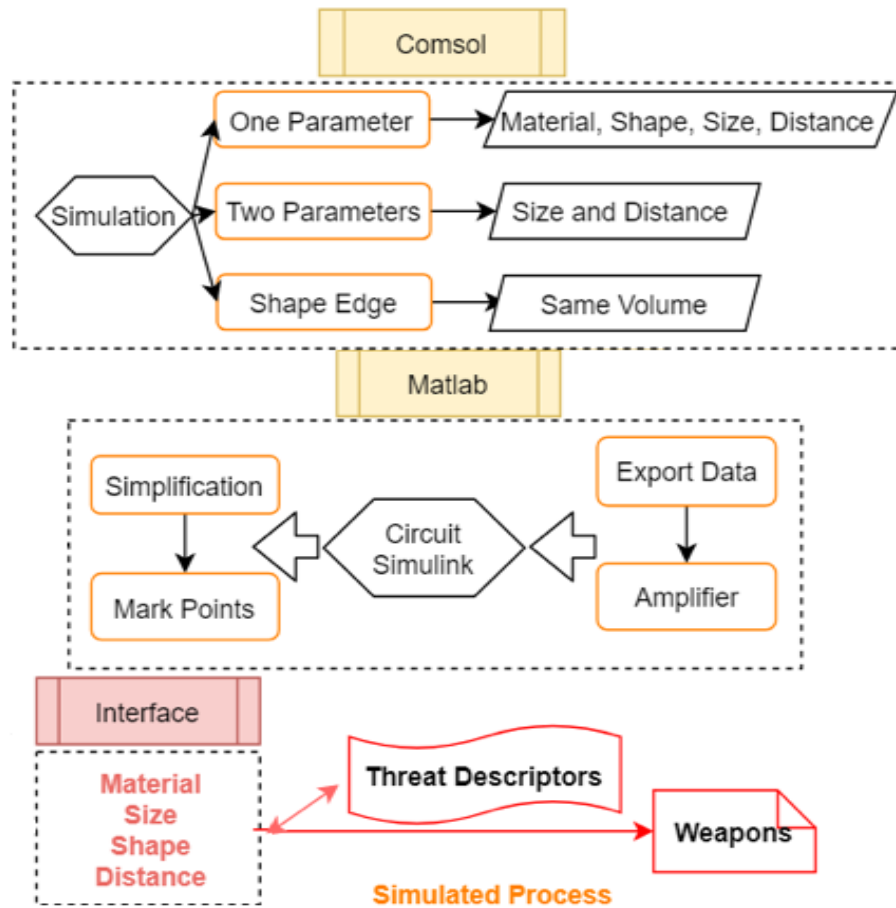


Figure 4.2: Detection system structure for simulation processing

The primary step for the simulation procedure is to obtain the simulated result of different cases and imitate the practical process of data simplification and threat object recognition in Figure 4.2. The simulation with varied parameters is initially achieved to determine the influence on the induced response. At the next stage, the analogue signature is exported into the MATLAB platform for further adjustment. The sigma-delta method is processed via a simulated circuit, and the mark points are eventually measured based on the simplified single-digit flow.

Furthermore, the same issue of changed sharpness on edge is separately operated by practical and simulated procedure, whereby the connection of two modules achieves the verification of practicability and performance of the proposed algorithm in the detection system.

4.2 Detection device scheme

The design and development of a weapon detection system in terms of the hardware device scheme, the processing program on FPGA and the object identification technique, as seen in Figure 4.3 [129], is presented. Firstly, the proposed weapon detection system supplies pulses to a search coil while the detection device collects the induced responses from the target object. The circuit scheme transfers and adjusts the electromagnetic signature before the conversion translates the analogue to the digital domain for data processing. The program design on the FPGA platform engages in digital data simplification and classification, and characterisation of the sensed object signal. The implemented module of the weapon identification determines the characteristics of detected objects so that the interface will ultimately deliver the description of a potential threat item.

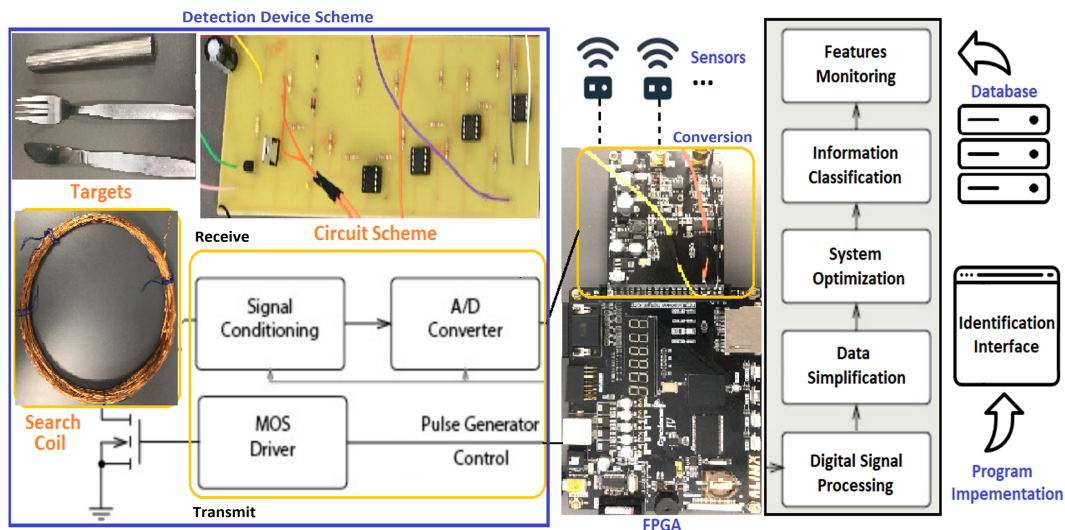


Figure 4.3: Fundamental structure of detection scheme

For the hardware-based framework, the system acquires the pulse to drive the transmission, while the receiver antenna obtains the induced response from a detected target. Hence, a search coil serves as both the driver and sensor to construct the electromagnetic generation and induction environment. Initially, a pulse signal is required to produced and applied to the loaded on the search coil in order to develop a time-varying electromagnetic field in the transmit mode. Correspondingly, the arrived response from the search coil is configured to amplify and amend the information with the purpose of digital processing. The experimental apparatus requires the electrical circuit interfacing with an FPGA platform for the signature treatment procedure. Therefore, the detection device structurally consists of the search coil for signal excitation and

collection, a dedicated circuit of amplification and adjustment stages for analogue processing.

4.2.1 Search coil

The detection scheme, using a PI technique, requires a continuous electrical pulse as the supply source through a coiled wire, which results in a magnetic field being generated. As the conductive item/s within the magnetic field alter the behaviour of magnetic flux, the subsequent coil received induced response in the opposite direction. Therefore, the single search coil servers as both transmitter and receiver, in this work, constructing the magnetic field and detecting the induced response.

The geometrical design of circuit conductors regarding the winding structure significantly influences the inductance of the coil for electromagnetic field interaction [117]. The project develops the electrical pulses through the search coil that acts as the induction excitation to load the magnetic field. Therefore, the inductance L of a multi-layer coil within an air core in this work determines the strength of magnetic flux and induced electric current, given by Wheeler approximation [118]:

$$L = \frac{0.8 \times a^2 \times N^2}{(6 \times a) + (9 \times l) + (10 \times c)} \quad (4.1)$$

Where N and l are the total turns and length of the coil respectively, a is the average winding radius, and c represents the difference between outside and inside coil radius.

From equation 4.1, increasing the total turns enhances the inductance of a coil, strengthening the magnetic field and sense of the induced current from the conductive object at the receiver. The detection range is extended as the coil diameter increased, whereas the identification sensitivity for small targets inversely decreases. That is because the reduced inductance weakens the surrounding magnetic field with the same electrical source. Therefore, the design of the coil decides the value of inductance in consideration of the detection sensitivity and range. The winding turns and coil diameter are increased in this project to realize the strengthened induced response at the practical detection range for the required target testing, as the parameters listed below [119].

Table 4.1: Search coil parameters

| Coil Parameter | Number of Turns | Diameter of Wire | Diameter of Coil |
|----------------|-----------------|------------------------|------------------|
| Search Coil | 20 | 0.5 mm | 400 mm |
| Resistance | Inductance | Conductivity | Material |
| 1.6 | 300 μ H | 5.88×10^7 s/m | Copper |

4.2.2 Circuit scheme

For the transmitter, the primary circuit switches the power to introduces the pulse current flowing through the coil, driving the alternating magnetic field in Figure 4.4. As the signal induced from a target, the first stage of receive scheme amplifies the analogue signal for the accurate distinction. The modification stage removes the initial pulse to highlight the induced response. The following adjustment intends to adapt the analogue signal correspondent within the input range of the conversion processing further. Therefore, the requirement of circuit design involves pulse generation, analogue signature amplification and signal modification.

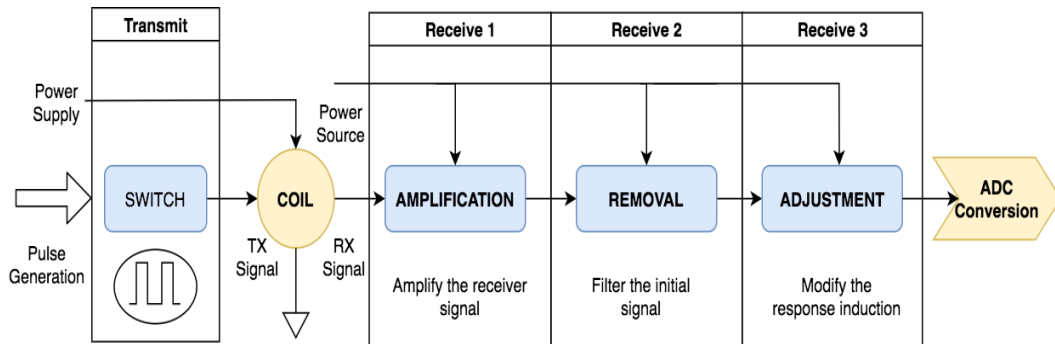


Figure 4.4: Analog circuit design

Pulse generation

The pulse generation intends to produce a continuous pulse signal with the required transmitting frequencies to drive the alternating magnetic field. As the initial power supplied on the board, the pulse generation scheme manages the output signal to provide the pulse frequencies via the MOSFET. The MOSFET is considered as a switch controlling the behaviour of the load circuit to generate the pulse sequence, as the low-voltage input required. Primarily, the MOSFET switch provides a considerable switching speed to manage the frequency of transmitting pulse on the search coil.

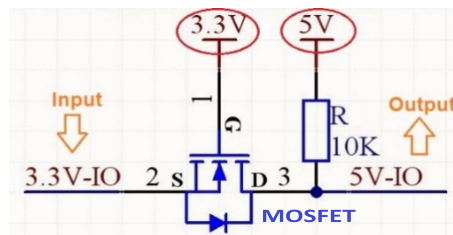


Figure 4.5: MOSFET conversion 3.3 V and 5 V

The experiment practically introduces the input source from the FPGA board that reaches 3.3 V. On the other hand, the typical MOSFET at the gate threshold of 5 V can drive a high-load circuit. Hence, the preceding conversion, in Figure 4.5, employs a small signal MOSFET that switches low-current input of 3.3 V into 5 V. Compared with the low-level power at 3.3 V, the input voltage launches the closure of the circuit so that the reference power directly supplies the output terminal at 5 V. MOSFET switches the pulse off to present the rapid decline at the falling edge that introduces the magnetic field immediately. Then, the PI technology can receive the induced response through the search coil after the initial pulse ends. The system gives the frequency of transmitting pulse (hundreds of Hz) to present the clear decaying response signature and avoids the pulse distortion based on the MOSFET design.

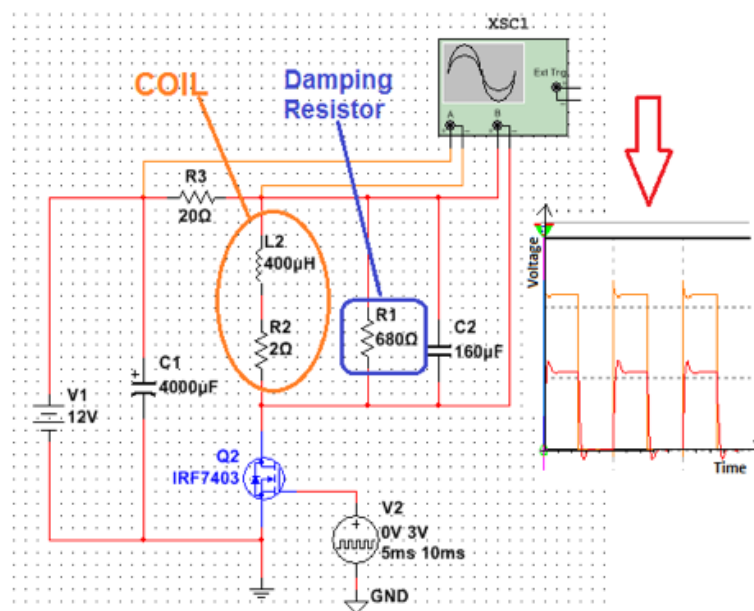


Figure 4.6: Pulse generation block

From Figure 4.6, the gate voltage of a short input pulse drives the connection of power supply and coil. On the contrary, no supplied power disconnects the closed circuit. Accordingly, the input pulse triggers MOSFET, located in series with the power supply and coil. The result

shows that circuit actually amplifies the voltage of introduced current through the coil.

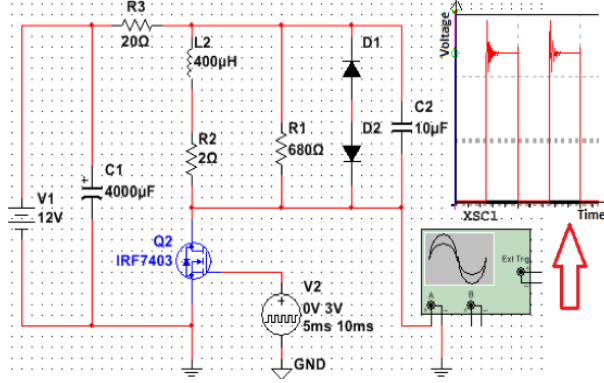


Figure 4.7: Improved pulse generation block

The developed structure of two Zener diodes (D1 and D2) paralleling the damping resistor (R1) and coil eliminates the burr that appeared at the declining edge of the pulse. Despite the alternating current introduced around the coil, the Zener diodes provide the stable voltage and avoid the overload to protect the circuit. Figure 4.7 shows that the distinct outcome occurs at the falling edge of the pulse without disturbing noise.

The pulse generation circuit achieves the introduced pulse with considerable electrical force supplying the search coil that can develop a powerful magnetic field. It also distinctly improves the pulse formation, avoiding interfered spike at the decline edge.

Signal amplification

When the induced response lands after the shutoff of the transmitting pulse, the receiver circuit should amplify the analogue signature to observe the difference between cases significantly. The signal amplification decides to outstand the variation of the base, effectively representing the feature of analogue induction.

The circuit implements the amplifier (LM358N) to establish the construction of two-stage amplification. The design decides the achievement of ten times amplification for each stage, so the individual scheme is identified based on the function of inverting operational amplifier [120].

$$V_{out} = A_{ol}(V1 - V2) \quad (4.2)$$

Where A_{ol} is the gain of no-feedback amplification, $V1$ and $V2$ mean the non-inverting and inverting input respectively, and V_{out} is the output voltage.

The current access the input resister (R1) through the negative pin, which equals the current travelling through the feedback resistor (R2) to output.

$$\frac{V_2 - V_{in}}{R_1} = \frac{V_{out} - V_2}{R_2} \quad (4.3)$$

Combining Eq and Eq, the gain of the inverting operational amplifier G is inferred:

$$G = \frac{V_{out}}{V_{in}} = -\frac{A_{ol} \cdot R_2}{R_1 + R_2 + A_{ol} \cdot R_1} \quad (4.4)$$

Where A_{ol} is considered as the infinitely great ($A_{ol} \rightarrow \infty$). The gain can be ideally represented:

$$G = -\frac{R_2}{R_1} \quad (4.5)$$

The resistor design at the input and feedback arrangements decides the magnification of output voltage in the circuit loop. The circuit design suggests that the inputting current accesses an input resister of 1 K to the negative pin of an amplifier. Simultaneously, the output connected with a feedback resistor of 10 K offers the feedback to the input terminal. Hence, the amplifier magnifies the received signature ten times and reverse it at each stage. After inverting operational amplification twice, the two-stage amplification can magnify the induced signature 100 times without inverting the direction of input voltage.

Signature adjustment

The required operation selects the section of an induced waveform from the amplified signature and then adjusts the voltage within the input range of the following ADC processing. The amplified result involves the introduced pulse and acquired induction response due to the transmitter and receiver sharing the coil. To demonstrate the induced response solely, the active filter selects the responding result at the range of higher voltage. Fundamentally, the entire waveform subtracts the given voltage to offset the initial pulse.

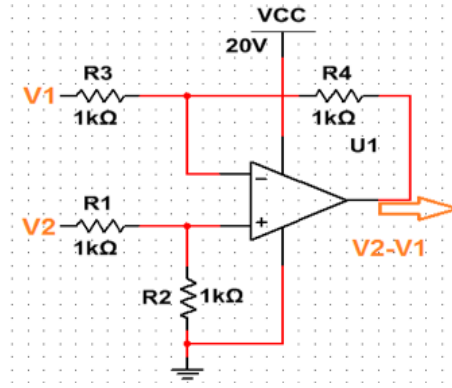


Figure 4.8: Differential amplifier building block

The differential amplifier, in Figure 4.8, generates the difference between the two inputs ($V1$ and $V2$) by a negative feedback loop. the output voltage is calculated based on the circuit transfer function using the superposition theorem [121]:

$$V_{out} = \frac{R1 + R4}{R1} \left(V2 \frac{R3}{R2 + R3} - V1 \frac{R4}{R1 + R4} \right) \quad (4.6)$$

The design provides the same value for all resistors ($R1=R2=R3=R4$), so the equation is simplified that the output voltage is the difference between inverting $V1$ and non-inverting $V2$. Consequently, the subtraction of given voltage from the landed signature leaves the induced response that is only a result for display.

The next operation adjusts the induced current within the range from -5 V to 5 V, the input scope of the FPGA module for data transformation. As the inverting terminal connected to 5 V, the same differential amplifier is placed to shift the voltage down. Hence, the adjustment of induced response achieves the scope requirement of FPGA input signals.

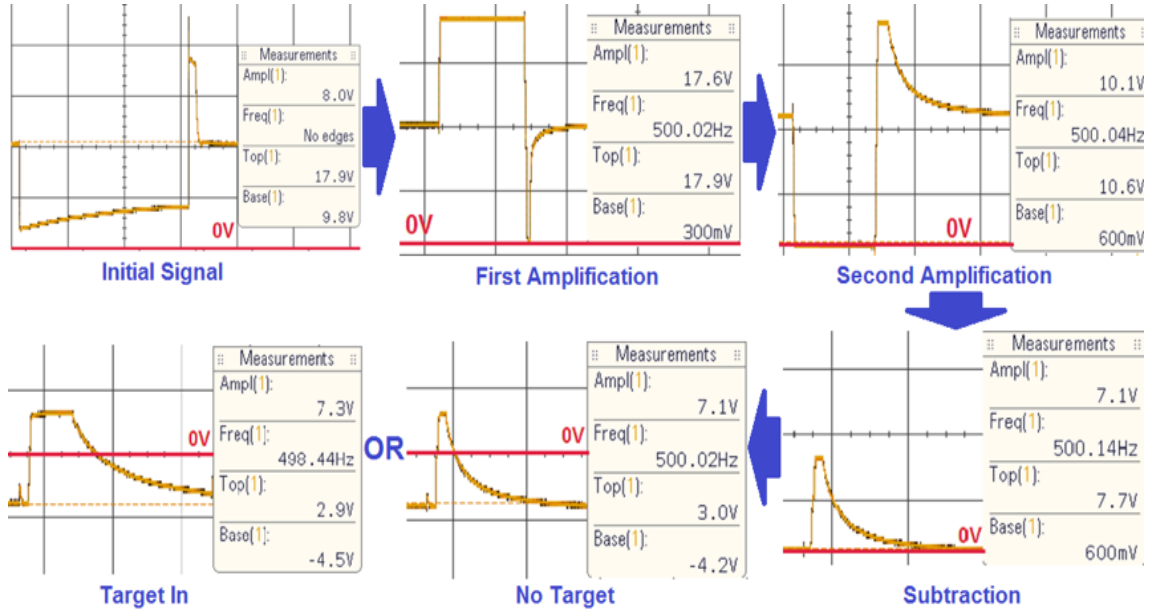


Figure 4.9: Results for amplification and adjustment

Figure 4.9 shows the individual result of the analogue signature sequentially at each step, as the testing frequency of 500 Hz provided for the clear signature processing. The two-stage amplification procedure magnifies the initial signal 100 times, reversing the direction twice concurrently. The subtractor selects the induced response at the higher range (10 V to 20 V) to remove the initial section of the pulse (0 to 10V). Eventually, the final result is modified at the range of -5 V and 5 V, preparing to introduce the FPGA board. Therefore, the extended period of the processed signature can experimentally reveal the appearance of a conductive target.

4.3 Response configuration

The analogue signal received of a target object induced response and the extended duration reflects the different detection of targets. The experimental scheme is required to store the results for targets and select the valuable information for analysis based on the elemental portions in the meantime. The essential sensed signature without any located targets is examined as the background because the conductive material of the coil inevitably produces the self-induction in the same circuit [122]. By comparing the background and practical targets, the experiment configuration is scheduled to present the precise result for the distinction of detected cases.

After collecting the experimental result, the typical approach divides the resultant signature according to the sampling period regarding the rise, delay and fall sections, The rapid increase

is defined as the rise section initially, and then the signature remains the high level at the delay duration. The following stage is the fall section once the signature starts to decline until the end, seen in Figure 4.10. Specifically, concerning the fall stage, the decaying signature is regularly divided into four plots dependent on the different declining levels.

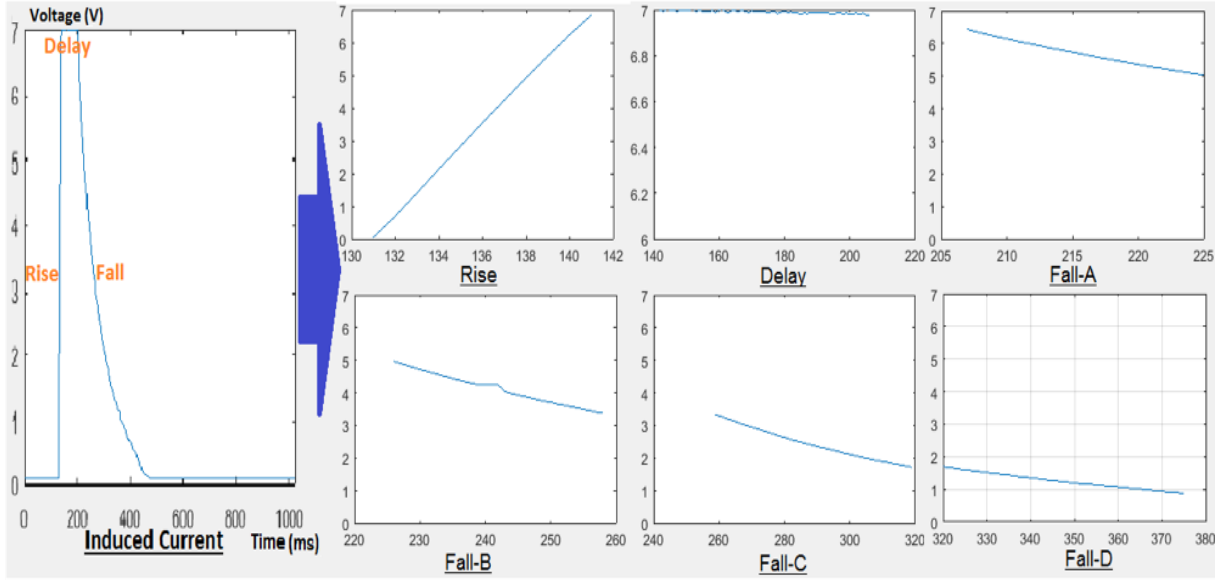


Figure 4.10: Record and division via MATLAB. Reproduced from [Yuxiang, 2018][129].

The distinct difference of extensive result provides the basis to distinguish the targets from the background efficiently. For the experimental scheme, the decreasing frequency of transmitting pulse contributes to the sufficient time for a conductor to fully absorb the electromagnetic force [123]. The consequence of expansion in analogue waveform results from the strengthened electromagnetic induction [124].

The experimental scheme distinguishes the induced responses of the practical testing objects to configure the frequency with different levels. Besides the slight fluctuation inherently from the analogue signature modification design, the deformation and noise emerge at the delay and decay periods at 200 Hz. As the frequency increased to 800 Hz, the signal difference becomes indistinct, leading to a reduced discrimination between the target object signatures in Figure 4.11. A frequency of 400 Hz exhibits the recognisable analogue results for the background and targets. Therefore, the experimental device equipped with configured frequency develops the identifiable difference between induced response, enhancing the accuracy of targets recognition.

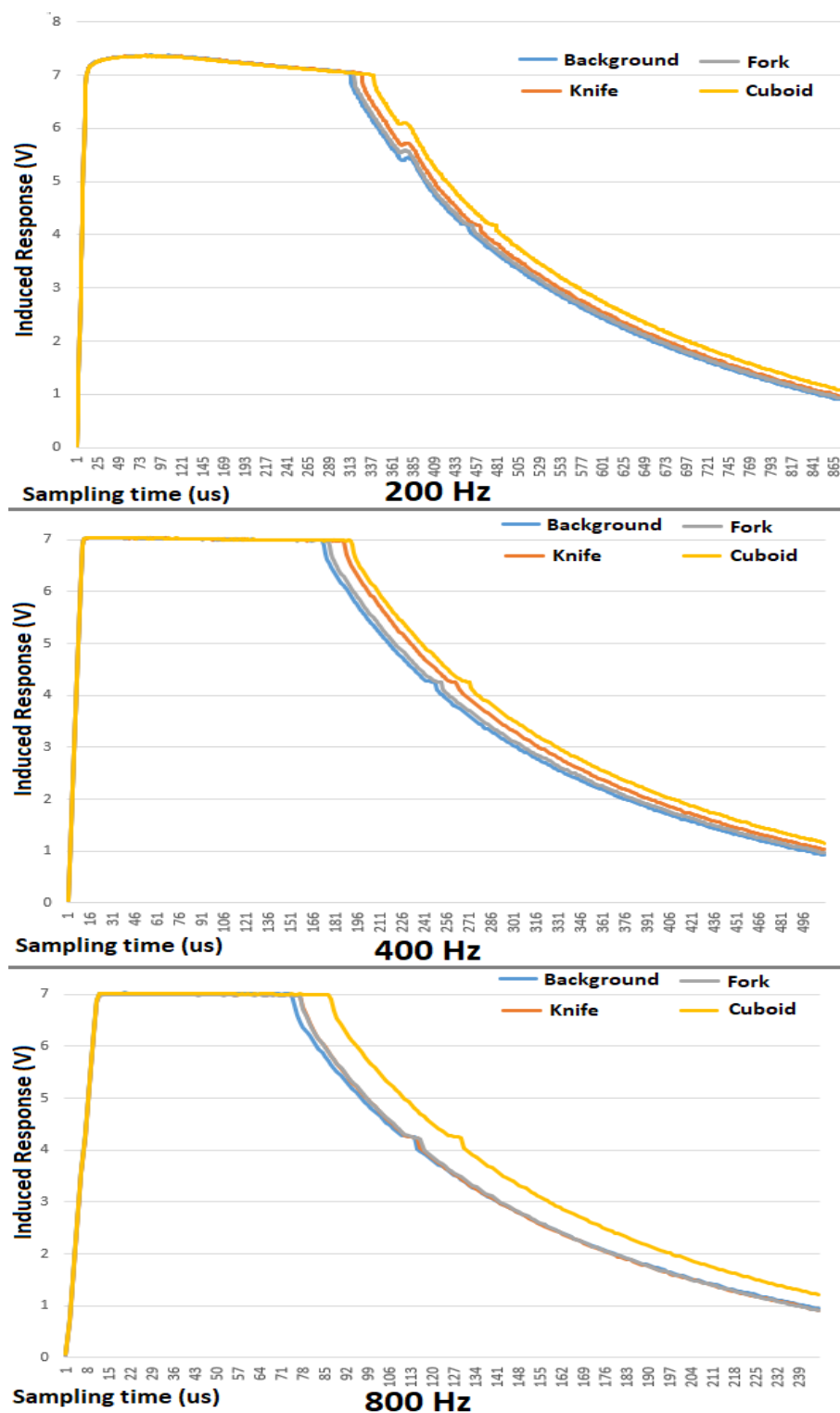


Figure 4.11: Distinction between targets and background in 200 Hz, 400 Hz and 800 Hz

4.4 Program design

The accomplishment of the experimental device is the collection and amendment of the induced response, and the configured scheme exhibits the recognizable analogue results. The following

onboard programming procedure requests the effective analysis method after the digital data conversion, including section division and data simplification.

4.4.1 ADC conversion

The essential operation translates the analogue signal from the circuit into the digital words, enabling the data analysis and processing on the FPGA platform. The resolution of the ADC converter to perform the binary data translation is relevant to the output pins standing for bit number. The project connects the expansion board of the ADC module with the main chip AD9226 to the platform. The additional capability of error correction reaches the high-speed data conversion date (65 MSPS) with 12-bit accuracy because of multistage differential pipelined architecture for error correction [125]. The digital conversion delivers the synchronous translation for the analogue changes of induced response, occupying the multiple bits to present the real-time sample.

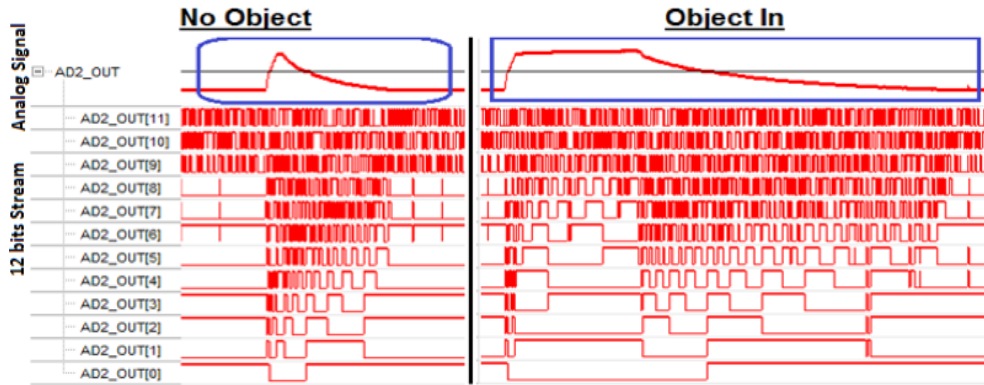


Figure 4.12: ADC conversion for object detection. Reproduced from [Yuxiang, 2018][129].

The landing of the analogue signature in the ADC module launches the digital translation at 12 channels simultaneously, sorting binary digits by low to high. According to the working clock, the induced information is converted into binary digital words distributed at 12 single-bit registers synchronously, no matter the background or targets in Figure 4.12. Therefore, the parallel digital data determines a unique analogue induced response, representing the characteristics of a target.

4.4.2 Section division

When the analogue result of induced response starts the digital data conversion after the collapse of the initial pulse, the system should divide it into sections to underline the signature

characteristics. The first period of rapid increase for the charge of induction, and then the signal remains the peak value at the delayed duration. The decay section gives a gradually decreasing trend over the extensive time, providing a recognizable feature.

The scheme applies the difference monitor design to define the sampling periods based on the response change, comparing the real-time variation to the prior sample. The difference within the accepted range barely affects the division of sections, resisting the slight fluctuation.

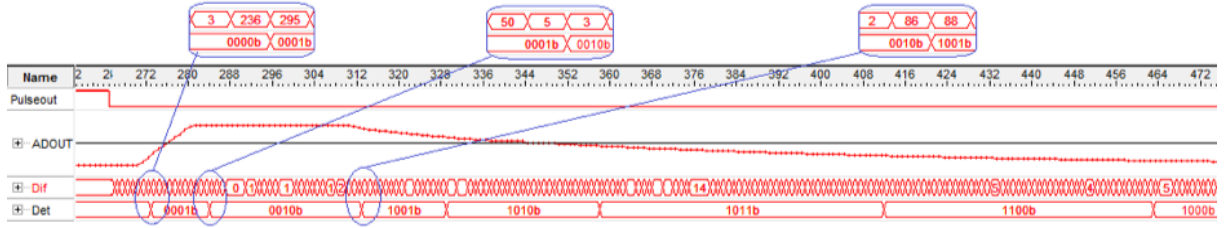


Figure 4.13: Difference monitor for the section division

The monitor initially detects the rapidly increasing difference from the previous sample that determines the beginning of the rise section in Figure 4.13. Afterwards, the delay duration appears once the difference returns to insignificance. The rapid change of difference occurs again regarded as the decay section, indicating the declining of signature.

As the detailed information acquired at the decay stage, the reference value decides the subsections for the division of a decaying signature. The classical method depends on the time-domain division concerning defaulted percentages of initial value as the reference. However, the noise, distortion and interference signal dramatically disturb the section division, hindering data analysis in each segment.

4.4.3 Data simplification

The digital data investigation with a 12-bit width requires powerful processors and massive space usage to handle the identification of induced responses. In the detection structure, the heavy task to analyse the 12 bits wide digital words excessively reduces the processing rate and occupies the storage memory. Hence, the data simplification employs the sigma-delta modulation to produce the reduced size of information, reflecting the analogue result of induction.

The program scheme can apply the $\Sigma\Delta$ structure to translate the time-varying induced response into a single bit sequenced wave for targets recognition. The time-domain analogue result is collected at the sampling clock, introduced to the programming arrangement of the $\Sigma\Delta$

modulation, including accumulation, comparison and quantisation.

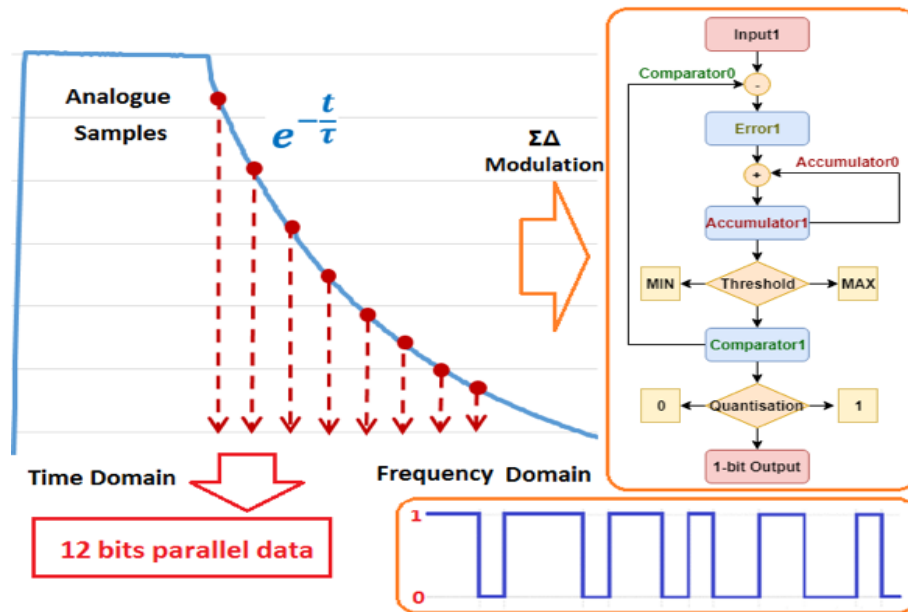


Figure 4.14: Sigma-Delta processing

Figure 4.14 shows that the frequency-domain data flow as the output result replaces the standard 12-bit parallel digital data. Therefore, the conversion to a sequenced binary word with frequency achieves the data simplification, featuring the analogue induced result varying over time.

The comparison of analogue results for experimental targets produces the corresponding single-bit digital sequence by the implemented $\Sigma\Delta$ programme, seen as in Figure 4.15.

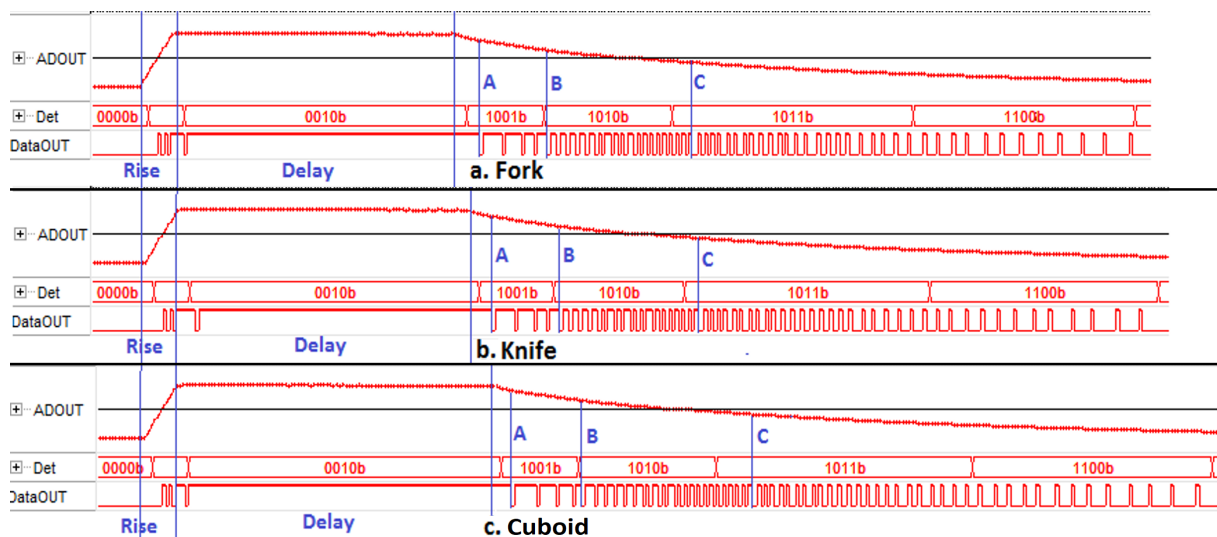


Figure 4.15: Binary sequence between background and targets after the $\Sigma\Delta$ module

When the induced response begins, the rapidly rising signal initially contributes to the presence of a high-level signal at the binary sequence. The single-bit output stays at a high level over

the ‘Delay’ stage due to the continuous analogue signal restricted at maximum. The decaying trend of analogue signal progressively reduces the density of high-level signal for the one-bit output, where the continuous signal 0 determines the decline stages of A, B and C. Therefore, the analysis of the single bit sequence identifies the unique induced response in the time domain, which describes the object detection.

4.4.4 Decay monitoring

The $\Sigma\Delta$ conversion produces the continuous high-level signal of extension at the delay section. By contrast, the distribution of low-level signal reflects the decaying response of different induction. Hence, the monitoring at the decay stage, depending on the variation of single-bit data flow, exhibits the significant identification of targets.

It is observed that the increasing duration of the high-level signal represents the time-varying change at the rising stage. On the contrary, the gradual reduction of a decaying waveform steadily expands the length of the low-level signal at the single-bit digital result. As the time increased at the decay stage, the one-bit data flow reaches the growing repeated signal of 0, such as single 0, double 0, triple 0. Accordingly, the length of continuous signal 0, which occurred at the first time, is considered as the mark point (A, B, C) to monitor the degree of signal attenuation at the decay phase.

Table 4.2: Marked points record from rise section (unit: μs). Reprinted from [Yuxiang, 2019]

| Mark Point | Fork | Knife | Cuboid |
|------------|------|-------|--------|
| A (0) | 104 | 106 | 113 |
| B (00) | 170 | 171 | 188 |
| C (000) | 206 | 219 | 234 |
| D (0000) | 238 | 249 | 269 |

The time points collected at the different length of low-level signal in Table 4.2 give the extensive times for inductive targets from the sampling beginning. However, the recorded times start from the emergence of induction, involving rise, delay and decay stages. For the significant identification of the decaying waveform, the collection of mark points begins at the end of delay duration, launching a declining trend for an induced response.

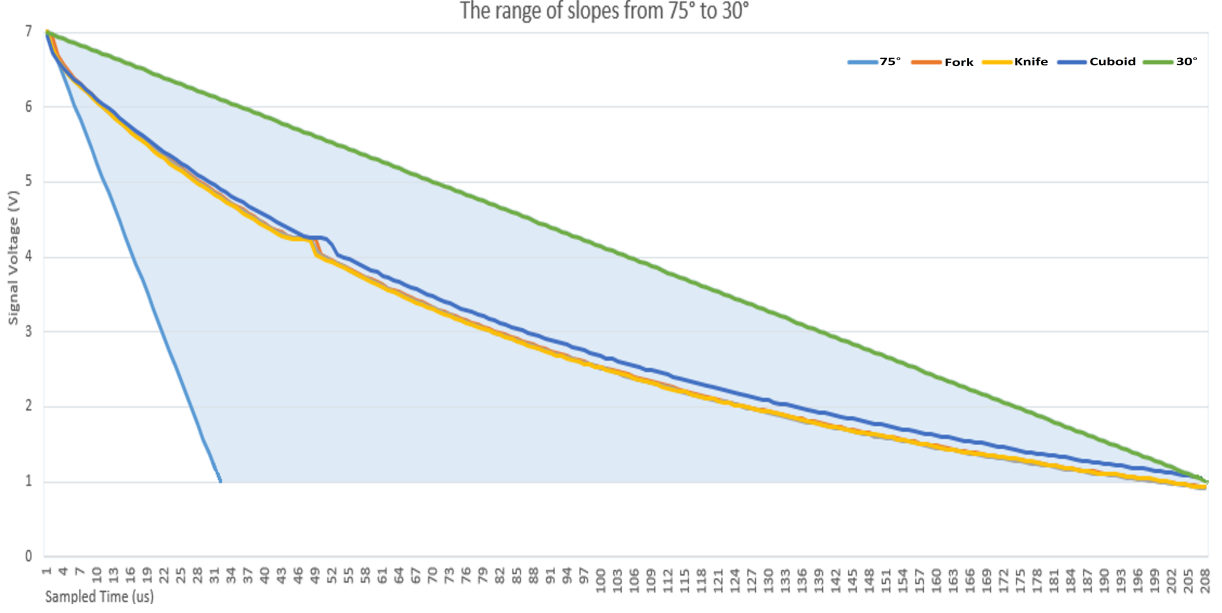


Figure 4.16: Range of slopes for the decay signal

To estimate the method capacity, the decline rate of a decaying signature gradually reduces, intuitively reflecting the degrees of slope at the waveform. The assumed area in Figure 4.16 over the slope range from 75° to 30° contains the entire decay phases of the background and targets, describing the decline variation rate. Afterwards, the method of collecting the mark points processes the analogue waveforms, as the slope progressively altered in the step of 5° .

Table 4.3: The statistics for the range of slopes (unit: μs)

| Mark Point | 75° | 70° | 65° | 60° | 55° | 50° | 45° | 40° | 35° | 30° |
|------------|------------|------------|------------|------------|------------|------------|------------|------------|------------|------------|
| A (0) | 5 | 6 | 7 | 7 | 8 | 9 | 10 | 11 | 12 | 13 |
| B (00) | 22 | 31 | 35 | 46 | 56 | 63 | 78 | 99 | 109 | 127 |
| C (000) | 25 | 38 | 46 | 58 | 64 | 79 | 98 | 110 | 139 | 164 |
| D (0000) | NA | 37 | 50 | NA | NA | NA | 106 | 125 | 151 | 179 |
| E (00000) | NA | NA | NA | 62 | 75 | 91 | NA | NA | 161 | 181 |

As demonstrated in Table 4.3, the early monitoring of single, double and triple 0 can efficiently discriminate the decline levels within the range of varied induction result. Nevertheless, the insufficient samples provided at four and five continuous signal 0 possibly lose the mark collections due to the limitation of the sampling clock. Hence, the experiment decides to monitor the first three lengths of low-level signal for response distinction, satisfactorily offering the valid mark points. Therefore, the collection of mark points is a feasible method to feature the decaying trend, distinguishing the characteristics of targets.

As the analysis step defined, the collected points at single 0 likely give the same level, influencing

the declining rate identification. Hence, the repeated results span the reduced slopes determining the distinction capacity. As a matter of fact, the lower slope offers an extended duration, so the particular analysis concentrates on the scope around the maximum and minimum of the assigned slopes respectively.

Table 4.4: Mark points around the maximal slope (unit: μs)

| Maximal Range | 72.5° | 73° | 74° | 75° | 76° | 77° | 78° | 79° |
|---------------|-------|-----|-----|-----|-----|-----|-----|-----|
| A (0) | 6 | 5 | 5 | 5 | 5 | 5 | 5 | 4 |
| B (00) | 27 | 25 | 24 | 22 | 21 | 20 | 18 | 17 |
| C (000) | 32 | 29 | 27 | 25 | 24 | 23 | 21 | 20 |

Table 4.5: Mark points around the minimal slope (unit: μs)

| Minimal Range | 27° | 27.5° | 28° | 29° | 30° | 31° | 32° | 32.5° |
|---------------|-----|-------|-----|-----|-----|-----|-----|-------|
| A (0) | 14 | 13 | 13 | 13 | 13 | 13 | 13 | 12 |
| B (00) | 145 | 142 | 137 | 131 | 127 | 125 | 123 | 111 |
| C (000) | 183 | 180 | 177 | 174 | 164 | 160 | 156 | 152 |

The same level at the single 0 extends the length of 6° around the maximal slope, as seen in Table 4.4. On the other hand, the result in Table 4.5 repeats the value for the span of 5° at the minimal range. At the same time, the record at the double and triple 0 avoids repetition of mark points. Therefore, the separate evaluation at the single 0 reaches the 5° to 6° distinction of decline slope, and it is developed in conjunction with double and triple 0, as a comprehensive measurement, to improve the identification of a decaying induced response.

4.5 Process simulation

The induced response for single parameter change gives the effective distinction at the decay duration for the data analysis. The simulation processing operates the induced result of the two simultaneous variation to define the decaying response as the unique target identification. As the single object parameter varied initially, the response identification depends on the distinguishing delay duration for the induction strength. To define the decaying change for result distinction, the study assessment develops the object model with two variable parameters of size and distance that results in the same peak value. Hence, the simulation processing conducts the variable size configuration of a target, allocated in the corresponding detection distance, to produce the similar induction strength. Nevertheless, the practice investigates the decay

duration for the target characteristics description.

Additionally, the variable edge of a target in the same volume brings the similar response alteration for the same induction strength. The simulation procedure models the same volume object with a varying edge to focus on the declining response for the detection case distinction. Therefore, the assessment processes the output results to examine the decay identification, featuring the edge changes of a target.

As the method defined, the simulation procedure operates the distinction between the specific cases, regarding the variation of two parameters and levels of sharp edge, by evaluating the mark points. The measurement proceeding initially amplifies the base of induced response once transferring the simulated data from COMSOL, as illustrated in Figure 4.17[130]. Based on a digital binary bit sequence via $\Sigma\Delta$ conversion, the record of mark points at the decay stage discriminates against the specific characteristics of a target.

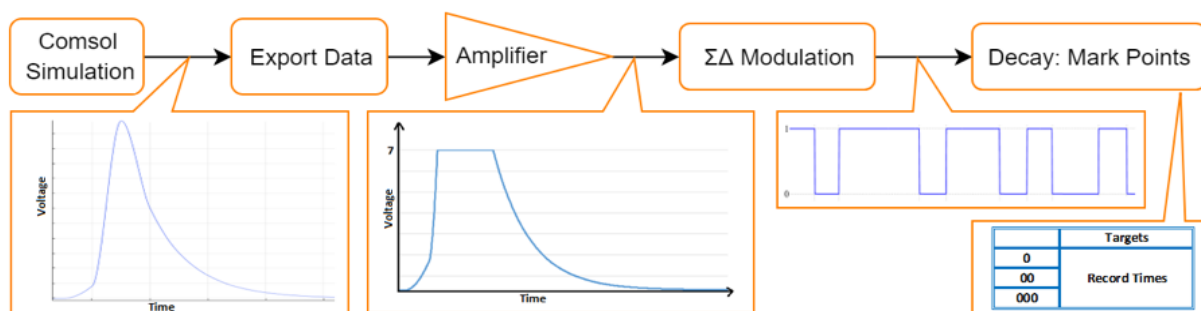


Figure 4.17: Measurement simulation procedure. Reproduced from [Yuxiang, 2019][130].

4.5.1 Two variable parameters

The exact strength of electromagnetic induction decides the similar response, resulting from the variable size of a target located at a different distance to the coil. Accordingly, the simulation conducts the two variable parameters of size and distance simultaneously attains the similar peak of induced response in Figure 4.18 [130]. As the amplification followed, the bottom section of the response is compared for specific cases.

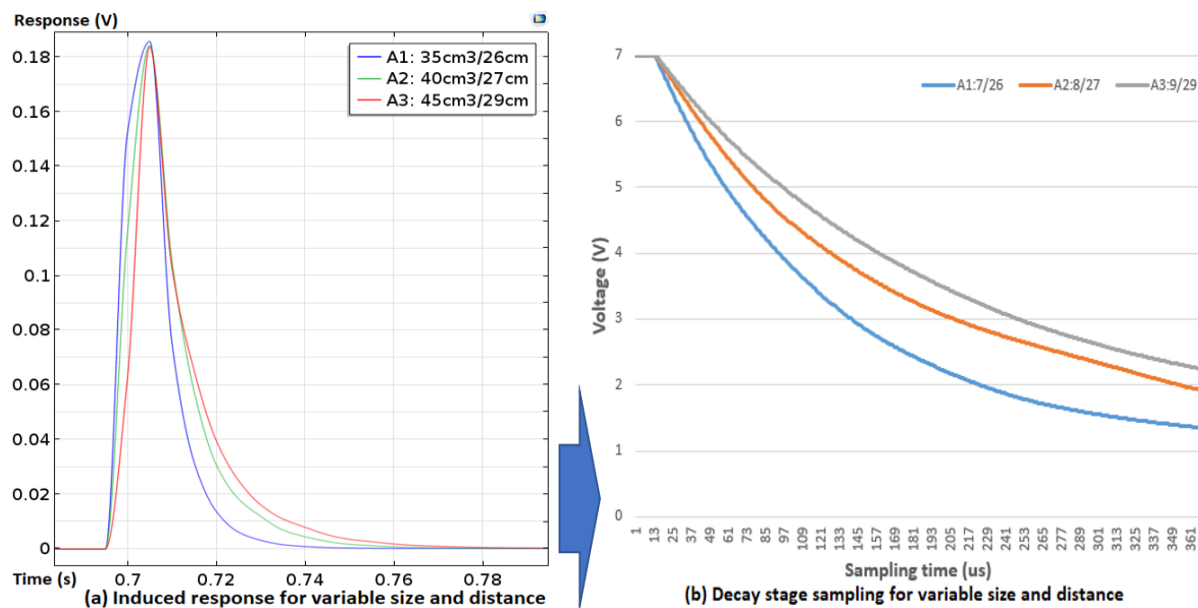


Figure 4.18: Analysis for two variable parameters

Despite the similar waveform with the same peak, the decline rate of a larger-sized object maintains slower over the decay duration. Hence, the analysis procedure measures the mark points to discriminate a larger size of the target, significantly providing the extensive results in Table 4.6.

Table 4.6: Record time for variable size and distance (unit: μs). Reprinted from [Yuxiang, 2019][130]

| Mark Point | $7 \times 3cm^3$ for 26cm | $8 \times 3cm^3$ for 27cm | $9 \times 3cm^3$ for 29cm |
|------------|---------------------------|---------------------------|---------------------------|
| A (0) | 11 | 14 | 15 |
| B (00) | 92 | 145 | 162 |
| C (000) | 151 | 212 | 257 |

4.5.2 Edge variable

The subsequent analysis simulation focuses on the levels of sharpness on the edge of targets, considered as the decisive criterion to identify a potential weapon. Figure 4.19 compares different degrees of pointedness at the base of response after magnifying and adjusting the induced signature [130].

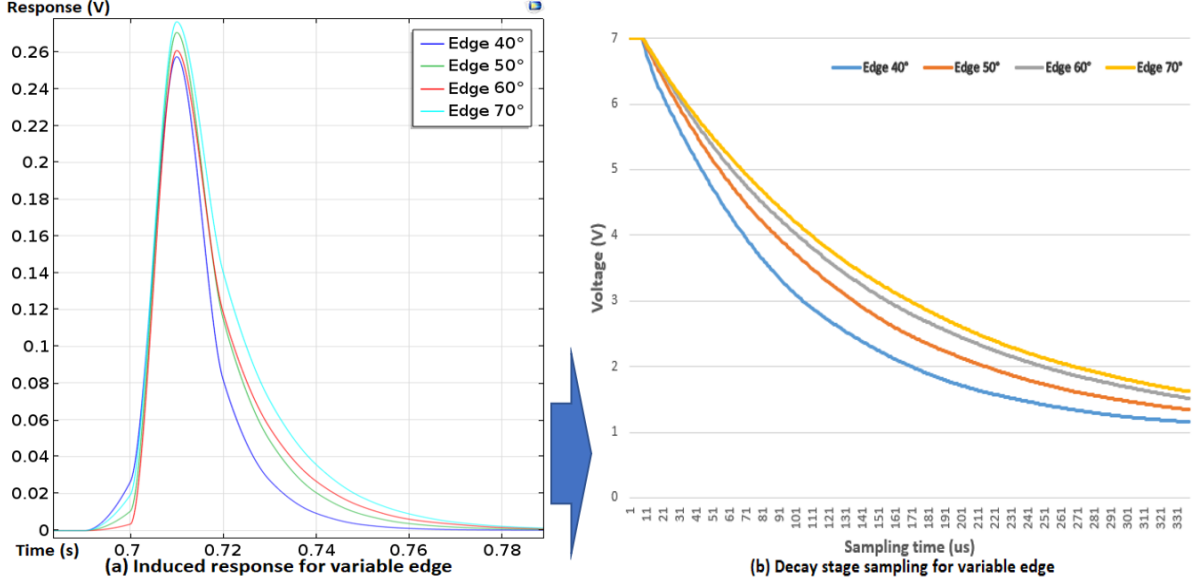


Figure 4.19: Analysis for shape edge

From the decaying result, a pointed edge of 40° features the rapid discharge speed of induced response while the release rate at the degree of 70° becomes slower. Despite the same value at single 0 in Table 4.7, the comprehensive measurement at the assigned time points can achieve the distinction between the different levels of a sharp edge.

Table 4.7: Record time for sharpness (unit: μs). Reprinted from [Yuxiang, 2019][130]

| Mark point | 40° | 50° | 60° | 70° |
|------------|------------|------------|------------|------------|
| A (0) | 11 | 13 | 15 | 17 |
| B (00) | 90 | 98 | 110 | 118 |
| C (000) | 118 | 136 | 165 | 174 |

4.6 Summary

The overall system structure mainly involves the analogue detection device, onboard processing programme and threat identification algorithm design regarding the practical and simulated development procedure. The project configures the experimental detection scheme to achieve the induced response processing and analysing based on the FPGA platform. Meanwhile, the procedure simulation verifies the system feasibility and practical performance, contributing to the object identification method development.

The basic detection device scheme firstly realizes the coil design for the transmitting pulse to supply the magnetic field and the induced response collection from conductive target detection.

The analogue circuit design delivers the pulse generation at the transmitting module, and then adjusts the received response for the digital conversion after the signal amplification stage. The project configures the system frequency to acquire the identifiable analogue distinction between the detected targets.

The detection system design achieves the data simplification module for the digital result conversion, determining the characteristics of the analogue response. The single binary sequence replaces the conventional multiple-bit digital translation to define the analogue changes with the simplified outcome. The data analysis depends on signature monitoring at the decay section to identify the target features for the weapon detection.

The signal processing simulation verifies the practical result analysis regarding the variable parameter of conductive objects. The simulated verification procedure provides the practicability of the target identification, and facilitates the algorithm development for the classification of object characteristics.

Chapter 5

Results and Discussion

This chapter provides the result analysis of the developed experimental weapon detection system and discusses the demonstration results of the data evaluation method for concealed weapon identification. For the achieved experimental system scheme, the project compares the practical and simulated results concerning the variable object parameters to develop and verify a target object distinction capability. Additionally, the algorithm development to identify the main features of a detected target, based on the object signature mark points evaluation, is presented, thereby characterizing the sharpness characteristic of an object edge for weapon recognition.

5.1 Experimental configuration

The primary experiment defines the result differences between the practical testing and simulation verification procedure. The system setup processes the variable changes of object detection regarding the sharp edge and cylindrical size. The practical examination configures the variable degree of sharp edge in the same location for target detection, meanwhile the same case of model simulation delivers the simulated experiment as the result reference. In addition, the detecting experiment determines the variable size scenario of cylinder target to verify the simulation procedure, comparing the practical and simulated outcomes.

The following experiment develops the induced response evaluation testing for the influencing parameters of variable targets. The study investigation for individual parameter variation provides the same detection scenes while it alters the specific target attribute, aiming to spotlight the results of a single change. The experiment produces the induced signature, then processes

and analyses the output data for the variables of material, shape, size and distance individually. The object modelling also configures the different levels of sharpness on the edge for the result assessment, contributing to the algorithm development.

5.2 Experimental processing

The experimental process configures the functional outcomes individually at the development stages concerning the transmitting and receiving sections, the adjustment circuit, the data processing and analysis modules in Figure 5.1. The progress result primarily involves the generated pulse at the transmitter while the induced response at the receiver, and then the adjusted signal, a binary sequence, and mark points evaluation based on FPGA processing. In order to verify the practical results, the simulation scheme operates the detection system procedure to provide the theoretical outcomes for comparison.

The transmitting stage of the detection system structure produces a continuous pulse stream configured with the experimental frequency, launching the alternating magnetic field. The following receiving scheme collects the sensing response of the coil to represent the induction changes of a detected target. In order to distinguish the response for different targets, the conditioning circuitry section provides the amplified and adjusted waveform for the onboard data processing.

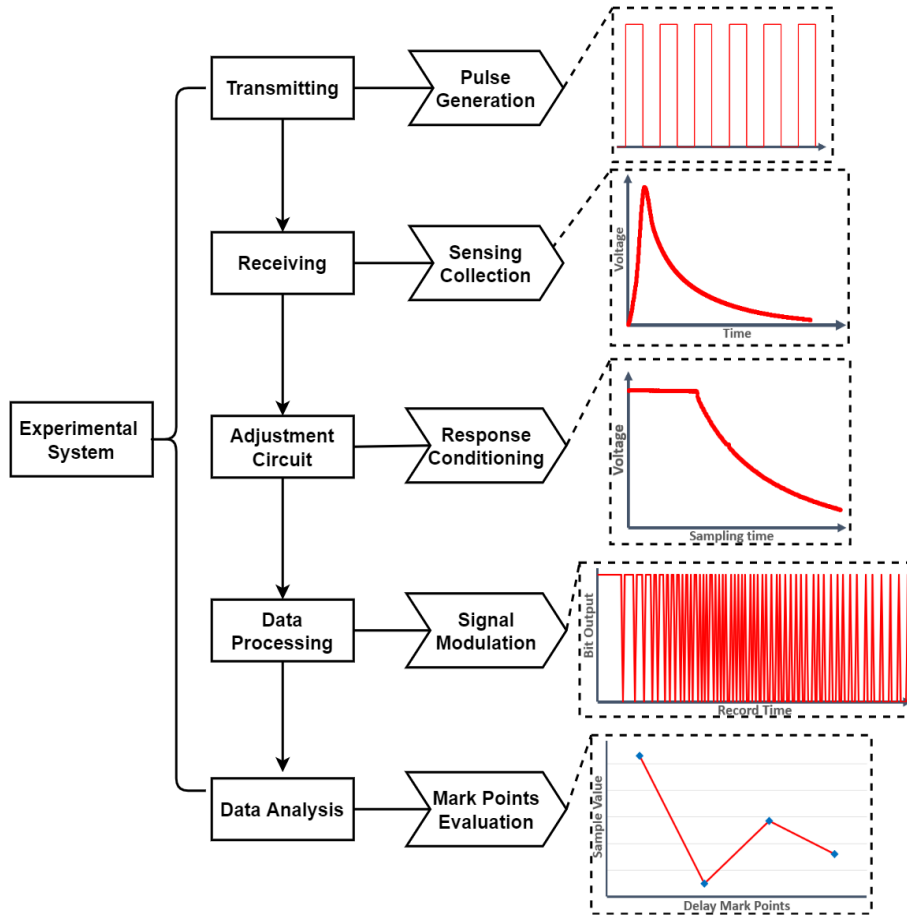


Figure 5.1: Practical signature procedure.

The implementation of the program on the platform monitors the delay duration to define the strength of induction and the density of low-level signal at the decay stage. As the analogue signal converted, the modulation procedure of FPGA presents the binary sequence, where the delay extension and the changes of decay describe the characteristics of induced response from a sensed target. For the data analysis and classification, the evaluation method of mark points outputs the data distribution to investigate the main features of the potential threat object, identifying the weapon from the detected items.

Meanwhile, the detection system simulation scheme processes the functional modules, including the induced response receiving, signal amplifying and conditioning, digital data processing, and the mark point assessment. The simulation model firstly produces the simulated response of electromagnetic inductance to emulate the characteristics of a target object. Following the same modification procedure, the simulated system structure amplifies and adjusts the received signal for data transformation. According to the delay sampling section, the examination design measures the duration to specify the electromagnetic induction power of a detected target.

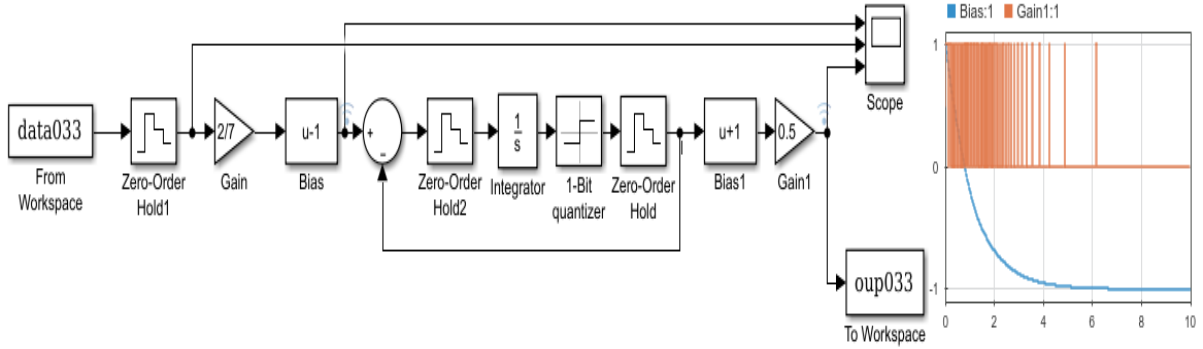


Figure 5.2: Modulation simulation procedure.

The data modulation simulation scheme delivers the same processing method and analytical procedure to evaluate the digital outcome of the decay study, as illustrated in Figure 5.2. As the input conditioned signal provided, the signature adjustment stage initially conducts the introduced data in the processing range via a gain and bias operator. Then the data conversion, concerning the integration and quantization, generates the binary digital sequence. The adjusted result eventually shows a single-digit flow within the signal 0 and 1.

5.3 Experimental verification

The experimental identification program produces the practical result on the device platform and the simulated result to verify the system outcome, based on the detection scenarios of varying edge and cylinder analysis. As the practical objects distinguished at the decay stage, the identification programme develops the evaluation method to acquire detailed information for accurate distinction. The decay analysis develops the critical description of a declining response to determine the characteristics of a detected target. Hence, the achievement of the proposed measurement at the decay phase dramatically defines the induction changes, classifying the variable features for object detection demonstration.

5.3.1 Edge demonstration

For the increasingly angled edge of a target, the slight difference of response results in the difficulty to distinguish the level of sharpness. The single record at each mark points becomes limited to identify the sharp edge of a target, considered as the potential weapon. Accordingly,

the development of double measurements at the mark points provides the detailed description of a decaying induction, benefiting the recognition of a variable edge.

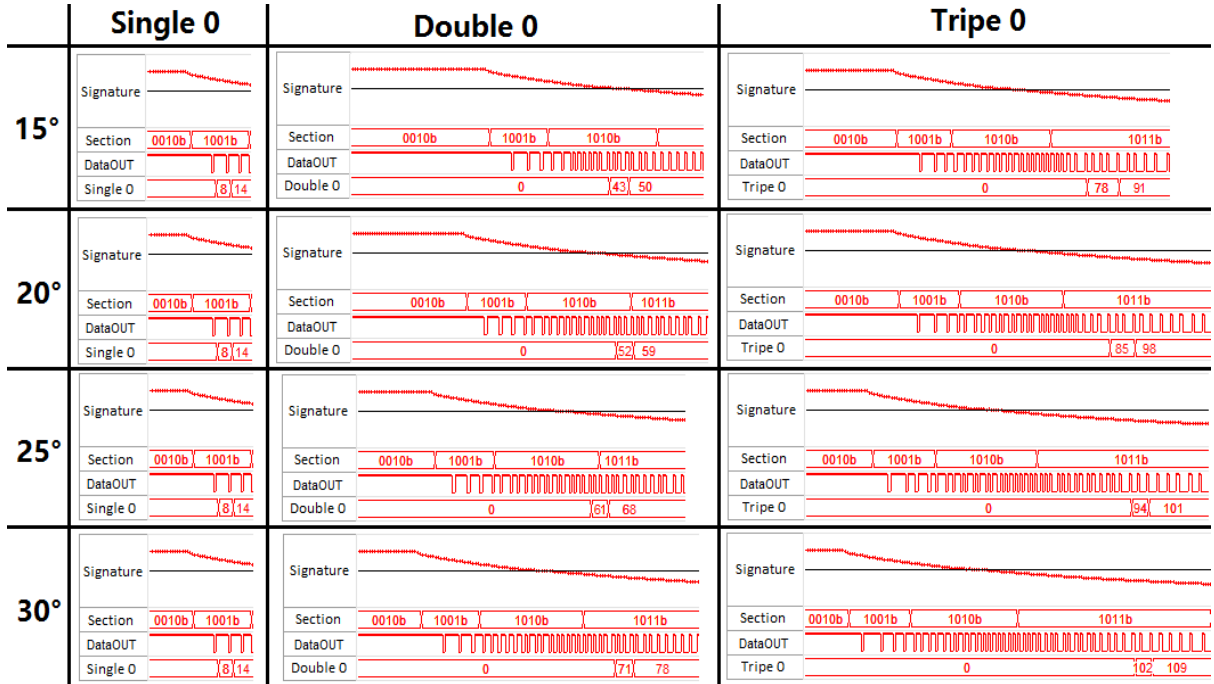


Figure 5.3: Experimental result of variable edge

The onboard registers evaluate the two-consecutive evidence for the individual mark points once they occurred, as seen in Figure 5.3. Although the variance of targets at the single 0 is hardly recognizable for difference, the record successively evaluates the mark points of double 0, which significantly determines the shape edge. The experimental result definitely shows the noticeable difference at the specific spot of tripe 0 for the lower degree angle of targets. Therefore, the consecutive evaluation of mark points enhances the reliable distinction of a unique response and thus, achieves the classification of sharpness at pointed levels.

The result verification applies the simulation procedure to demonstrate the identical variance of sharpness of a target. At a specific sharp angle, the simulated model produces a unique decaying response of induction, used as the input source for analysis. The subsequent data processing optimizes the information in accordance with the practical operations.

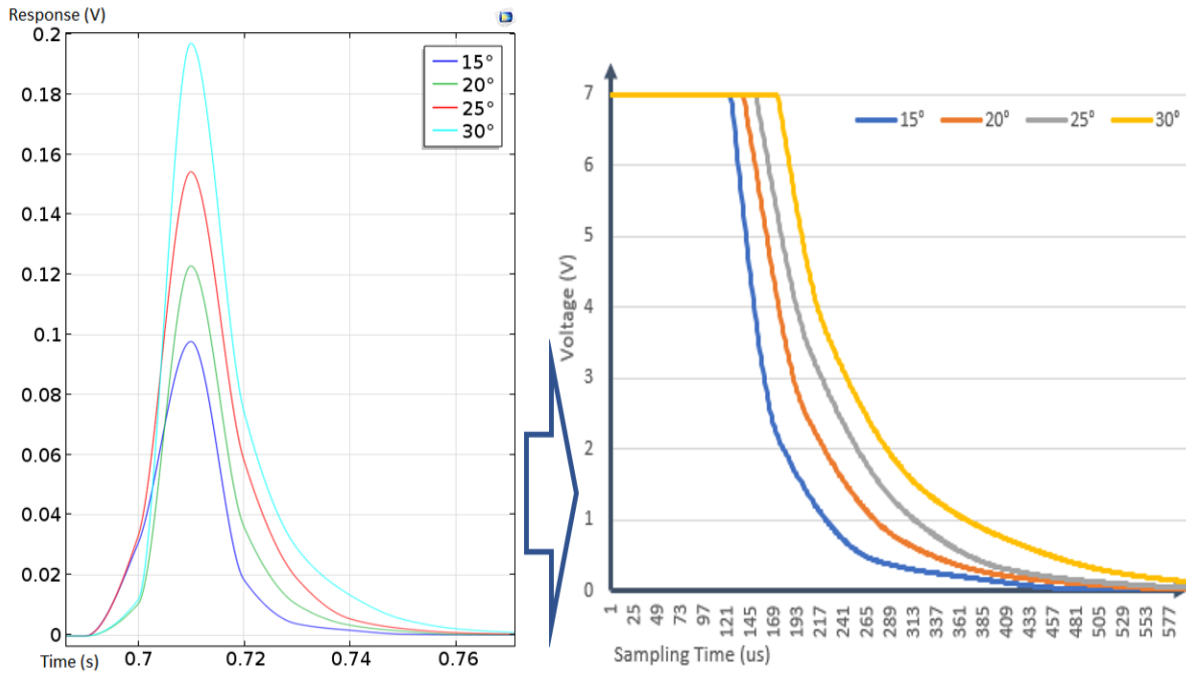


Figure 5.4: Verification procedure for variable edge

The simulation models generate the induced responses corresponding to the variable changes of edge, as seen in Figure 5.4. The following procedure of signal conditioning delivers the sampling data after digital conversion and amplification. The experimental consequence shows the extensive delay duration used to reflect the induction strength while decaying response changes describe the characteristics of the specified edge. The result indicates that the decline becomes rapid as the degree of edge decreases, where the 15° edge drops from the initial voltage of the decay section speedily.

Table 5.1: Practical and simulated edge comparison

| Sharpness | Name | Delay | 1st 0 | 2nd 0 | 1st 00 | 2nd 00 | 1st 000 | 2nd 000 |
|-----------|------------|-------|-------|-------|--------|--------|---------|---------|
| 15° | Practical | 121 | 8 | 14 | 43 | 50 | 78 | 91 |
| | Simulated | 124 | 9 | 15 | 44 | 51 | 80 | 92 |
| | Difference | 3 | 1 | 1 | 1 | 1 | 2 | 1 |
| 20° | Practical | 132 | 8 | 14 | 52 | 59 | 85 | 95 |
| | Simulated | 136 | 9 | 15 | 55 | 61 | 87 | 97 |
| | Difference | 4 | 1 | 1 | 3 | 2 | 2 | 2 |
| 25° | Practical | 147 | 8 | 14 | 61 | 68 | 94 | 101 |
| | Simulated | 150 | 10 | 16 | 63 | 70 | 96 | 105 |
| | Difference | 3 | 2 | 2 | 2 | 2 | 2 | 4 |
| 30° | Practical | 170 | 8 | 14 | 71 | 78 | 102 | 109 |
| | Simulated | 172 | 10 | 16 | 74 | 81 | 105 | 113 |
| | Difference | 2 | 2 | 2 | 3 | 3 | 3 | 4 |

The consecutive evaluation at the mark points processes the simulation evidence for sharpness levels, compared with the experimental result. Table 5.1 reveals that the simulated measurement can distinguish the variable degree of an angled edge, presenting the limited error with the onboard assessment. Besides, with the increasing length of continuous signal 0, the simulation procedure provides the evident variation of sharp edge targets for distinction.

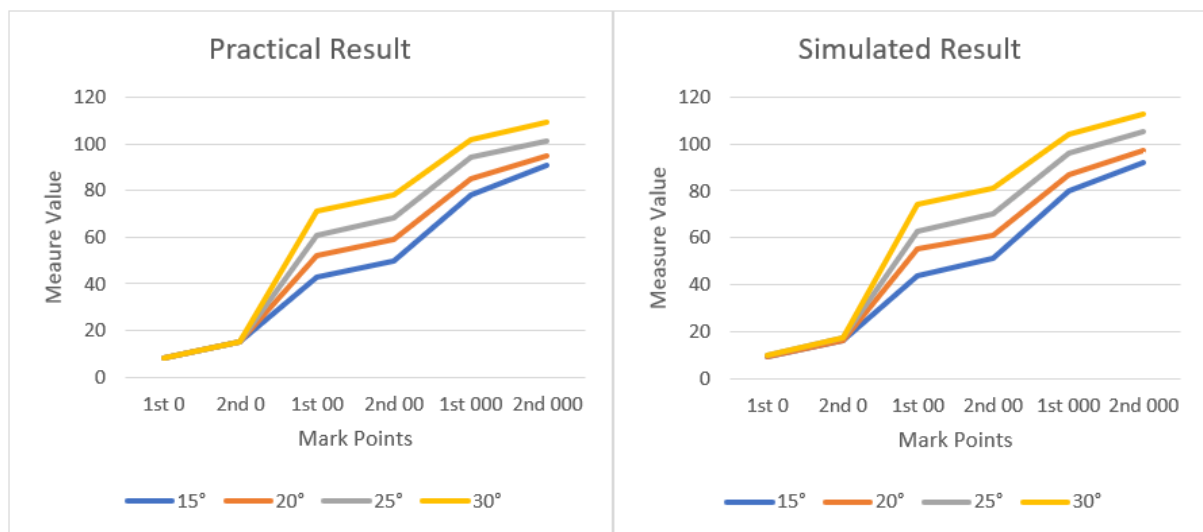


Figure 5.5: Practical and simulated variable edge comparison

However, the distribution of mark points for both practical and simulated evidence, in Figure

5.5, gives a similar tendency towards discrimination between sharpness levels. In fact, the combination of different locations of mark points in the binary data flow becomes the characteristics of a specific sharp-edged object. Therefore, the simulation verification proves that the comprehensive evaluation of mark points on the FPGA platform accomplishes the distinction of sharpness levels at a target edge, identifying the potential hazard.

5.3.2 Cylinder demonstration

The achievement of a novel algorithm in the detection system discriminates the threat targets with the sharp edge and recognizes the changes of licit and secure items concurrently. The general prismatic geometry without the pointedness considered no threat to the security typically includes the cuboid and cylinder. The targets' geometric figure obtains the cubic transformation, assuming the sharpness at the corner increases to the right angle. On the other hand, as the reference of a non-threatening component, the cylinder structure features a curved circular surface without the pointed prism. Hence, the variable sizes of cylinders as the experimental subject are operated to demonstrate the practicability of combined evaluation at the mark points for targets identification.

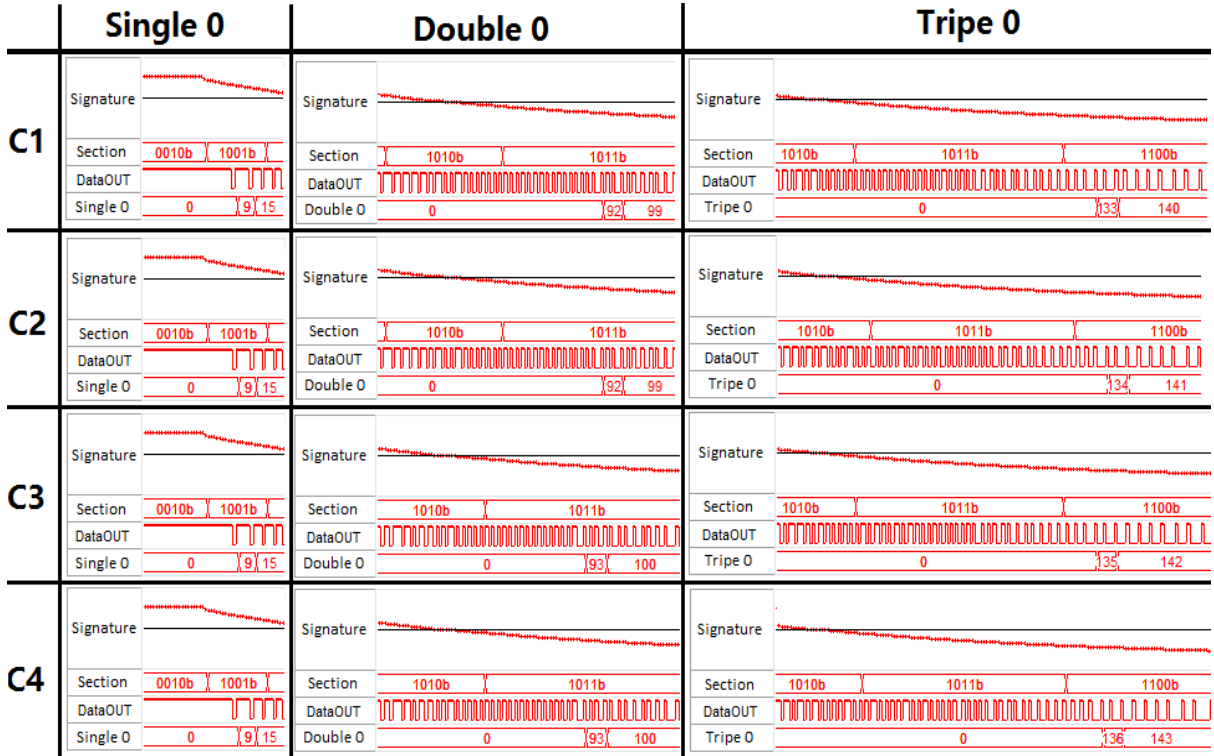


Figure 5.6: Experimental result of variable cylinder

For the embedded scheme, the double measurement at the mark points compares the practical evidence according to the gradually varying sizes of cylinder targets. Figure 5.6 gives the equivalent of indications for single 0, and likewise, the double-0 result gains the negligible difference between the variable sizes. Although the record value increases at the labelled triple 0, the variance for changing cylinders stays in a limited scope. Overall, the practical measurement at the mark points slightly fluctuates with the variety of cylindrical targets, remaining within a specific range.

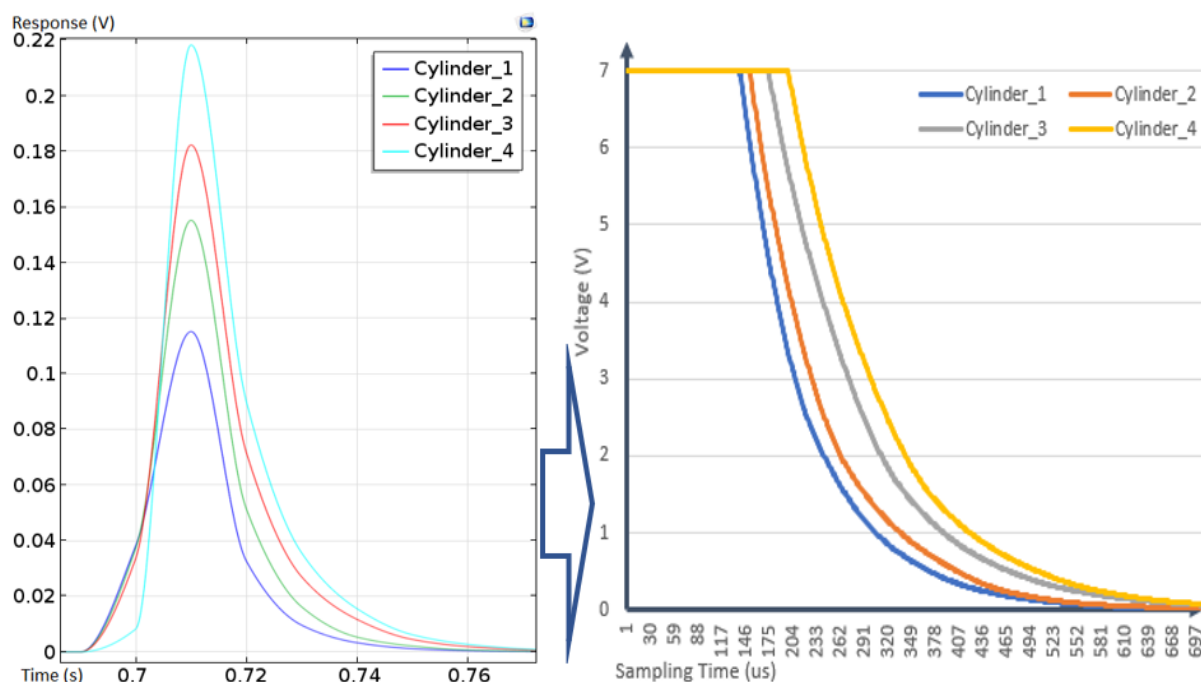


Figure 5.7: Response simulation and signal conditioning for variable cylinder.

As the induced response obtained, the simulation procedure operates the signal processing of amplification and adjustment functions to produce the sampling waveform in Figure 5.7. The result suggests that the larger volume of a cylinder target provides the extended delay duration, reflecting the more considerable peak value of the response signal.

Table 5.2: Practical and simulated variable cylinder comparison

| Sharpness | Name | Delay | 1st 0 | 2nd 0 | 1st 00 | 2nd 00 | 1st 000 | 2nd 000 |
|------------|------------|-------|-------|-------|--------|--------|---------|---------|
| Cylinder_1 | Practical | 138 | 9 | 15 | 92 | 99 | 133 | 140 |
| | Simulated | 140 | 10 | 16 | 94 | 102 | 134 | 142 |
| | Difference | 2 | 1 | 1 | 2 | 3 | 1 | 2 |
| Cylinder_2 | Practical | 151 | 9 | 15 | 92 | 99 | 134 | 141 |
| | Simulated | 154 | 11 | 16 | 95 | 103 | 135 | 143 |
| | Difference | 3 | 1 | 1 | 3 | 4 | 1 | 2 |
| Cylinder_3 | Practical | 174 | 9 | 15 | 93 | 100 | 135 | 142 |
| | Simulated | 177 | 11 | 17 | 96 | 104 | 137 | 145 |
| | Difference | 3 | 2 | 2 | 3 | 4 | 2 | 3 |
| Cylinder_4 | Practical | 198 | 9 | 15 | 93 | 100 | 136 | 143 |
| | Simulated | 202 | 12 | 18 | 97 | 105 | 139 | 147 |
| | Difference | 4 | 3 | 3 | 4 | 5 | 3 | 4 |

The following procedure models the same variation of a cylinder-shaped object, which produces the associative measurement of simulated evidence located at the label spots. Table 5.2 reveals the reduced error between the experiment and simulation outcomes in general, compared with the sharp-edge instances.

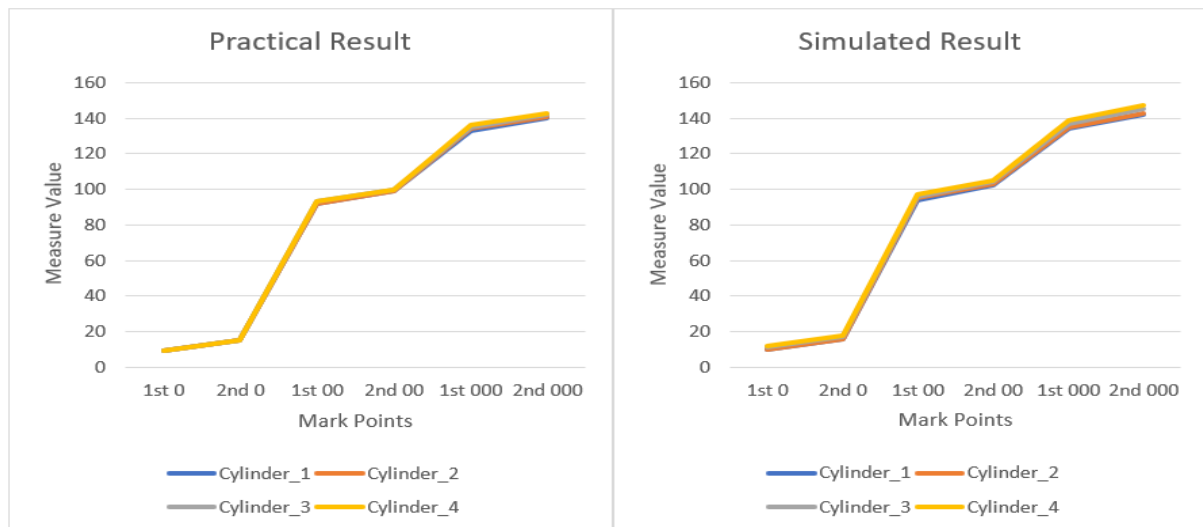


Figure 5.8: Practical and simulated cylinder comparison

Afterwards, the practical and simulated evidence are allocated and associated on the basis of the sequential mark points, respectively. Although the simulation provides a clear difference,

Figure 5.8 gives a similar distribution for the cylindrical variation. Therefore, the combined evaluation at the successive mark points forms a distinctive variation tendency, featuring the change of a cylinder target.

5.4 Algorithm development

The detection system develops the object recognition method to distinguish the variable response of targets, depending on the delay duration and mark points evaluation of decay phase. The comprehensive evaluation at the voltage and time domains proposes the identification algorithm, achieving the featured description for the sharpness of a potential target.

As a reasonable concordance with the practical and simulated results, the mark point assessment by the simulation processing identifies the features of objects for the detection scenes concerning the material, size, shape and distance. The identification method identifies the characteristics of a separate component for the variable parameters, defining the principal features.

In order to distinguish the illicit objects with the sharp edge from the non-threatening items, the feasible examination practice assigns the sharpness analysis for weapon recognition. The mark points evaluation algorithm provides a unique description for the specific sharp edge changes, thereby determining the threat components based on the specified sharpness.

5.4.1 Mark points evaluation

The evaluation method approach delivers the data analysis to distinguish the induced response of variable parameters for object detection, based on the delay duration and mark points of the decay phase. The practicable assessment solution analyses the specified voltage for signal declining distinction; meanwhile, the mark points examination defines the properties of a decaying response at the sampling time domain, used to identify the characteristics of a target. The signal process amplifies the induced response and emphasizes the base section, and the delay duration primarily determines the peak changes for the characteristic's identification. The degree of voltage decline identified the decaying changes for the decay period, substantially distinguishing the object features. Hence, the corresponding values decreased from the beginning of decay can determine the signature changes, thereby characterizing the mark points for object distinction.

The sampling-domain assessment of mark points reflects the specific changes of a sampling

signature, which differs the features of objects regarding the material, shape, size and distance. The duration evaluation at the single, double and triple 0 provides the featured measurement at the specified stages, based on the particular decline in response sampling. According to the periodical change analysis, the mark points evaluation method investigates the time-domain transform at the declining phrases, enabling the attributes description of a detected target.

Material Evaluation

The material analysis procedure operates the same volume of block-shaped targets made of a different material. The mark points assessment at the voltage and time-domain differs the feature changes of the induced response in terms of delay and decay duration. The scaled waveform involves the delay duration that indicates the peak changes of induction and the decay period describing the voltage changes at the mark points.

Table 5.3: Sampling-domain mark points evaluation for material

| | Delay | 1st 0 | 2nd 0 | 1st 00 | 2nd 00 | 1st 000 | 2nd 000 |
|--------|-------|-------|-------|--------|--------|---------|---------|
| Steel | 162 | 9 | 16 | 54 | 59 | 79 | 86 |
| Iron | 532 | 16 | 28 | 204 | 217 | 324 | 334 |
| Alum | 299 | 19 | 34 | 303 | 318 | 459 | 487 |
| Copper | 262 | 21 | 36 | 434 | 449 | 674 | 693 |

From Table 5.3, the delay duration for the sampling extension defines the peak value for the material changes. At the decaying signal, the sampling measurement at the single, double and triple 0 characterizes the identification at the sampling time domain. Meanwhile, the voltage assessment processes the declined samples at the mark points and the corresponding ratio compared with the peak value from the beginning.

Table 5.4: Voltage-domain mark points evaluation for material

| | Steel | | Iron | | Alum | | Copper | |
|---------|-------|-------|------|-------|------|-------|--------|-------|
| | Volt | PCT | Volt | PCT | Volt | PCT | Volt | PCT |
| 1st 0 | 6.13 | 87.6% | 6.54 | 93.5% | 6.63 | 94.7% | 6.65 | 95.0% |
| 1st 00 | 2.99 | 42.7% | 3.20 | 45.7% | 3.32 | 47.5% | 3.11 | 44.3% |
| 1st 000 | 1.94 | 27.7% | 2.06 | 29.5% | 2.32 | 33.1% | 2.16 | 30.9% |

The result suggests that steel material presents the lower voltage sample at all mark points featuring the rapid declining response in Table 5.4. The decrease becomes slower for the copper at the initial stage, while the rapid change occurs for the lower voltage measured at the following

phrases. Compared with the material of Iron, the voltage assessment of aluminum evidently delivers the higher values at all mark points, showing the extended decay duration.

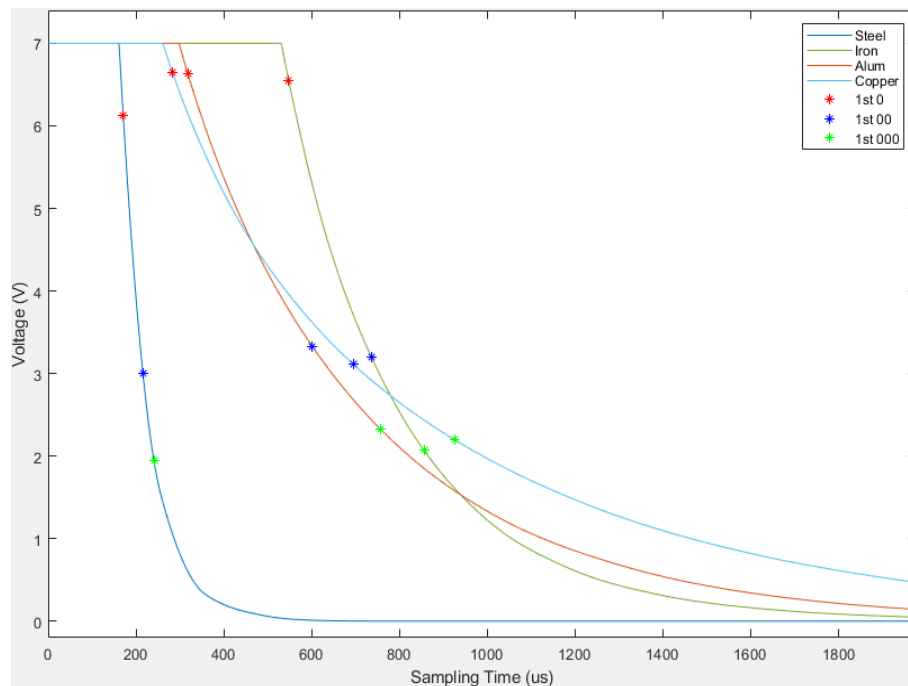


Figure 5.9: Voltage analysis for material.

The voltage distribution over the sampling time, shown in Figure 5.9, concludes the mark points assessment distinguishes the specified material of targets. The voltage declines slowly, indicating the extension of the decaying response based on the previous samples. The voltage-domain changes represent the distinction between the material, cooperating with the sampling time evaluation.

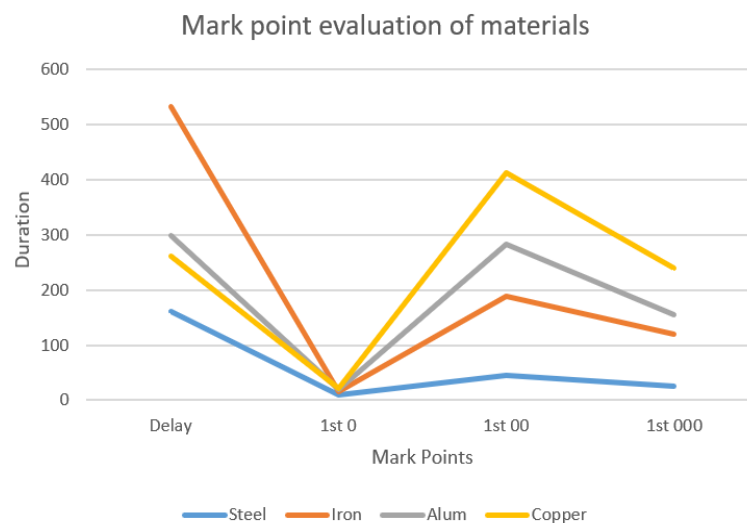


Figure 5.10: Mark points identification for material.

The algorithm development primarily delivers the evaluation distribution visualizing the length for delay phase, associated with the duration of the single, double and triple 0 as first emerging at the decay stage. The result in Figure 5.10 gives the algorithm analysis for different materials based on the combination duration assessment. It indicates that the copper material of a target generates a lower value of duration for delay and mark points, resulting from the strengthened induction and extended decaying response.

Shape Evaluation

The evaluation approach processes the shape changes of a target while other parameters remain constant, which underlines the mark point assessment for the shape study. The delay extension differentiates the peak changes for response signature with the corresponding amplification. Meanwhile, the decay evaluation analyzes the signature changes regarding the mark points distribution over the sampling time. The voltage assessment specifically determines the declined response of a specific shape, featuring the waveform drop of mark points.

Table 5.5: Sampling-domain mark points evaluation for shape

| | Delay | 1st 0 | 2nd 0 | 1st 00 | 2nd 00 | 1st 000 | 2nd 000 |
|--------|-------|-------|-------|--------|--------|---------|---------|
| Knife | 79 | 6 | 9 | 16 | 21 | 37 | 44 |
| Block | 137 | 16 | 29 | 274 | 287 | 421 | 440 |
| Torus | 192 | 18 | 32 | 302 | 317 | 490 | 506 |
| Sphere | 302 | 19 | 33 | 279 | 296 | 461 | 477 |

The mark points distribution, shown in Table 5.5, indicates that the sphere-shaped target gives the strengthened response with the more significant delay value, despite the same volume provided. Obviously, the decaying induction signature exhibits the extension because of the longer record time for mark points. The single 0 point for the sphere signature suggests the extension of a decaying signature, while the knife figure features the rapid decline at a later stage for the quick changes at the double and triple 0 pieces of evidence. The mark points evolution offers the noticeable distinction between the block and cylinder figures with the same detection practice.

Table 5.6: Voltage-domain mark points evaluation for shape

| | Knife | | Block | | Torus | | Sphere | |
|---------|-------|-------|-------|-------|-------|-------|--------|-------|
| | Volt | PCT | Volt | PCT | Volt | PCT | Volt | PCT |
| 1st 0 | 4.83 | 69.5% | 6.36 | 90.9% | 6.60 | 94.3% | 6.62 | 94.6% |
| 1st 00 | 2.95 | 42.3% | 2.98 | 42.6% | 3.31 | 47.4% | 3.38 | 48.2% |
| 1st 000 | 1.74 | 24.9% | 2.04 | 29.2% | 2.36 | 31.9% | 2.22 | 31.7% |

The voltage assessment of a knife object gives the rapid decline initially as the significant distinction with the shape of block, torus and sphere. From Table 5.6, the lower voltage measured at the double and triple 0 points decides a unique identification for the knife target. The same voltage assessment method occurs at the mark points that distinguish the shape between block and torus. Although a cone gives the extended samples at the sampling domain, the voltage-domain assessment of a sphere accounts for a more significant proportion over mark points, which defines a steadily decaying change.

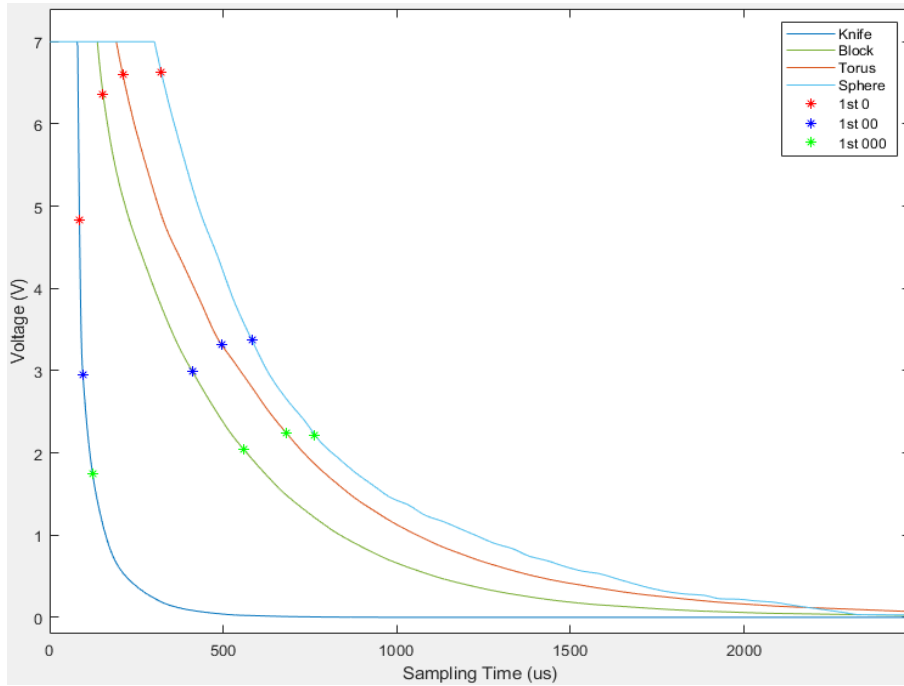


Figure 5.11: Voltage analysis for shape.

Therefore, the voltage evaluation effectively characterizes the decaying changes of variable shapes regarding the decline weight, based on the mark points sampling. Figure 5.11 distributes the mark points in terms of sampling time and decreased voltage, which visualizes the distinction between the shape changes. In general, the decline weight evaluation develops the mark points study for the voltage domain, and thus it advances the shape identification.

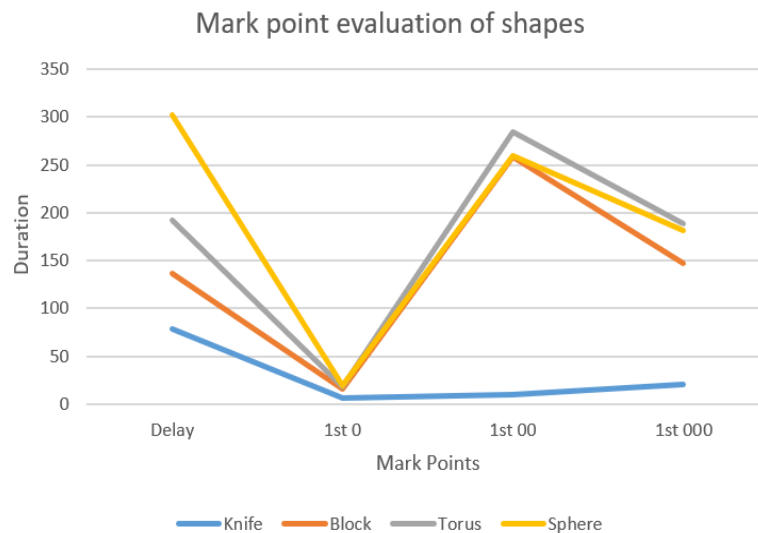


Figure 5.12: Mark points identification for shape.

The evaluation method delivers a comprehensive analysis of delay and mark points duration. The result in Figure 5.12 shows that the knife produces significantly slight changes of duration value, providing the evident distinction from the regular shape of a target. Therefore, the algorithm can characterize the rapidly declining response, defining the sharp edge of a knife to identify the threat components.

Size Evaluation

The detection practices of the changeable sizes for a cubical shape produces the induced signal of different volumes, concerning $2 \times 2 \times 2 \text{ cm}^3$ (size_1), $3 \times 3 \times 3 \text{ cm}^3$ (size_2), $4 \times 4 \times 4 \text{ cm}^3$ (size_3) and $5 \times 5 \times 5 \text{ cm}^3$ (size_4). The evaluation method assesses the delay duration and records the mark points once the signal declines.

Table 5.7: Sampling-domain mark points evaluation for size

| | Delay | 1st 0 | 2nd 0 | 1st 00 | 2nd 00 | 1st 000 | 2nd 000 |
|--------|-------|-------|-------|--------|--------|---------|---------|
| size_1 | 104 | 8 | 18 | 70 | 77 | 105 | 118 |
| size_2 | 158 | 10 | 20 | 91 | 99 | 137 | 150 |
| size_3 | 243 | 14 | 24 | 129 | 140 | 194 | 205 |
| size_4 | 309 | 15 | 26 | 152 | 161 | 230 | 241 |

The result shows that the extended delay duration implies the larger volume, as the strengthened induction received in Table 5.7. The progressive changes at the mark points differ the variable volumes of induced response, which determine the size characteristics of a cubic target.

Table 5.8: Voltage-domain mark points evaluation for size

| | size_ 1 | | size_ 2 | | size_ 3 | | size_ 4 | |
|---------|---------|-------|---------|-------|---------|-------|---------|-------|
| | Volt | PCT | Volt | PCT | Volt | PCT | Volt | PCT |
| 1st 0 | 6.41 | 91.6% | 6.40 | 91.5% | 6.44 | 92.1% | 6.47 | 92.5% |
| 1st 00 | 3.13 | 44.7% | 3.20 | 45.7% | 3.18 | 45.5% | 3.18 | 45.5% |
| 1st 000 | 2.15 | 30.7% | 2.15 | 30.7% | 2.14 | 30.6% | 2.12 | 30.2% |

The voltage analysis delivers the distinction of a declining response to define the behavioural change of size in Table 5.8. The result suggests that the varying size of detection remains the same level of a decline change over the mark point sampling, although the different value for delay measurement. Despite the variable size, the declining percentage from the start point is restricted within 0.6 % at the specified sampling points, suggesting the critical features of a target.

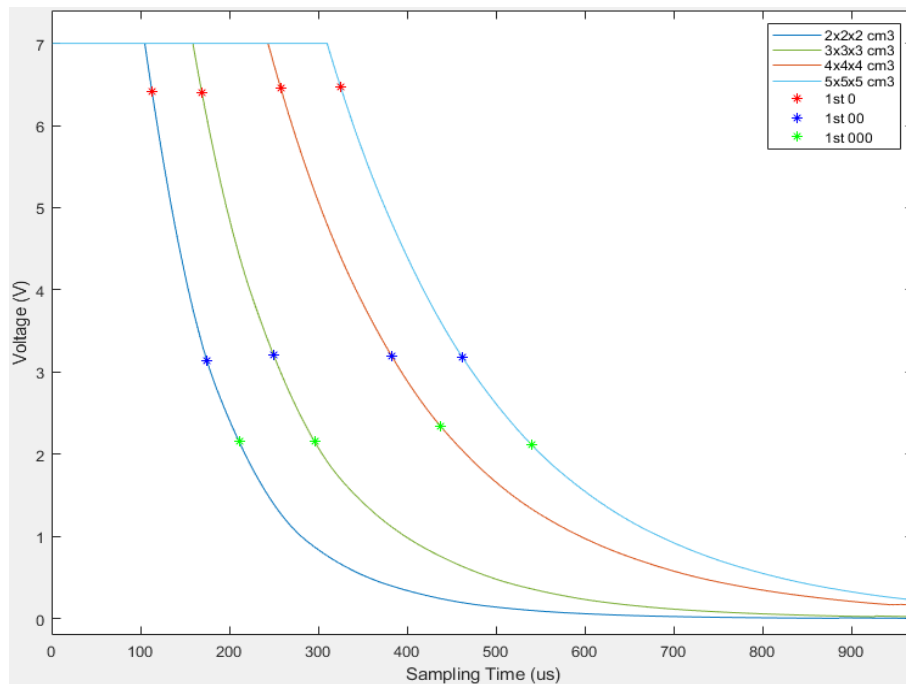


Figure 5.13: Voltage analysis for size.

The voltage evaluation results in Figure 5.13 visually provides the declining changes at the mark points. The measurement of delay duration can distinguish the induction strength of variable size, while the voltage at a first single, double and triple signal 0 remains the same level to describe the identical parameters of target excepting the size.

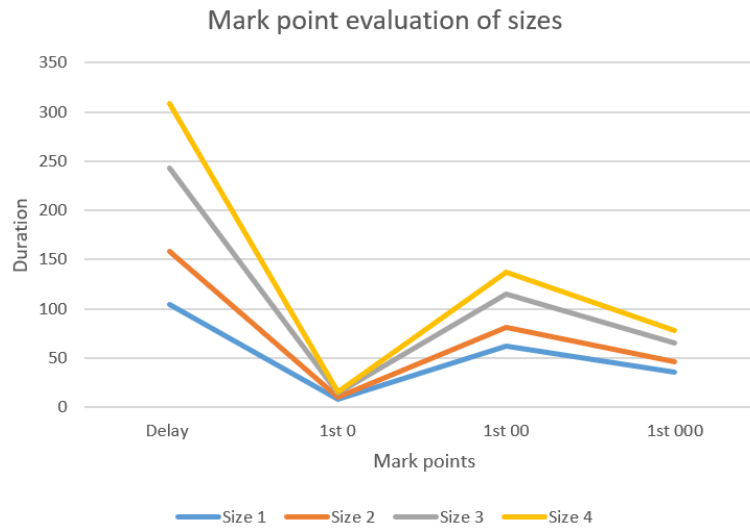


Figure 5.14: Mark points identification for size.

The size identification in Figure 5.14 indicates that the increased duration of delay evaluation determines the larger size. Meanwhile, the mark points duration assessment suggests a similar distribution within the variation range, reflecting the variable size of a specified target.

Distance Evaluation

As the induced response obtained at the different distances for the same target, the distance detection study processes the mark points evaluation for the voltage and sampling time analysis. The measurement operation assesses the delay section and records the mark points after the data modulation processing and data transformation.

Table 5.9: Sampling-domain mark points evaluation for distance

| | Delay | 1st 0 | 2nd 0 | 1st 00 | 2nd 00 | 1st 000 | 2nd 000 |
|------------|-------|-------|-------|--------|--------|---------|---------|
| Distance20 | 486 | 17 | 29 | 190 | 201 | 290 | 306 |
| Distance22 | 408 | 16 | 28 | 189 | 200 | 283 | 296 |
| Distance24 | 345 | 16 | 28 | 190 | 201 | 284 | 297 |
| Distance27 | 255 | 16 | 28 | 187 | 198 | 281 | 294 |
| Distance30 | 148 | 15 | 27 | 189 | 200 | 287 | 296 |

The mark points over the sampling time deliver the different delay changes while the similar alteration for the decay phase, as seen in Table 5.9. The more significant value of delay duration represents the closer distance of target detection.

Table 5.10: Voltage-domain mark points evaluation for distance

| | Distance20 | | Distance22 | | Distance24 | | Distance27 | | Distance30 | |
|---------|------------|-------|------------|-------|------------|-------|------------|-------|------------|-------|
| | Volt | PCT | Volt | PCT | Volt | PCT | Volt | PCT | Volt | PCT |
| 1st 0 | 6.53 | 93.3% | 6.54 | 93.4% | 6.52 | 93.1% | 6.54 | 93.4% | 6.51 | 93.0% |
| 1st 00 | 3.26 | 46.6% | 3.24 | 46.3% | 3.24 | 46.3% | 3.21 | 45.9% | 3.20 | 45.7% |
| 1st 000 | 2.25 | 32.1% | 2.23 | 31.8% | 2.21 | 31.6% | 2.20 | 31.4% | 2.19 | 31.3% |

The voltage measurement in Table 5.10 suggests that the same declining level at the mark points describe the same feature of a decaying response. The voltage assessment provides the same description of a detection target regardless of the distance placed.

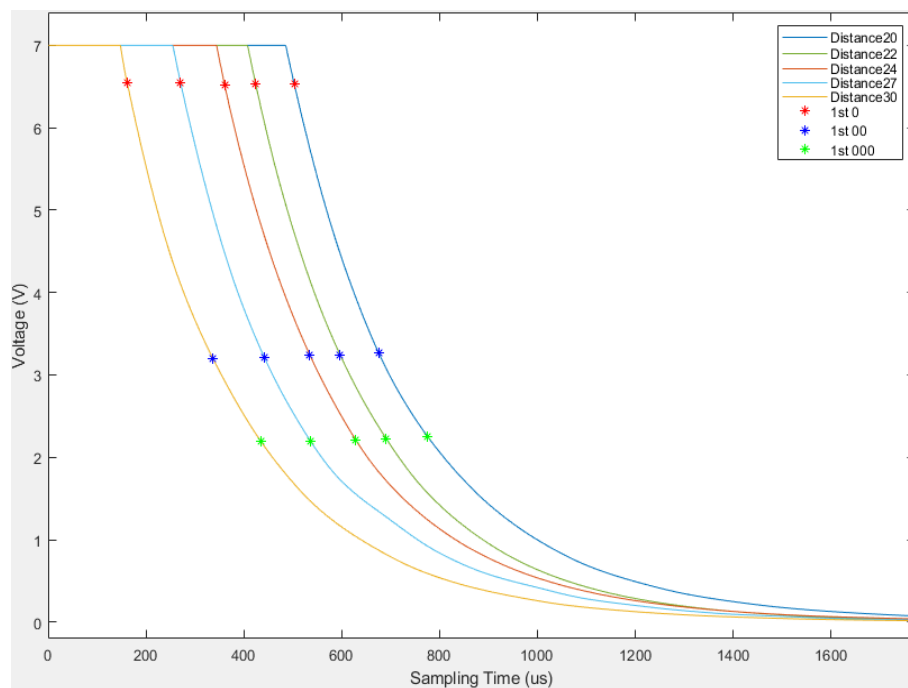


Figure 5.15: Voltage analysis for distance.

The voltage evaluation result in Figure 5.15 visually provides the declining changes at the mark points for variable detection distance. The result indicates the detection distance affects the induction strength to change the delay duration, while the declining voltage at the same level results from the same target wherever detection occurs.

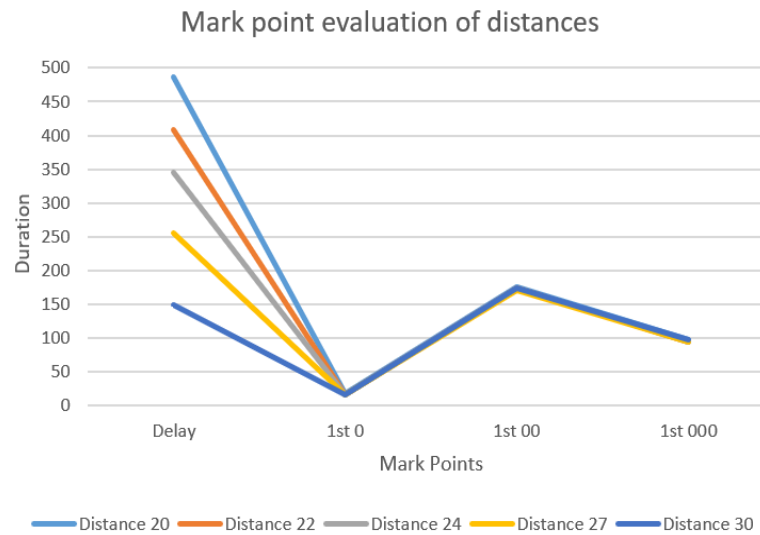


Figure 5.16: Mark points identification for distance.

The evaluation approach produces the comparison results in Figure 5.16, illustrating the more significant value of delay duration for the closer detection distance due to the strengthened induction. Besides, the identical value distribution over the mark points at the decay period suggests the unique induced response from the same detected target.

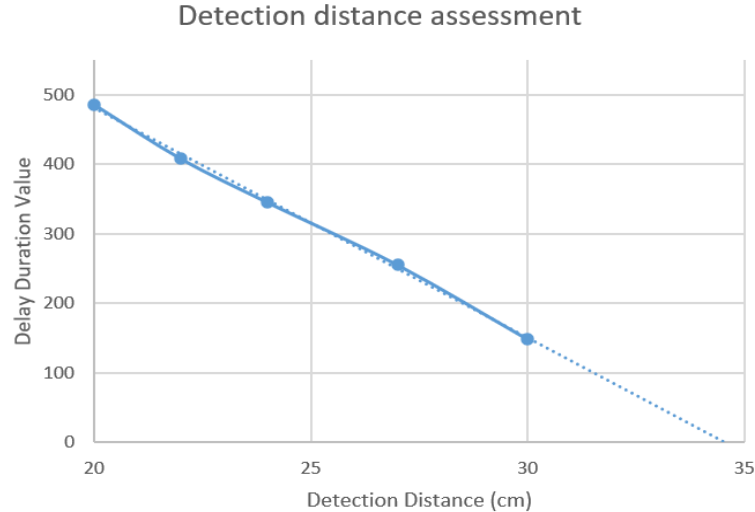


Figure 5.17: Detection distance assessment.

According to the detection distance measured, the assessment approach applies the sample distribution to describe the trendline of distance over 30 cm. The result in Figure 5.17 suggests that the detection distance is limited at 34 cm, resulting from no measurement for delay duration.

Sharpness Evaluation

In order to detect the sharp edge of a threat component, the sharpness analysis changes the volume of targets (10 cm³, 20 cm³, 30 cm³ and 40 cm³) with a shaped edge of 5° while the shape, material and other parameters remain the same.

Table 5.11: Sampling-domain mark points evaluation for sharpness 5°

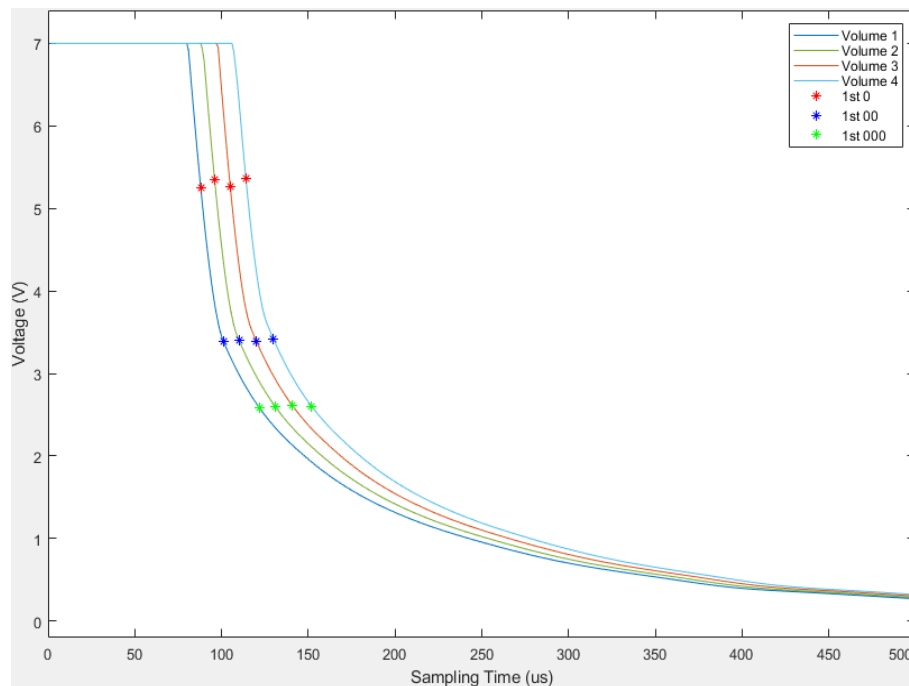
| | Delay | 1st 0 | 2nd 0 | 1st 00 | 2nd 00 | 1st 000 | 2nd 000 |
|-----------|-------|-------|-------|--------|--------|---------|---------|
| sharp5_ 1 | 81 | 7 | 12 | 20 | 26 | 41 | 48 |
| sharp5_ 2 | 89 | 7 | 12 | 21 | 27 | 42 | 49 |
| sharp5_ 3 | 98 | 7 | 12 | 22 | 28 | 43 | 50 |
| sharp5_ 4 | 107 | 7 | 12 | 23 | 29 | 45 | 51 |

The collection of mark points at the sampling time shows no difference occurs at the first single 0 while the extended delay duration for larger volume, as seen in Table 5.11. The distinction becomes significant as the signal declined at double and triple 0.

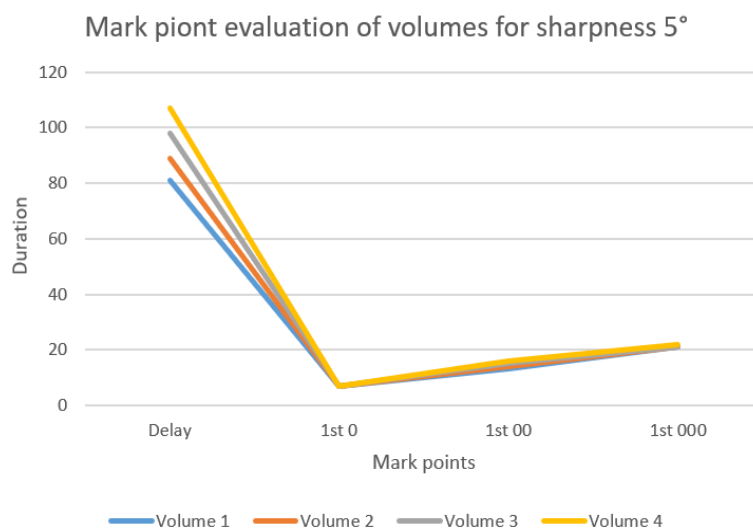
Table 5.12: Voltage-domain mark points evaluation for sharpness 5°

| | sharp5_ 1 | | sharp5_ 2 | | sharp5_ 3 | | sharp5_ 4 | |
|---------|-----------|-------|-----------|-------|-----------|-------|-----------|-------|
| | Volt | PCT | Volt | PCT | Volt | PCT | Volt | PCT |
| 1st 0 | 5.25 | 75.0% | 5.34 | 76.4% | 5.26 | 75.2% | 5.36 | 76.7% |
| 1st 00 | 3.39 | 48.4% | 3.40 | 48.6% | 3.39 | 48.5% | 3.41 | 48.7% |
| 1st 000 | 2.58 | 36.8% | 2.59 | 37.1% | 2.60 | 37.2% | 2.60 | 37.2% |

The voltage evaluation gives the same level of decline at mark points in Table 5.12. The difference between variable volumes is limited within the declining percentage of 0.3% when the assessment occurs at first double and triple signal 0, reflecting the same level of sharpness.

Figure 5.18: Voltage analysis for sharpness 5° .

The visual result in Figure 5.18 indicates the same declining level at the decay phase characterizes the sharpness 5° , even though the different delay duration for the variable volume of a detected target. Hence, the mark point evaluation can determine the level of sharpness to define the threat target, despite the volumes changed.

Figure 5.19: Mark points identification for sharpness 5° .

The evaluation algorithm suggests that the increased delay duration decides the larger volume of a shaped component, as seen in Figure 5.19. The mark points duration assessment delivers

the same allocation representing the particular decaying response of induction. Furthermore, the increasing duration in sampling order of mark points within the less span of 20 characterizes the unique rapidly declining response, defining the 5° sharpness. Therefore, the mark points evaluation method achieve the sharpness identification to recognize the potential threat component.

5.5 Discussion

The result discussion based on the experimental demonstration primarily conducts the evaluation methods analysis of induced response at the delay and decay phases for weapon identification. The investigation of system outcome, measuring the delay duration, suggests the induction strength of object detection. Meanwhile, the mark points examination from a digital binary consequence at the decay stage, defining the critical characteristics of a target. Therefore, the comprehensive evaluation development delivers the combination analysis of delay and mark points at the decay to identify the sharpness of an edge, distinguishing the concealed threat components from riskless items.

5.5.1 Delay phase analysis

After amplifying the induced response received at the circuit, the experimental operation adjusts the signature within the range of data conversion so that the waveform transforms the peak point into the delay phase. The delay duration mainly reflects the strength of the responding signature induced by a conductive target. The size of a target and distance to the search coil dramatically determines the electromagnetic induction power, resulting in the extension value for the delay stage.

The program based on the platform measures the extended duration, which decides the specific size of targets located at the respective distance. According to the particular delay value, the collection of samples in the variable combination of size and distance analyses the logical relationship for feature identification.

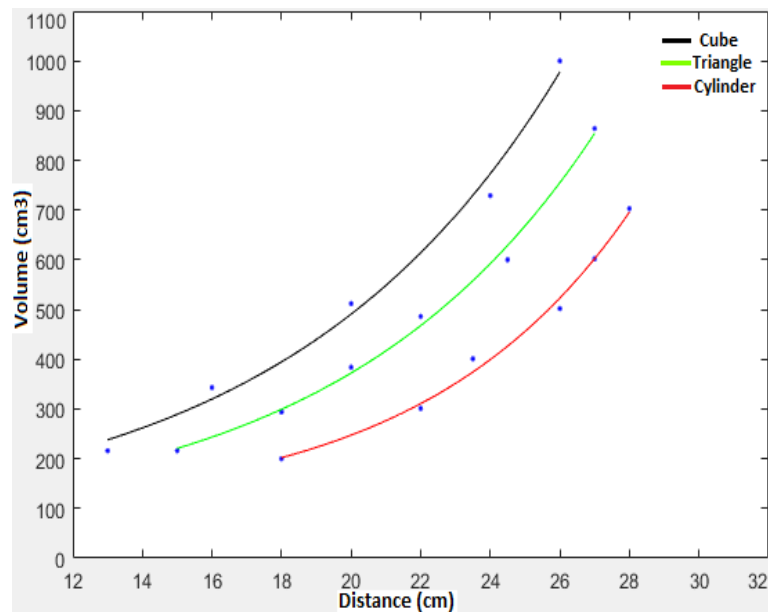


Figure 5.20: Size and distance relationship

Figure 5.20 reveals the different size of targets give the same value for delay phase located at the variable distance regarding cube, triangle and cylinder shape. On the basis of connection with the scattered samples for individual targets, the general expression provides the exponential function to describe the variation waveform:

$$f(x) = a \cdot e^{b \cdot x} + c \quad (5.1)$$

It suggests that the volume of targets actually becomes the exponential growth for the distance, as the delay value defined. The formula model with assigned coefficients approximates the scattered points respectively in terms of a cubic, triangular and cylindrical target.

Table 5.13: Cube, triangle and cylinder coefficients

| Coefficients | Cube | Triangle | Cylinder |
|--------------|--------|----------|----------|
| a | 34.85 | 21.5 | 5.635 |
| b | 0.1258 | 0.1336 | 0.1672 |
| c | 59.12 | 61.19 | 87.84 |

Table 5.13 shows that the different shapes of targets characterize the natural exponential function regarding the coefficients of a, b and c. According to the delay value measured, the specific formula expression provides the relationship between the size and distance once the shape of targets is defined. Hence, the experimental measurement of delay duration can

precisely calculate the size of a target and detected distance.

The formula models associating with the different shapes of components are defined for the delay phase and stored in the system. When the detection schedule assesses the delay value, it directly calls the reference models to examine the specific size and distance identification. Therefore, the analysis of the delay phase, depending on the function model, reasonably infers the size of a specific target located at a distance to the sensing coil.

5.5.2 Decay phase analysis

The decaying response dramatically reflects the characteristics of electromagnetic induction, enabling the effective identification of conductive targets. The simulation examination proves that the features of a target in terms of material, shape and size produce a unique waveform at the decay duration. On the other hand, the basic equipment configuration, deploying the transmitting pulse frequency, generates the distinct difference between the background and targets. The experimental amplification of the received signature practically spotlights the base section of a decay response, which provides detailed information for distinction.

The weapon detection system features programmable prototyping on the FPGA platform as a flexible, speedy and economical solution, different from the typical computer and microcontroller processing. As the analogue signature converted by the ADC module, the $\Sigma\Delta$ modulation outcomes the single-bit digital flow to describe the induction variation, significantly simplifying the data acquisition. As a matter of fact, the conversion scheme translates the time-domain decaying response into frequency-domain digital information, enabling the optimization design system. Hence, the high level of the signal at the frequency in the binary sequence characterizes the decaying induction to recognize targets' features beneficially.

The binary signal distribution regularly changes the length of continuous low levels at a sequence of discrete values. The valuation of mark points, assigned at the increased length of signal 0, essentially divides a decaying response into the dynamic sections with the sampling time. The experiment verifies the measurement at the mark points as an effective solution to distinguish the multi-parameter variation of targets. Additionally, the method achieves the identification of a target with a sharp edge, considered as the threat item to the security.

The system assessment schedule develops the successive mark point measurement to characterize the induced response of a specific target, providing increasingly distinguishable information. The experimental results of varying edge and cylinder demonstration realize the practical distinction

between targets depending on the critical features description. The simulation procedure provides similar results to verify the performance of the novel method proposed for practical application.

The detection system scheme employs the mark point evaluation method for the delay and decay study to achieve the object feature identification. The delay and mark point duration examination determine the main characterizes description involving the material, shape, size and distance for object distinction. Additionally, the detection approach defines the sharp edge of a target which identifies the potential threat components from the inspection items. Therefore, the developed evaluation algorithm accomplishes the description of a variable induced response, distinguishing the object characteristics for identification and classification.

The specific change over the successive mark points decides the unique induced response, thereby representing the critical characterizes of a target. Furthermore, the object identification development applies the fitting curve algorithm to specify the mark point change for feature distinction, including the trigonometric expression and polynomial regression methods.

Trigonometric expression

The scattered points of normalized results, as the representative reference, are distributed regarding the variable sharpness and size of the cylinder. According to the overall fluctuation, the scheme applies the trigonometric Fourier transform in terms of the sine and cosines series to describe the specific variation [126] [127]:

$$F(x) = a_0 + \sum_{n=1} (a_n \cdot \cos(nwx) + b_n \cdot \sin(nwx)) \quad (5.2)$$

Where a and b are the coefficients associated with the term, w is called the base frequency of signal.

The Fourier transform principle is that the time-domain function is fundamentally considered the sum of elementary sinusoids at the constituent frequencies. According to the located evidence at the mark points, the transform decomposes the waveform into the constituent expressions of odd and even functions, characterizing a unique induced response.

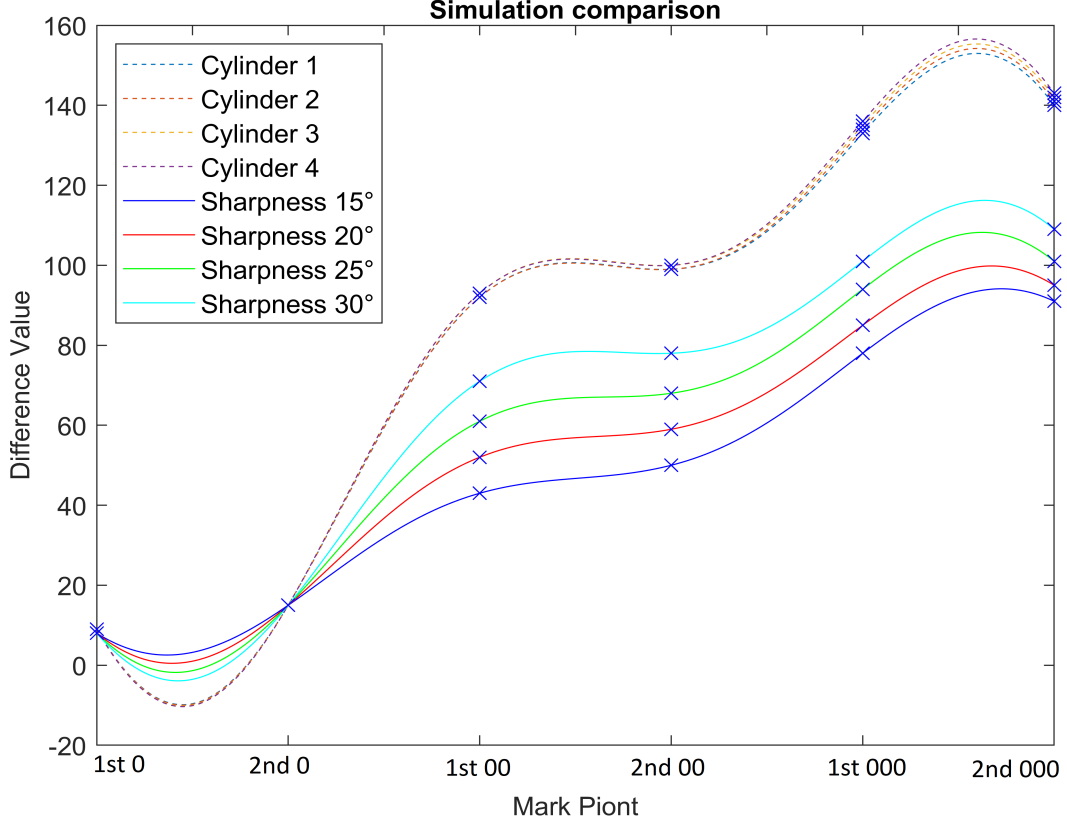


Figure 5.21: Trigonometric expression for object distinction.

Figure 5.21 obtains the apparent distinction between the threat targets with a sharp edge and no threat items of a cylinder using the Fourier series. The transformed waveform precisely expresses the distribution of labelled points to enable the classification of variable sharp-edge components, significantly different from the variation of cylindrical volumes.

The experiment employs a 2-term Fourier formula to approximate the distribution of evaluation results at the assigned spots, connecting the scattered points. The constant term a_0 is the foundation of a waveform that decides the fundamental value. The coefficients a_1 of cosine and b_1 of sine in the first term explain the general variation trend, and the increased terms provide the detailed description of fluctuation:

$$F(x) = a_0 + a_1 \cdot \cos(wx) + b_1 \cdot \sin(wx) + a_2 \cdot \cos(2wx) + b_2 \cdot \sin(2wx) \quad (5.3)$$

From the record in Table 5.14, the increased size of the cylinder enhances the constant term compared with variable sharpness, whereas the value difference significantly classifies the irregular edge of targets. The characteristics of a cylinder in different sizes give the more considerable value at the a_1 of cosine term than the changeable edge of targets. The difference

of sine value can identify the degrees of sharpness while the b1 of a variable cylinder is restricted at the low level.

Table 5.14: Fourier coefficients for cylinder and sharpness

| Target | a0 | a1 | b1 |
|--------------|-------|-------|--------|
| Cylinder 1 | 81.24 | 13.72 | -61.97 |
| Cylinder 2 | 81.58 | 14.03 | -62 |
| Cylinder 3 | 82.24 | 14.34 | -62.86 |
| Cylinder 4 | 82.58 | 14.75 | -63.2 |
| Sharpness 15 | 47.85 | 8.94 | -35.47 |
| Sharpness 20 | 52.43 | 8.56 | -38.44 |
| Sharpness 25 | 57.77 | 8.03 | -42.62 |
| Sharpness 30 | 63.59 | 7.26 | -47.03 |

Therefore, the algorithm is developed to evaluate the sine and cosine coefficients of Fourier transform based on the successive measurement at the mark points. The achievement can identify the sharpness to characterize the threat targets, differentiating from the variable nonthreatening items.

Polynomial regression

Although the trigonometrical functions can describe the change of mark points distribution, it faces limited programming application and processing speed. An alternative solution uses the nonlinear model of polynomial regression to identify the relationship of independent samples at the different mark points.

The experimental function is achieved by the embedded programming applications with a higher processing speed than the Fourier series description. The regression analysis, considered as a statistical estimation solution, models the expected multiple linear values at the degree terms, generally expressed as:

$$y = \sum_{j=1} w_j x^j \quad (5.4)$$

Where the coefficients w and predictor variable x of j degrees polynomial.

An assumption with polynomial terms typically fits the curvilinear pattern to describe the scattering phenomenon. Therefore, the parameters of the series can be evaluated to characterize the description of noted samples independently for a specific target.

The regression analysis approximates the fitting model based on the ordinary least squares,

which addresses the computational and inferential polynomial challenges. The principal operations minimize the sum of the residuals calculated at the individual equation, as shown below:

$$\hat{\beta} = \min \|A\beta - Y\|_2^2 \quad (5.5)$$

Where $\hat{\beta}$ is offset coefficients for the fitted value Y while the observed value A assigns the parameters β .

The result presents the most petite length for model and samples measurement, which closely fits the change. The fitted model identifies the variance in a prediction of the assigned mark points and minimizes the deviation from the desired value.

The analysis algorithm, based on the 6th degree polynomial, places the samples (x1, y1), (x2, y2), (x3, y3), (x4, y4), (x5, y5), (x6, y6) in the 6*6 matrix at the increasing series, as shown:

$$\begin{bmatrix} x1 & x2 & x3 & x4 & x5 & x6 \\ x1^2 & x2^2 & x3^2 & x4^2 & x5^2 & x6^2 \\ x1^3 & x2^3 & x3^3 & x4^3 & x5^3 & x6^3 \\ x1^4 & x2^4 & x3^4 & x4^4 & x5^4 & x6^4 \\ x1^5 & x2^5 & x3^5 & x4^5 & x5^5 & x6^5 \\ x1^6 & x2^6 & x3^6 & x4^6 & x5^6 & x6^6 \end{bmatrix} \begin{bmatrix} \beta_0 \\ \beta_1 \\ \beta_2 \\ \beta_3 \\ \beta_4 \\ \beta_5 \end{bmatrix} = \begin{bmatrix} \text{sum}(y) \\ \text{sum}(y^2) \\ \text{sum}(y^3) \\ \text{sum}(y^4) \\ \text{sum}(y^5) \\ \text{sum}(y^6) \end{bmatrix} \quad (5.6)$$

The solution eliminates with maximum column pivoting, where it finds the most significant absolute value as the pivot, then interchange the row and substitute backward for the answer. The embedded software program is designed to calculate the coefficients by the elimination method, which can predict the behaviour of independent collections. Accordingly, the programming design interfaces the hardware development solution, assisting the target identification based on the marked data collection.

Table 5.15: Polynomial parameters for cylinder and sharpness

| Target | x^5 | x^4 | x^3 | x^2 | x^1 | x^0 |
|--------------|-------|-------|-------|-------|-------|-------|
| Cylinder 1 | -3.24 | 58.54 | -398 | 1252 | -1743 | 842 |
| Cylinder 2 | -3.27 | 59.08 | -401 | 1261 | -1254 | 847 |
| Cylinder 3 | -3.31 | 59.70 | -405 | 1276 | -1274 | 857 |
| Cylinder 4 | -3.34 | 60.25 | -409 | 1285 | -1286 | 862 |
| Sharpness 15 | -1.35 | 23.75 | -156 | 478 | -646 | 310 |
| Sharpness 20 | -1.61 | 28.67 | -192 | 595 | -815 | 393 |
| Sharpness 25 | -1.93 | 34.67 | -234 | 730 | -1007 | 485 |
| Sharpness 30 | -2.15 | 39.16 | -267 | 845 | -1177 | 570 |

Table 5.15 gives the coefficients for different terms used to differentiate the specific cases between the regular shape and sharp edge targets. The experimental result indicates that for the basis and first degrees, the parameters present a considerable difference for threat identification. Therefore, the prototype, defined by basic parameters of polynomial equations, determines the general description for features classification.

As the series increased, the result gives a detailed description that fits the required model to the samples for precise classification. Therefore, the evaluation of the basis coefficients coordinates the assessment at higher terms achieves the threat identification and the recognisable differentiation for target characteristics.

The algorithms using trigonometric and polynomial expression are innovatively developed to produce a unique waveform that involves the samples collected at the mark points. The coefficients of the algorithmic function determine the distribution of evaluation evidence at the mark points, enabling the feature identification of sharpness. However, the preprocessing for algorithm application conducts the signal normalization for the specific induced responses of all targets. The detection techniques challenge the overall calibration to enable particular parameters to be identified.

5.5.3 Comprehensive analysis

The detection project employs the advanced method to identify the induced response based on the delay duration evaluation in conjunction with the decay assessment. It also confirms the feasibility of the novel algorithm to comprehensively measure the mark points, contributing to threat identification of a target regarding the sharpness analysis.

For the practical application of detection structure, the proposed system measures delay duration from the received data of induction on the FPGA platform. It can provide a reasonable

estimation of the size and distance depending on the relationship model. Simultaneously, the identification of decay phase evaluates the mark points at the single bit sequence after the $\Sigma\Delta$ conversion, forming the associative digit group for distinction.

The distribution of the serial labelled spots produces a unique waveform that represents the characteristics of a specific target. The algorithm gives the distinguishable coefficients to identify the critical features of sharpness, deciding a threat component. Eventually, the system result displays the primary features of a detected target in terms of material, size, shape and distance, and estimates the potentiality of danger depending on the sharpness.

Overall, the novelty of the weapon detection scheme applied the FPGA-based evaluation of delay duration and the algorithm of mark points for the decay analysis to describe the featured induced signature and define the significant characteristics of a target. Therefore, the research proves that the innovative algorithm defines the decisive features to discriminate a threat target, concealed under the cloth across the open detection area.

5.6 Summary

The experimental detection scheme fundamentally evaluates the system results based on the object modelling configured with varying parameters individually. The system processing provides the progress outcomes at the module stages for the functional analysis. Meanwhile, the functional processing simulation produces the digital outcome assessment to define the target characteristics description.

The experimental verification compares the practical results on the FPGA platform and simulated solution to achieve the analytical correspondence. The system delivers the outcome evaluation to identify the threatening feature changes based on the variable edge of the detected object. In addition, the simulated analysis realizes the varying size of cylinder demonstration to determine the same examination results as the practical processing.

The feature identification algorithm develops the mark points evaluation based on the delay and decay sections to determine the induced response changes, describing the target characteristics. The system solution investigates the main parameter variation in terms of material, shape, size and detection distance for the feature recognition. Furthermore, the algorithm development contributes to the potential threat identification for the sharpness assessment.

The result discussion delivers the result analysis for the delay phase to present the mathematical

relationship between the target size and detection distance. The project also provides the feature distinction solution of trigonometric expression and polynomial regression to evaluate the decay phase of response signature for the object characteristics classification.

Chapter 6

Conclusions and Future Work

The achievements and conclusions for the proposed concealed weapon detection design in the open area environment are presented. Additionally, further work to improve the detection accuracy and processing speed of the detection system implementation and application is proposed.

6.1 Conclusions

This research project was committed to proposing an innovative detection system for concealed weapons recognition in open area environments. For threat target identification hidden under clothes, the developed solution applied the PI technology to pinpoint a featured component of a conductive target object, using the electromagnetic response. The novelty of the classification scheme was demonstrated to functionally define the induced response, thereby determining the characteristics of the target detection. From the framework of the project, the simulation procedure and practical experiment examined the feasibility and effectiveness of the alarm application for the open area under surveillance. The proposed algorithm realised the systematic optimisation to efficiently identify the characteristics of an object which presents the potential threat.

As the conventional techniques reviewed, electromagnetic detection exposed the functional deficiency of threat recognition intelligence and the potential for information leaks to occur with the imaging display applications. However, neither the image-based nor signal-based method solves real-time threat identification due to the massive information for analysis. The

efficient and economical platform of FPGA provided tremendous advantages over the different signal digitalization apparatuses in the open area practices. As a result, the project decided to implement the detection scheme on the FPGA to improve efficiency, dynamically identifying the potential of the threat.

The project demonstration structurally depended on the specific cases with the variable parameters, realized in both simulated and practical scenes. The mutual verification and supplement of module achievements functionally testified to the feasibility of a systematic detection procedure as a whole. Firstly, the electromagnetic induction theory clarified the operating principle of detectors, deploying the multi-sensor structure in the open area. The design employed the PI architecture to capture the induced response, conveniently disposed at a standoff distance for the concealed weapons recognition. Moreover, the mathematical derivation proved the theoretical basis that a unique induced response determines the characteristics of the detected object, also demonstrated by the simulation cases analysis.

The developed scheme fundamentally required the search coil and experimental circuitry in coordination with the FPGA expansion board. According to the arrangement of the analogue circuit, the pulse was produced to the coil as the transmitter while the receiver achieved the signal amplification and wave adjustment. The practical experimentation produced the distinct difference between cases by the frequency configuration, benefiting the objects recognition.

For the analogue waveform conversion, the induced response landed on the programming board and synchronously obtained the digital data translation. The FPGA-based procedure realized the data simplification to represent the time-varying signal for distinction, where the onboard $\Sigma\Delta$ modulation developed a single-bit data flow. The section division of binary sequence spotlighted the decay monitoring to examine the continuous low-level signal, considering the efficient recognition of object features. Therefore, the assessment of mark points at the decay duration was testified to distinguish the objects for the variable characteristics.

Meanwhile, the process simulation of two-variable cases demonstrably discriminated the similar induced response from the record of mark points. The classification of noted samples at the decay also was capable of distinguishing between the varying simulated cases of varying edge. The experimental result initially verified that the delay extension record decides the induction density, smoothing the peak of the response. The mark points collection at the single, double and triple 0 subsequently realized the distinction between the practical objects with variable parameters.

The algorithm optimization of successive assessment at mark points enhanced the identification and classification of specific events for the weapons detection system. The practical testing of the scheduled approach classified the characteristics of targets regarding the irregular edge and variable cylinder demonstration, thereby achieving feature description. Meanwhile, the simulation procedure verified the feature identification and classification of object detection practices.

The weapon detection design developed the object identification algorithm to determine the critical characteristics of a specified target object parameter - material, size, shape and detection distance. The delay and mark points duration within the object signature enables realize the object parameter identification. The detection method examined the sharpness to define the potential threat, where the system development can distinguish the threatening components and the innocuous items.

Overall, the suggested detection system contributes a hybrid evaluation method at the delay and decay phrases, which demonstrates high efficiency and performance of threat features. As the delay extension defined, the mathematical function reveals a reasonable inference of the size and distance of a target based on the exponential relationship. Furthermore, the decay analysis of a target induction uniquely identifies the characteristics of a potential threat, thus digitalizing and optimizing the data process.

The advantage of mark points measurement provides the efficient identification of a variable target, significantly avoiding the information excess and overload. The developed algorithm functionally extracts the featured digital data to represent the unique induced response, which defines the object characteristics for threat discrimination. It benefits the auto-classification of potential weapons once positive match with the risk descriptors. The technique also features the rapidly synchronous data acquisition for real-time detection instead of imaging, reducing manual misjudgements.

The proposed solution realizes the multiple array detection for an uncontrolled visitor flow under the open area surveillance, contributing to the efficient assessment speed over the serial walk-through metal scanning. Meanwhile, the project achieves the autonomous threat identification ability to alarm the potential weapons, replacing the artificial decision-making by imaging. The economical application based on the FPGA processing saves the cost of computational data analysis and supporting devices like cameras for the imaging detection system.

Therefore, the development of a CWD system with the novel algorithm evaluates the characteristics of an object to define the potential threat, depending on the evidence distribution of mark points. The technique performance realizes the accurate distinction between the threat and no-threat targets and efficiently classifies the levels of risk at an open area.

6.2 Future work

The achievement of the weapon detection project develops the novel identification method to define and distinguish the critical characteristics of a threat component, as the experimental work demonstrated. The system development requires efficient data processing and precise threat determination to realize the real-time weapon detection performance in the further stage. The prospective advancement involves the developed detection techniques for complex object structures and multiple objects recognition. In addition to the system design of the sensor arrangement within an open area array configuration, the integration of a facility for tracking, recording and display of threat object trajectories will enable a comprehensive system to be realized.

The sigma-delta modulation realizes the analogue signal translation to a digital binary sequence signature for data simplification; however, to enhance the performance of the detection system, the future processing scheme will need to consider the inclusion of a specialized modulation chip with a stable and speedy response to process the analogue signal. Simultaneously, proficient data processing reduces the error and resists disturbance to enhance the reliability of digital conversion, synchronizing the object identification in real-time.

The work demonstrates the effective recognition method for the single target description, while the multi-object detection requires further development to monitor the multiple and combined components in the detecting environment. To realize the multi-target monitoring necessary, the functional improvement of target identification applications requires identifying segmentation for multiple objects investigation. Additionally, the detection design realizes the intelligent recognition to extract the decisive information from the combination of different particular components in the simultaneous detection phenomenon.

The sensor system arrangement requires the tracking function to exhibit the moving path of weapon assignment in an open area, suggesting the carrier in the uncontrolled pedestrian flow. The robust detection program of the sensor framework logically connects the elemental

transducers to monitor the individual domain, which infers a moving path of suspicious items accessing the zone. The sensor placement applications of the identification algorithm implementation visualize positive tracks of a concealed weapon once defining the threat features. Therefore, the detection system development incorporates the benefits of efficient target recognition and powerful weapon tracking, contributing to public security in an open area.

References

- [1] Shanthi, P., Richard, S., & Gabor, T. (2017). Understanding Delta-Sigma data converters (2nd ed.). Wiley, doi: 10.1002/9781119258308.
- [2] Bandyopadhyay, S. K., Datta, B., & Roy, S. (2012). Identifications of concealed weapon in a Human Body. International Journal of Scientific & Engineering Research, doi: arXiv:1210.5653.
- [3] Westminster Group (2015) <https://www.wi-ltd.com/product/walk-through-metal-detector> (accessed July 29, 2021).
- [4] Westminster International LTD. (2019). WG SX-I Walk Through Metal Detector [brochure]. Westminster International LTD.
- [5] İşiker, H., Ünal, L., Tekbaş, M., & Özdemir, C. (2018). An auto-classification procedure for concealed weapon detection in millimeter-wave radiometric imaging systems. Microwave and Optical Technology Letters, 60(3), 583-594. doi: 10.1002/mop.31005.
- [6] Xiang, S., & Jian, C. (2019). Development of a standoff terahertz imaging system for concealed weapon detection. Microwave and Optical Technology Letters, 61(4), 1116-1120. doi: 10.1002/mop.31688.
- [7] Parande, M., & Soma, S. (2015). Concealed Weapon Detection in a Human Body by Infrared Imaging. International Journal of Science and Research, 4(9), 182-188.
- [8] Patriot One Technologies. (2021). Multi-Sensor Gateway: Threat Detection Of Concealed Weapons. Patriot One Technologies. <https://patriot1tech.com/patscan/multi-sensor> (accessed Aug 24, 2021).

- [9] Dempsey, M. (2020). The hidden detectors looking for guns and knives. BBC News. <https://www.bbc.co.uk/news/business-52734768> (accessed Aug 24, 2021).
- [10] Buckchash, H., & Raman, B. (2017). Raman. A robust object detector: Application to detection of visual knives, Hong Kong, China, 633-638. doi:10.1109/ICMEW.2017.8026214.
- [11] Zhuge, X., & Yarovoy, A. G. (2011). A Sparse Aperture MIMO-SAR-Based UWB Imaging System for Concealed Weapon Detection. *IEEE Transactions on Geoscience and Remote Sensing*, 49(1), 509-518. doi: 10.1109/TGRS.2010.2053038.
- [12] Shi, X., & Chen, J. (2019). Development of a standoff terahertz imaging system for concealed weapon detection. *Microwave and optical technology letters*, 61(4), 1116-1120, doi: 10.1002/mop.31688.
- [13] Jyo, T., Hamada, H., Kitayama, D., Yaita, M., & Nosaka, H. (2018). An Accurate Permittivity Measurement Using Interferometric Phase Noise Averaging for Terahertz Imaging. *IEEE Transactions on Terahertz Science and Technology*, 8(3), 278-286, doi: 10.1109/TTHZ.2018.2803445.
- [14] Malik, M. U., Ahmed, W., Majid, A., & Yaqoob, Z. (2017). Learning augmented standoff Concealed Weapon Detection. 2017 14th International Bhurban Conference on Applied Sciences and Technology, , 830-837, doi: 10.1109/IBCAST.2017.7868153.
- [15] Haynes, W. M. (2011). *CRC Handbook of Chemistry and Physics* (92th ed.). Boca Raton, Florida, United States: CRC Press.
- [16] Shen, X., Charles, R.D., Erich, G., & Zoya, P. (2008). Detection and Segmentation of Concealed Objects in Terahertz Images. *IEEE Transactions on Image Processing*, 17 (12), 2465-2475.
- [17] Ospald, F., Zouaghi, W., Beigang, R., Matheis, C., & Jonuscheit, J. (2014). Aeronautics composite material inspection with a terahertz time-domain spectroscopy system. *OPTICAL ENGINEERING*, 53 (3).
- [18] John H. Glenn Research Center (2011). Non-Contact Measurement of Density and Thickness Variation in Dielectric Materials. Retrieved from <https://www.techbriefs.com/component/content/article/tb/techbriefs/physical-sciences/3523> (accessed July 19, 2021).

- [19] Dolganova, I. N., Zaytsev, K. I., Metelkina, A. A., Yakovlev, E. V., Karasik, V. E., & Yurchenko, S. O. (2016). Combined terahertz imaging system for enhanced imaging quality. *Optical and quantum electronics*, 48(6), 1-8, doi: 10.1007/s11082-016-0590-2.
- [20] Piotr Garbacz. (2016). Terahertz Imaging - Principles, Techniques, Benefits and Limitations. Retrieved from <https://www.researchgate.net/publication/298911597-Terahertz-Imaging-Principles-Techniques-Benefits-and-Limitations>.
- [21] Lewis, R.A. (2012). *Terahertz Physics*. The Edinburgh Building, Cambridge CB2 8RU, UK: Cambridge University Press.
- [22] Kathryh, V.L., David, J.B., Edward, A.D., & Leon, F.M. (2017). Millimeter Wave Advanced Imaging Technology. In. (Ed.) *Airport Passenger Screening Using Millimeter Wave Machines* (pp. 16-22). Washington, DC: The national academic press.
- [23] Meng, Y., Qing, A.Y., Lin, C., & Zhao, Y.Z. (2018). Passive Millimeter Wave Imaging System Based on Helical Scanning. *Scientific Reports*, 8 (1), 7852-7864. doi: 10.1038/s41598-018-25637-9.
- [24] Harwood, M. (2010). Companies Seek Full-Body Scans That Ease Health, Privacy Concerns. *Security Management*. Retrieved from <https://web.archive.org/web/20141006112416/http://securitymanagement.com/news/companies-seek-full-body-scans-ease-health-privacy-concerns-006852>. (accessed July 19, 2021).
- [25] May, J.W. & Rebeiz, G.M. (2010). Design and Characterization of W-Band SiGe RFICs for Passive Millimeter-Wave Imaging. *IEEE Transactions on Microwave Theory and Techniques*, 58 (5), 1420-1430. doi: 10.1109/TMTT.2010.2042857.
- [26] Laskey, M. (2010). An Assessment of Checkpoint Security: Are Our Airports Keeping Passengers Safe?. Retrieved from <https://web.archive.org/web/20121213155345/http://democrats.homeland.house.gov/SiteDocuments/20100317140311-88574.pdf>. (accessed July 19, 2021).
- [27] Michael, A.J. & Chang, Y.W. (2001). Portable concealed weapon detection using millimeter-wave FMCW radar imaging. *Proceedings of SPIE*, 4231 (1), 134-141. doi:

10.1117/12.417525.

- [28] Schopper, F., Ninkovic, J., Richter, R., Schaller, G., & Selle, T. (2018). High resolution X-ray imaging with pnCCDs. *Nuclear Inst. and Methods in Physics Research*, 912, 11-15. doi: 10.1016/j.nima.2017.10.004.
- [29] Iwanczyk, J.S., Nygard, E., Meirav, O., Arenson, J., & Barber, W.C. (2009). Photon Counting Energy Dispersive Detector Arrays for X-ray Imaging. *IEEE Transactions on Nuclear Science*, 56 (3), 535-542. doi: 10.1109/TNS.2009.2013709.
- [30] Kim, Y.C., Kim, K.H., Son, D.Y., Jeong, D.N., & Seo, J.Y. (2017). Printable organometallic perovskite enables large-area, low-dose X-ray imaging. *Nature International journal of science*, 550 (7674), 87-91. doi: 10.1038/nature24032.
- [31] U.S. Food & Drug Administration (2019). Medical X-ray Imaging. Retrieved from <https://www.fda.gov/radiation-emitting-products/medical-imaging/medical-x-ray-imaging#description> (accessed July 19, 2021).
- [32] Pastorino, M. (2010). *Microwave imaging*. John Wiley & Sons, Inc., Hoboken, New Jersey: Wiley.
- [33] Kurrant, D., Bourqui, J., & Fear, E. (2017). Surface estimation for microwave imaging. *Sensors (Switzerland)*, 17 (7), 1658-1678.
- [34] Vakalis, S., & Nanzer, J. A. (2018). Microwave Imaging Using Noise Signals. *IEEE Transactions on Microwave Theory and Techniques*, 66 (12), 5842-5851.
- [35] Abou-Khousa, M.A., Rahman, M.S.U., & Xie, X. (2019). Dual-Polarized Microwave Imaging Probe. *IEEE Sensors Journal*, 19 (5), 1767-1776.
- [36] Meola, C. (2012). *Infrared thermography: recent advances and future trends*. Sharjah, United Arab Emirates: Bentham Science.
- [37] Giri, L. & Tuli, S. (2014). Frequency modulated infrared imaging for thermal characterization of nanomaterials. *Infrared Physics and Technology*, 67, 526-630. doi: 10.1016/j.infrared.2014.09.033.
- [38] Lahiri, B.B., Bagavathiappan, S., Jayakumar, T., & Philip, J. (2012). Medical applications of infrared thermography: A review. *Infrared Physics and Technology*, 55 (4), 221-235. doi:

- 10.1016/j.infrared.2012.03.007.
- [39] Chen, H.M., Lee, S., Rao, R.M., Slamani, M.A., & Varshney, P.K. (2005). Imaging for concealed weapon detection: a tutorial overview of development in imaging sensors and processing. *IEEE Signal Processing Magazine*, 22 (2), 52-61. doi: 10.1109/MSP.2005.1406480.
- [40] José, M. C. (2015). *Wave Fields in Real Media: Wave Propagation in Anisotropic, Anelastic, Porous and Electromagnetic Media* (3rd ed.). Amsterdam, Netherlands: Elsevier Science.
- [41] Johnson, W. C. (2014). *Electromagnetic wave transmission*. In AccessScience. McGraw-Hill Education. <https://doi.org/10.1036/1097-8542.222900>.
- [42] Marsh, L.A., Christos, K., & Armitage, D.W. (2013). Three-dimensional object location and inversion of the magnetic polarizability tensor at a single frequency using a walk-through metal detector. *Measurement Science and Technology*, 24 (4), doi: 10.1088/0957-0233/24/4/045102.
- [43] Mesnik, B. (2018). How Walk-Through Metal Detectors Work. Retrieved from <https://kintronics.com/walk-metal-detectors-work>. (accessed July 19, 2021).
- [44] Garrett Metal Detectors. (2019). Garrett PD 6500i Enhanced Pinpoint Walk-Through Metal Detector [Online image]. Retrieved from <https://www.garrett.com/security/walk-through/pd-6500i-walk-through-metal-detector>. (accessed July 19, 2021).
- [45] Marsh, L. A., Makkonen, J., Vihonen, J., Visa, A., Järvi, A., Armitage, D. W., & Peyton, A. J. (2013). Investigation of the significance of the ‘body effect’ on sensitivity to metallic objects in a walk-through metal detector. *Journal of Physics: Conference Series*, 450(1), doi: 10.1088/1742-6596/450/1/012037.
- [46] Horowitz, P., & Hill, W. (2015). *The Art of Electronics: The x Chapters* (3rd ed.). United States: Cambridge University Press.
- [47] Tian, G., Al-Qubaa, A., & Wilson, J. (2012). Design of an electromagnetic imaging system for weapon detection based on GMR sensor arrays. *Sensors & Actuators: A. Physical*, 174(1), 75-84. doi: 10.1016/j.sna.2011.11.034.

- [48] Shi, X., & Chen, J. (2019). Development of a standoff terahertz imaging system for concealed weapon detection. *Microwave and Optical Technology Letters*, 61(4), 1116-1120. doi: 10.1002/mop.31688.
- [49] Rob, W., Max, J., Abbi, L., Stuart, T., & Joe, C. W. (2017). Magnetic induction tomography of objects for security applications. *Proceedings of SPIE - The International Society for Optical Engineering*, 10438, doi: 10.1117/12.2278888.
- [50] Ma, L., & Soleimani, M. (2017). Magnetic induction tomography methods and applications: A review. *Measurement Science and Technology*, 28(7), doi: 10.1088/1361-6501/aa7107.
- [51] Wei, H. Y., Ma, L., & Soleimani, M. (2012). Volumetric magnetic induction tomography. *Measurement Science and Technology*, 23(5), doi: 10.1088/0957-0233/23/5/055401.
- [52] Li, F., Abascal, J. F. P. I., Desco, M., & Soleimani, M. (2017). Total Variation Regularization With Split Bregman-Based Method in Magnetic Induction Tomography Using Experimental Data. *IEEE Sensors Journal*, 17(4), 976-985. doi: 10.1109/JSEN.2016.2637411.
- [53] Renner, A., Marschner, U., & Fischer, W. (2014). A new imaging approach for in situ and ex situ inspections of conductive fiber-reinforced composites by magnetic induction tomography. *Journal of Intelligent Material Systems and Structures*, 25(9), 1149-1162. doi: 10.1177/1045389X13507349.
- [54] Walker, D. W., Kramer, S. C., Biebl, F. R. A., Ledger, P. D., & Brown, M. (2019). Accelerating magnetic induction tomography-based imaging through heterogeneous parallel computing. *Concurrency and Computation: Practice and Experience*, 31(17), doi: 10.1002/cpe.5265.
- [55] Zolgharni, M., Griffiths, H., & Ledger, P. D. (2010). Frequency-difference MIT imaging of cerebral haemorrhage with a hemispherical coil array: numerical modelling. *Physiological Measurement*, 31(8), 111-125. doi: 10.1088/0967-3334/31/8/S09.
- [56] Pacheco, P. S. (2011). *An Introduction to Parallel Programming*. Amsterdam, Netherlands: Elsevier/Morgan Kaufmann.
- [57] Rosenberg, J. (2017). Chapter 6 - Security in embedded systems. In A. Vega, P. Bose, & A. Buyuktosunoglu (Eds.) *Rugged Embedded Systems*. (pp. 149-205) . Burlington,

- Massachusetts: Morgan Kaufmann.
- [58] Bertil, S., Jorge, G., & Moritz, S. (2017). *Parallel Programming: Concepts and Practice*. Burlington, Massachusetts: Morgan Kaufmann Publishers Inc.
- [59] Wolf, M. (2017). *Computers as components: principles of embedded computing system design* (4th ed.). Burlington, Massachusetts: Morgan Kaufmann Publishers.
- [60] Tan, L., & Jiang, J. (2019). *Digital Signal Processing: Fundamentals and Applications* (3rd ed.). Cambridge, Massachusetts: Academic Press.
- [61] Oshana, R. (2006). *DSP software development techniques for embedded and real-time systems*. Oxford and Boston: Newnes.
- [62] Yiu, J. (2010). *The Definitive Guide to the ARM Cortex-M3* (2nd ed.). Oxford and Boston: Newnes.
- [63] Parker, M. Altera Corporation. (2017). *FPGA vs. DSP Design Reliability and Maintenance*. Retrieved from <https://www.intel.com/content/dam/www/programmable/us/en/pdfs/literature/wp/wp-01023.pdf>. (accessed July 19, 2021).
- [64] Sinclair, L. (2011). *Electronics Simplified* (3rd ed.). Oxford, London: Newnes.
- [65] Wade, M. T., Sun, C., Lee, Y., & Orcutt, J. S. (2015). Single-chip microprocessor that communicates directly using light. *Nature*, 528(7583), 534-538. doi: 10.1038/nature16454.
- [66] Wachter, S., Polyushkin, D., & Bethge, O. (2017). A microprocessor based on a two-dimensional semiconductor. *Nature communications*, 8(1). doi: 10.1038/ncomms14948.
- [67] Kong, J., chung, S., & Skadron, K. (2012). Recent thermal management techniques for microprocessors. *ACM Computing Surveys (CSUR)*, 44(3), 1-42. doi: 10.1145/2187671.2187675.
- [68] Uttamchandani, D. (2016). *Wireless MEMS Networks and Applications*. Sawston, Cambridge: Woodhead Publishing.
- [69] Wilson, P. (2017). *The Circuit designer's companion* (4th ed.). Oxford and Boston: Newnes.
- [70] Mittal, S. (2018). A survey of FPGA-based accelerators for convolutional neural networks. *Neural Computing and Applications*, 32(4), 1109-1139. doi: 10.1007/s00521-018-3761-1.

- [71] Peter, W. (2016). Design Recipes for FPGAs: Using Verilog and VHDL (2nd ed.). Oxford and Boston: Newnes Publisher.
- [72] Winser, A., & Cranos, W. (2017). Digital Signal Processing: Principles, Algorithms and System Design. Cambridge, Massachusetts: Academic Press.
- [73] Brownlee , J. (2019). A Gentle Introduction to Object Recognition With Deep Learning. Retrieved from <https://machinelearningmastery.com/object-recognition-with-deep-learning>. (accessed July 19, 2021).
- [74] Bavirisetti, D. P., & Dhuli, R. (2016). Two-scale image fusion of visible and infrared images using saliency detection. *Infrared Physics and Technology*, 76, 52-64. doi: 10.1016/j.infrared.2016.01.009.
- [75] Lee, D., Yeom, S., & Kim, S. (2010). Automatic image segmentation for concealed object detection using the expectation-maximization algorithm. *Optics express*, 18(10), 10659-10667. doi: 10.1364/OE.18.010659.
- [76] Du, L., Li, L., Wei, D., & Mao, J. (2019). Saliency-Guided Single Shot Multibox Detector for Target Detection in SAR Images. *Institute of Electrical and Electronics Engineers (IEEE)*, 58(5), 1-11. doi: 10.1109/tgrs.2019.2953936.
- [77] Liu, W., Anguelov, D., Erhan, D., Szegedy, C., & Reed, S. (2016). SSD: Single Shot MultiBox Detector. *Computer Vision – ECCV 2016* , 9905, doi: 10.1007/978-3-319-46448-0_2.
- [78] Miao, X., Liu, X., Chen, J., Zhuang, S., Fan, J., & Jiang, H. (2019). Insulator Detection in Aerial Images for Transmission Line Inspection Using Single Shot Multibox Detector. *Institute of Electrical and Electronics Engineers (IEEE)*, , 9945-9956. doi: 10.1109/ACCESS.2019.2891123.
- [79] Pierluigi, C., Marco, D., Marco , L., & Cosimo, D. (2015). Facial expression recognition and histograms of oriented gradients: a comprehensive study. *Springer Science and Business Media LLC*, 4(1), 1-25. doi: 10.1186/s40064-015-1427-3.
- [80] N. Dalal and B. Triggs. (2005). Histograms of oriented gradients for human detection, 2005 IEEE Computer Society Conference on Computer Vision and Pattern Recognition (CVPR'05), San Diego, CA, USA, pp. 886–893 vol. 1. doi: 10.1109/CVPR.2005.177.

- [81] Ross, G., Jeff, D., Trevor, D., & Jitendra, M. (2014). Rich Feature Hierarchies for Accurate Object Detection and Semantic Segmentation. IEEE Conference on Computer Vision and Pattern Recognition, Columbus, OH, USA.
- [82] Md Zahangir, A., Tarek, M. T., Chris, Y., & Stefan, W. (2019). A State-of-the-Art Survey on Deep Learning Theory and Architectures. MDPI AG, 8(3), doi: 10.3390/electronics8030292.
- [83] S, Pulkit. (2108). A Step-by-Step Introduction to the Basic Object Detection Algorithms. Analytics Vidhya. Retrieved from <https://www.analyticsvidhya.com/blog/2018/10/a-step-by-step-introduction-to-the-basic-object-detection-algorithms-part-1> (accessed July 19, 2021).
- [84] Pirkle, W. C. (2019). Designing Audio Effect Plugins in C++: For AAX, AU, and VST3 with DSP Theory (2nd ed.). London, United Kingdom: Routledge, Taylor & Francis Group.
- [85] Ineneji, C., & Kusaf, M. (2019). Hybrid weapon detection algorithm, using material test and fuzzy logic system. Computers and Electrical Engineering, 78, 437-448. doi: 10.1016/j.compeleceng.2019.08.005.
- [86] Li, Y., Tian, G., Bowring, N., & Rezgui, N. (2008). A microwave measurement system for metallic object detection using swept-frequency radar. Millimetre Wave and Terahertz Sensors and Technology, 7117(1), doi: 10.1117/12.801671.
- [87] Li, Y., & Tian, G. A radio-frequency measurement system for metallic object detection using pulse modulation excitation. 17th World Conference on Nondestructive Testing (WCNDT), Shanghai, China.
- [88] Sweet, D. M., Meissner, C. A., & Atkinson, D. J. (2017). Assessing law enforcement performance in behavior-based threat detection tasks involving a concealed weapon or device. Law and Human Behavior, 41(5), 411-421. doi: 10.1037/lhb0000243.
- [89] Alencar, P., & Cowan, D. (2012). Handbook of Research on Mobile Software Engineering: Design, Implementation, and Emergent Applications. Hershey, Pennsylvania, USA: IGI Global.
- [90] Rashvand, H. F., & Abedi, A. (2017). Wireless Sensor Systems for Extreme Environments: Space, Underwater, Underground, and Industrial. Hoboken, New Jersey: Wiley.

- [91] Meijer, G., Pertijs, M., & Makinwa, K. (2014). Smart sensor systems: emerging technologies and applications. Hoboken, New Jersey: IEEE Press.
- [92] Pati, P. (2016). Finite element analysis approach to open area concealed weapon detection system (Doctoral thesis). University of Huddersfield, Huddersfield.
- [93] Zhu, W., Yin, W., Dewey, S., Hunt, P., Davis, C. L., & Peyton, A. J. (2017). Modeling and experimental study of a multi-frequency electromagnetic sensor system for rail decarburisation measurement. *NDT and E International*, 86, 1-6. doi: 10.1016/j.ndteint.2016.11.004.
- [94] York, T., McCann, H., & Ozanyan, K. B. (2011). Agile Sensing Systems for Tomography. *IEEE Sensors Journal*, 11(12), 3086-3105. doi: 10.1109/JSEN.2011.2164905.
- [95] Law, J. & Rennie, R. (2015). *A Dictionary of Physics* (7th ed.). England: Oxford University Press.
- [96] Ammari, H., Han, W., Darko, V., Chen, J., & Chen, M. (2015). Detection and classification from electromagnetic induction data. *Journal of Computational Physics*, 301, 201-217. doi: 10.1016/j.jcp.2015.08.027.
- [97] Anderson, T. S., McCarthy, M. P., & Holzworth, R. H. (2020). Detection of VLF Attenuation in the Earth-Ionosphere Waveguide Caused by X-Class Solar Flares Using a Global Lightning Location Network. *Space Weather*, 18(3), doi: 10.1029/2019SW002408.
- [98] Kim, B., Yoon, J.W., Lee, S., Han, S., & Kim, K. (2015). Pulse-induction metal detector with time-domain bucking circuit for landmine detection. *Electronics Letters*, 51 (2), 159-161. doi: 10.1049/el.2014.3895.
- [99] Tyson, J. (2001). How Metal Detectors Work. Retrieved from <https://electronics.howstuffworks.com/gadgets/other-gadgets/metal-detector.htm>. (accessed July 19, 2021).
- [100] Reed, M.A. & Scott, W.R. (2014). Implementation of optimized electromagnetic induction coils. *Proceedings of SPIE - The International Society for Optical Engineering*, 9072. doi: 10.1117/12.2050464.

- [101] Rerkratn, A., Petchmaneelumka, W., Kongkauropham, J., Kraisoda, K., & Kaewpoonsuk, A. (2011). Pulse Induction Metal Detector Using Sample and Hold Method. 2011 11th International Conference on Control, Automation and Systems, 45-48.
- [102] Grant, I. S., & Phillips, W. R. (2013). *Electromagnetism* (2nd ed.). John Wiley & Sons.
- [103] Owen, G. E. (2017). *Electromagnetic Theory*. Mineola, NY: Dover Publications.
- [104] Billingham, J., & King, A. C. (2012). *Electromagnetic Theory*. Cambridge University Press.
- [105] Siegel, D. M. (2010). *Innovation in Maxwell's Electromagnetic Theory: Molecular Vortices, Displacement Current, and Light*. Cambridge University Press.
- [106] Fleisch, D. (2011). *A Student's Guide to Maxwell's Equation*. The Edinburgh Building, Cambridge, UK: Cambridge University Press.
- [107] Santiago, J.o.h.n. (2013). *Circuit Analysis For Dummies*. Hoboken, New Jersey: John Wiley & Sons, Inc.
- [108] Boylestad, R.L. (2016). *Introductory circuit analysis* (13th ed.). Cambridge, United Kingdom: Pearson.
- [109] COMSOL Multiphysics. Understand, Predict, and Optimize Physics-Based Designs and Processes with COMSOL Multiphysics. COMSOL. <https://uk.comsol.com/comsol-multiphysics> (accessed July 19, 2021).
- [110] Kovertz, A. (2006). *Electromagnetic theory*. Oxford science publications: Oxford University Press.
- [111] Bishop, O. (2011). *Electronics: circuits and systems* (4th ed.). Oxford, United Kingdom: George Routledge.
- [112] Baker, B.C. (2011). How delta-sigma ADCs work. *Analog Design Journal*, 3, 13-16. Retrieved from <http://www.ti.com/lit/an/slyt423a/slyt423a.pdf>. (accessed July 19, 2021).
- [113] Chen, F., Li, X., & Kraft, M. (2016). Electromechanical Sigma-Delta Modulators (M) Force Feedback Interfaces for Capacitive MEMS Inertial Sensors: A Review. *IEEE Sensors Journal*, 16 (17), 6476-6495. doi: 10.1109/JSEN.2016.2582198.

- [114] Rosa, J.M. & Rio, R. (2013). CMOS sigma-delta converters: practical design guide (3rd ed.). University of Seville, Spain: Wiley-Blackwell.
- [115] Rana, S., George, B., & Kumar, V.J. (2015). Sigma-Delta Digital Converter Suitable for a Resistive Displacement Sensor with a Floating Slide. *IEEE Transactions on Instrumentation and Measurement*, 65 (3), 502-509. doi: 10.1109/TIM.2015.2499018.
- [116] Krieger, J.D., Yeang, C., & Wornell, G.W. (2013). Dense Delta-Sigma Phased Arrays. *IEEE Transactions on Antennas and Propagation*, 61 (4), 1825-1837. doi: 10.1109/TAP.2013.2241719.
- [117] Serway, A. R., Jewett, J. W., Wilson, J., Wilson, A., & Rowlands, W. (2016). *Physics for global scientists and engineers* (2nd ed.). Australia: Cengage Learning.
- [118] All About Circuits. Inductor Sizing Equation Chapter 1 - Useful Equations And Conversion Factors. All About Circuits. <https://www.allaboutcircuits.com/textbook/reference/chpt-1/inductor-sizing-equation> (accessed July 19, 2021)
- [119] Mather, P., Pati, P. (2010) "Transmitter & Receiver Coil Design for Open Area Concealed Weapon Detection System", CWIEME Chicago 2010, Chicago, USA.
- [120] Franco, S. (2015). *Design with operational amplifiers and analogue integrated circuits* (4th ed.). New York, United States: McGraw Hill Education.
- [121] Raj, A. Circuit Digest. (2018). Differential Amplifier or Voltage Subtractor Circuit. Retrieved from <https://circuitdigest.com/electronic-circuits/differential-amplifier-or-voltage-subtractor-circuit> (accessed July 19, 2021).
- [122] Guatieri, S., Badaracco, G., Defilippis, I., & Barrettino, D. (2016). Pulse induction parking sensor. In 2016 IEEE SENSORS, Orlando, FL, USA, Retrieved from 10.1109/ICSENS.2016.7808806.
- [123] Sigman, J.B., Barrowes, B.E., O'Neill, K., Wang, Y., Simms, J.E., Bennett, H.H., & Yule, D.F. (2017). High-Frequency Electromagnetic Induction Sensing of Nonmetallic Materials. *IEEE Transactions on Geoscience and Remote Sensing*, 55 (9), 5254-5263. doi: 10.1109/TGRS.2017.2704102.

- [124] Yamada, T. & Fujisaki, K. (2008). Basic Characteristic of Electromagnetic Force in Induction Heating Application of Linear Induction Motor. *IEEE Transactions on Magnetics*, 44 (11), 4070-4073. doi: 10.1109/TMAG.2008.2002786.
- [125] TEXAS INSTRUMENT. (2013). ADC12L063 12-Bit, 62 MSPS, 354 mW A/D Converter with Internal Sample-and-Hold. Retrieved from <https://www.ti.com/lit/ds/symlink/adc12l063.pdf>. (accessed July 19, 2021).
- [126] Marian, K. K. (2015). *RF Power Amplifiers* (2nd ed.). Hoboken, New Jersey: John Wiley & Sons.
- [127] Herman, R. L. (2014). *Introduction to Partial Differential Equations*. Wilmington, NC: University of North Carolina Wilmington.
- [128] Fucik, L., & Vrba, R. (2016). Proceedings of the Third International Conference on Informatics in Control, Automation and Robotics, Signal Processing, Systems Modeling and Control,, Portugal, 2, 142-147. doi: 10.5220/0001207901420147.
- [129] Huang, Y., Mather, P. J., & Sibley, M. (2018). Open Area Concealed Weapon Detection Sensor System Development. 2018 Progress in Electromagnetics Research Symposium, Toyama, Japan, 611-620. doi: 10.23919/PIERS.2018.8598210.
- [130] Huang, Y., Mather, P. J., & Sibley, M. (2019). Open Area Concealed Weapon Detection (CWD) Sensor System and Algorithm Development. 2019 Photonics & Electromagnetics Research Symposium, Rome, Italy, 4078-4085. doi: 10.1109/PIERS-Spring46901.2019.9017665.
- [131] SH, Tsang. (2018). Review: SSD — Single Shot Detector (Object Detection). Towards data science. Retrieved from <https://towardsdatascience.com/review-ssd-single-shot-detector-object-detection-851a94607d11> (accessed July 19, 2021).

Appendix A

SCHEMATIC BLOCK DIAGRAM

The schematic to record the time at the mark points is achieved by the main modules of the difference monitor, digital conversion, modulation processing, data identification and distinction.

- The pulse generation provides the transmitting pulse to the circuit.
- Sampling the received signal and translating it into the digital data according to the clock.
- The difference monitor divides the entire induction into the assigned sections.
- The one-bit sequence is produced via the modulation module.
- The mark points evaluation program successively measures the evidence at the single, double and triple 0 to characterize the targets.

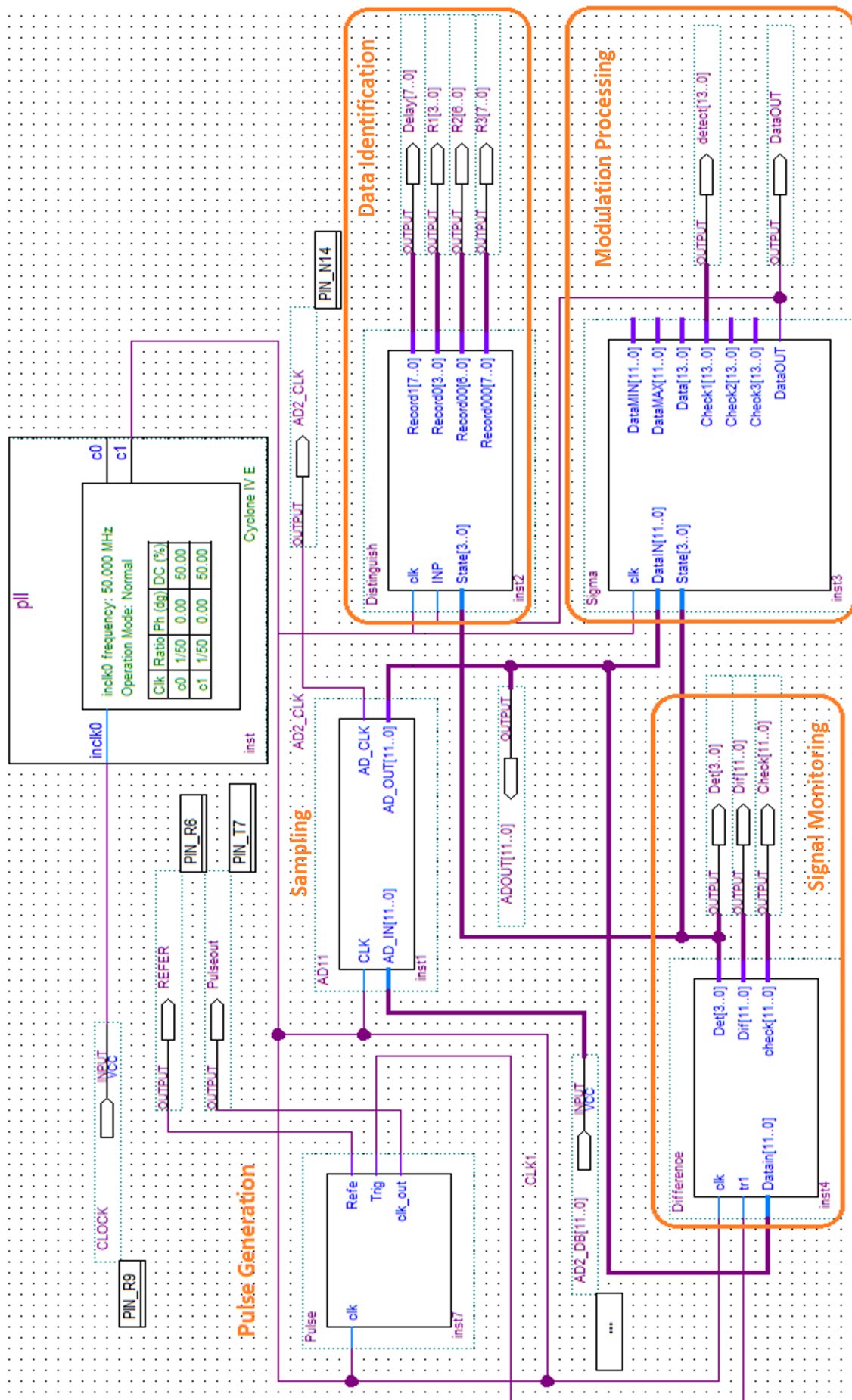


Figure A.1: Block diagram layout

Appendix B

VHDL PROGRAM FILES

The system program files involve the functional modules to realize the

B.1 Pulse generation – procedures the transmitting pulse to the coil;

B.2 Digital sampling conversion – collects and translates the analogue signal;

B.3 Signal monitoring – examines the changes of induced response;

B.4 Modulation processing - generates the single-bit data sequence;

B.5 Data Identification - the threat identification depends on the data distinction and classification to evaluate the mark points, defining the potential weapons.

B.1 Pulse Generation

Listing B.1: Transmitting pulse generation function

```
1. -----
2.  --Module Name: Pulse Generation
3.  --Create Date: 06/07/2017
4.  --Author Name: Yuxiang
5.  --Description:
6.  --Based on the system clock, the module generates the trigger signal for the further
7.  --use, as well as the pulse clock for signal transmitting on the coil .
8.  -----
9.  LIBRARY IEEE;
10. USE IEEE.STD.LOGIC_1164.ALL;
11. use ieee . std_logic_arith . all ;
12. use ieee . std_logic_unsigned . all ;      --Library head files
```

```

13.  ENTITY Pulse IS
14.  PORT ( clk:IN STD_LOGIC;    --Default clock input
15.         Refe: OUT STD_LOGIC;  --Refer signal output
16.         Trig:OUT STD_LOGIC;   --Trigger signal output
17.         clk_out:OUT STD_LOGIC); --System clock output
18.  END Pulse;
19.  ARCHITECTURE behavior OF Pulse IS
20.  SIGNAL cout: std_logic_vector(11 downto 0):="000000000000";  --Initial value
21.  SIGNAL tmp1,tmp2 :STD_LOGIC;  --Define temporary variables
22.  -----
23.  --Merge the default clock into the pulse clock
24.  -----
25.  BEGIN
26.  PROCESS(clk, tmp1,tmp2)
27.  BEGIN
28.  IF rising_edge ( clk ) THEN
29.      Refe<='1';
30.      cout<=cout+1;
31.  IF cout<"001011101110" THEN  --Trigger the high level
32.      tmp1<='1';
33.  ELSIF cout<"100111000100" THEN --Trigger the low level
34.      tmp1<='0';
35.  Else cout<="000000000000";  --Reset value
36.  END IF;
37.  IF cout<"001011101101" THEN  --Trigger the low level
38.      tmp2<='0';
39.  ELSIF cout<"100111000100" THEN --Trigger the high level
40.      tmp2<='1';
41.  Else cout<="000000000000";  --Reset value
42.  END IF;
43.  END IF;
44.  END PROCESS;
45.  clk_out<=tmp1;  --Output system clock
46.  Trig<=tmp2;
47.  END behavior;

```

B.2 Digital Sampling Conversion

Listing B.2: Analogue to digital data conversion

```

1.  -----
2.  --Module Name: ADC Conversion
3.  --Create Date: 05/10/2017
4.  --Author Name: Yuxiang
5.  --Description:
6.  --The signal received on the FPGA board is introduced to the ADC extension board for
7.  --data conversion. The program collects the digital data once it is accomplished.
8.  -----
9.  library IEEE;
10. use ieee . std_logic_1164 . all ;
11. use ieee . std_logic_arith . all ;
12. use ieee . std_logic_unsigned . all ;
13. ENTITY AD11 IS
14. PORT( CLK: IN std_logic;
15.        AD_IN : IN std_logic_vector (11 downto 0);    --Signal received
16.        AD_CLK : OUT std_logic;
17.        AD_OUT: OUT std_logic_vector(11 downto 0));    --Digital data output
18. END AD11;
19. ARCHITECTURE behavior OF AD11 IS
20.  -----
21.  --Opposite bit priority conversion
22.  -----
23. BEGIN
24. PROCESS(CLK,AD_IN)
25. BEGIN
26. if rising_edge (clk) then
27.     AD_OUT(0 to 11) <= AD_IN(11 downto 0);    --Assign digital data
28. end if ;
29. END PROCESS;
30.     AD_CLK <= CLK;    --Retain the project clock
31. END behavior;

```

B.3 Signal Monitoring

Listing B.3: Value difference monitoring function

```

1.  -----
2.  --Module Name: Difference Monitor
3.  --Create Date: 11/10/2017

```

```

4.      --Author Name: Yuxiang
5.      --Description:
6.      --The difference monitor program aimed to divide the entire induced response
7.      -- into the individual sections depending on the difference between the new and prior samples.
8.      -----
9.      library IEEE;
10.     use ieee . std_logic_1164 . all ;
11.     use ieee . std_logic_arith . all ;
12.     use ieee . std_logic_unsigned . all ;
13.     ENTITY Difference IS
14.     PORT(  clk,tr1: IN  std_logic ;
15.           Datain : IN  std_logic_vector (11 downto 0);
16.           Det: OUT std_logic_vector(3 downto 0);           --Sample Difference
17.           Dif: OUT std_logic_vector(11 downto 0);          --Data duration
18.           check: OUT std_logic_vector(11 downto 0));
19.     END Difference;
20.     ARCHITECTURE behavior OF Difference IS
21.     SIGNAL flag : std_logic :='0';
22.     SIGNAL flag2 : std_logic :='0';
23.     SIGNAL Reg1: std_logic_vector(11 downto 0);
24.     SIGNAL Reg2: std_logic_vector(11 downto 0);
25.     SIGNAL base1: std_logic_vector (11 downto 0);
26.     SIGNAL peak: std_logic_vector(11 downto 0);
27.     SIGNAL Standard75: std_logic_vector(11 downto 0);
28.     SIGNAL Standard50: std_logic_vector(11 downto 0);
29.     SIGNAL Standard25: std_logic_vector(11 downto 0);
30.     SIGNAL Standard00: std_logic_vector(11 downto 0);
31.     SIGNAL value1: std_logic_vector (12 downto 0);
32.     SIGNAL cout: std_logic_vector (1 downto 0);
33.     SIGNAL state: std_logic_vector (3 downto 0):="0000";
34.     -----
35.     --If the new value is bigger and difference rise beyond the range, that
36.     --means the signal increases rapidly referred as rise section (0001).
37.     -----
38.     BEGIN
39.     PROCESS(clk,tr1,Datain)
40.     BEGIN
41.     if rising_edge ( clk ) then
42.         if tr1='1' then

```

```

43.      cout<=cout+1;
44.      Reg1<=Datain;
45.      if cout ="10" then
46.          flag<='1';
47.      end if;
48.      if flag='1' then
49.          if Datain > Reg1 then
50.              Reg2<=Datain-Reg1;          --Provide the difference
51.          else Reg2<=Reg1-Datain;
52.          end if;
53.          if state = "0000" and Datain > Reg1 and Reg2 > "000001000000" then
54.              state<="0001";          --Rise stage
55.  -----
56.  --The difference within the range in the following stage is considered as the
57.  --delay section (0010)
58.  -----
59.          elsif state = "01" and Reg2 < "000000001010" then
60.              state<="0010";          --Delay stage
61.              flag2<='1';
62.              elsif state(3) = '1' and Datain < Reg1 and flag2 = '0' then
63.                  Standard75<=peak - ("00"&value1(11 downto 2));
64.                  Standard50<=base1 + ('0'&value1(11 downto 1));
65.                  Standard25<=base1 + ("00"&value1(11 downto 2));
66.                  Standard00<=base1 + ("000"&value1(11 downto 3));
67.  -----
68.  --For the decay section, it is further divided into subsections based on the
69.  --75%, 50%, 25% and 12% of the peak value.
70.  -----
71.          if Datain(11)='0' and Datain> Standard75 then --75%
72.              state<="1001";          --Section A in decay stage
73.          elsif Datain(11)='1' and Datain> Standard50 then
74.              state<="1010"; --Section B of negative in decay stage
75.          elsif Datain(11)='0' and Datain >= "000000000000" then --50%
76.              state<="1010"; --Section B of negative in decay stage
77.          elsif Datain(11)='1' and Datain> Standard25 then --25%
78.              state<="1011";          --Section C in decay stage
79.          elsif Datain(11)='1' and Datain> Standard00 then
80.              state<="1100";          --Section D in decay stage
81.          elsif Datain(11)='1' and Datain> base1 then

```

```

82.             state<="1000";           --Remaining part
83.             end if;
84.             elsif state = "0010" and Datain < Reg1 and Reg2 > "000000001111"
85.             and flag2 = '1' then
86.             state<="1001";           --Capture Peak
87.             peak<=Reg1;
88.             value1<=('1'& Reg1)-('0'&base1);    --Value=peak-base
89.             flag2<='0';
90.             end if;
91.         end if;
92.         elsif tr1= '0' then
93.             state<="0000";
94.             Base1<=Datain;
95.         end if;
96.     end if;
97. END PROCESS;
98.     check<=Standard00;    --Process check
99.     Dif<=Reg2;            --Output difference
100.    Det<=state;           --Give the phrases
101. END behavior;

```

B.4 Modulation Processing

Listing B.4: Signal sigma-delta modulation function

```

1.  -----
2.  --Module Name: Sigma Delta Modulation
3.  --Create Date: 07/02/2018
4.  --Author Name: Yuxiang
5.  --Description:
6.  --The sigma-delta modulation program is aimed to translate the 12-bit signal into the
7.  --one-bit sequence output.
8.  -----
9.  library IEEE;
10. use ieee . std_logic_1164 . all ;
11. use ieee . std_logic_arith . all ;
12. use ieee . std_logic_unsigned . all ;
13. ENTITY Sigma IS
14. PORT( clk: IN std_logic ;

```

```

15.      DataIN : IN  std_logic_vector (11 downto 0);
16.      State: IN  std_logic_vector (3  downto 0);
17.      DataMIN : OUT std_logic_vector(11 downto 0);
18.      DataMAX : OUT std_logic_vector(11 downto 0);
19.      Data : OUT std_logic_vector(13 downto 0);
20.      Check1 : OUT std_logic_vector(13 downto 0);
21.      Check2 : OUT std_logic_vector(13 downto 0);
22.      Check3 : OUT std_logic_vector(13 downto 0);
23.      DataOUT: OUT std_logic);
24.  END Sigma;
25.  ARCHITECTURE behavior OF Sigma IS
26.  SIGNAL Reg2: std_logic_vector(11 downto 0);    --Store the temporary data
27.  SIGNAL Reg1: std_logic_vector(11 downto 0);
28.  SIGNAL Reg0: std_logic_vector(11 downto 0);
29.  SIGNAL Regmin: std_logic_vector(11 downto 0);  --Minimum comparison
30.  SIGNAL Regmax: std_logic_vector(11 downto 0):= "101100110110"; --Maximum comparison
31.  SIGNAL Regstate: std_logic_vector (3  downto 0);
32.  SIGNAL flag : std_logic :='0';
33.  SIGNAL Datainput: std_logic_vector (13 downto 0);
34.  SIGNAL Comparator: std_logic_vector(13 downto 0);
35.  SIGNAL Error: std_logic_vector (13  downto 0);
36.  SIGNAL Accumulator: std_logic_vector(13 downto 0);
37.  -----
38.  --The new received signal is compared with the prior comparison value to get
39.  --new error.
40.  -----
41.  BEGIN
42.  PROCESS(clk,DataIN, State)
43.  BEGIN
44.      if clk'event and clk='1' then
45.          Reg2 <= DataIN;
46.          Reg1 <= Reg2;
47.          Reg0 <= Reg1;
48.          if State = "0000" then
49.              Accumulator <= "0000000000000000";    --Reset the value
50.              Comparator <= "0000000000000000";
51.          end if;
52.          if Regstate = "0000" and State = "0001" then
53.              Regmin <= Reg0;

```



```

54.             flag <= '1';
55.         end if ;
56.         if State = "0001" or State = "0010" or State = "1001" or
57. State = "1010" or State = "1011" or State = "1100" then
57.             if flag = '1' then
58.                 Datainput <= "00"&(Reg1 - Regmin);           --Input=signal-base
59.                 Error <= ("00"&(Reg1 - Regmin)) - Comparator; --Error=input-comparison
60.                 Accumulator <= Accumulator + ("00"&(Reg1 - Regmin)) - Comparator;
61.                 --Accumulation=prior+error
62.                 -----
63.                 --Then the error is accumulated. If the value is positive and bigger than
64.                 --threshold value, the comparison is assigned as maximum and output as 1.
65.                 --Otherwise the comparison is minimum and the result remains 0.
66.                 -----
67.                 if (Accumulator + ("00"&(Reg1 - Regmin)) - Comparator) > ("011111111111")
68. then           --Negative value
69.                 Comparator <= "00000000000000";
70.                 DataOUT <= '0';
71.                 elsif (Accumulator + ("00"&(Reg1 - Regmin)) - Comparator) > ("00010110011011")
72. then           --Threshold
73.                 Comparator <= ("00101100110110");           --Maximum
74.                 DataOUT <= '1';                               --Quantise as 1
75.                 else
76.                 Comparator <= "00000000000000";           --Minimum
77.                 DataOUT <= '0';                               --Quantise as 0
78.                 end if ;
79.                 end if ;
80.                 else
81.                     DataOUT <= '0';
82.                 end if ;
83.                 Regstate <= State;
84.             end if ;
85.         END PROCESS;
86.         DataMIN <= Regmin;
87.         DataMAX <= Regmax;
88.         Data <= Datainput;
89.         Check1 <= Error;           --Testing check pins
90.         Check2 <= Accumulator;
91.         Check3 <= Comparator;

```

92. **END** behavior;

B.5 Data Identification

Listing B.5: Digital data analysis and target identification function

```

1.  -----
2.  --Module Name: Data Identification
3.  --Create Date: 03/09/2018
4.  --Author Name: Yuxiang
5.  --Description:
6.  --The identification module measures the delay duration, and successively
7.  --evaluates the mark pinots of single, double and triple 0 at decay phrase.
8.  -----
9.  library IEEE;
10. use ieee . std_logic_1164 . all ;
11. use ieee . std_logic_arith . all ;
12. use ieee . std_logic_unsigned . all ;
13. ENTITY Distinguish IS
14. PORT( clk: IN std_logic ;
15.       INP : IN std_logic ;
16.       State: IN std_logic_vector (3 downto 0);
17.       Record1 : OUT std_logic_vector(7 downto 0);    --Delay measurement
18.       Record0 : OUT std_logic_vector(3 downto 0);    --Single 0
19.       Record00 : OUT std_logic_vector(6 downto 0);   --Double 0
20.       Record000 : OUT std_logic_vector(7 downto 0)); --Triple 0
21. END Distinguish;
22. ARCHITECTURE behavior OF Distinguish IS
23. SIGNAL Count1: std_logic_vector(7 downto 0);
24. SIGNAL Count2: std_logic_vector(7 downto 0);
25. SIGNAL Regist: std_logic_vector (3 downto 0):= "0000";
26. SIGNAL flag : std_logic :='0';
27. SIGNAL flag0 : std_logic_vector (1 downto 0):="00";
28. SIGNAL flag00 : std_logic_vector (1 downto 0):="00";
29. SIGNAL flag000 : std_logic_vector (1 downto 0):="00";
30. BEGIN
31. PROCESS(clk,INP, State)
32. BEGIN
33.   if clk'event and clk='1' then

```

```

34.         if State = "0000" then
35.             Count1 <= "00000000";  --Reset registers
36.             Count2 <= "00000000";
37.             Record0 <= "0000";
38.             Record00 <= "00000000";
39.             Record000 <= "00000000";
40.             flag <= '0';           --Reset flags
41.             flag0 <= "00";
42.             flag00 <= "00";
43.             flag000 <= "00";
44.         end if;
45.         if State = "0010" then --Delay phrase
46.             Count1 <= Count1 + 1;
47.         end if;
48.         if State = "1001" then --Decay phrase
49.             flag <= '1';
50.             elsif State <= "1000" then
51.                 flag <= '0';
52.             end if;
53.             if flag = '1' then
54.                 count2 <= count2 + 1;
55.                 Regist(0) <= INP;           --Introduce to registers
56.                 Regist(1) <= Regist(0);
57.                 Regist(2) <= Regist(1);
58.                 Regist(3) <= Regist(2);
59.             -----
60.             --Check the prior successive sample of value at the decay duration
61.             --Use the flag to count the double measurement
62.             -----
63.                 if INP = '1' and Regist(0) = '0' and Regist(1) = '1' and flag0 = "00" then
64.                     flag0 <= flag0+1;
65.                     Record0 <= count2(3 downto 0); --'0' marked
66.                 end if;
67.                 if INP = '1' and Regist(0) = '0' and Regist(1) = '1' and flag0 = "01" then
68.                     flag0 <= "11";
69.                     Record0 <= count2(3 downto 0); -- Double assessment of '0'
70.                 end if;
71.                 if INP = '1' and Regist(0) = '0' and Regist(1) = '0' and
72.                     Regist(2) = '1' and flag00 = "00" then

```

```

73.         flag00 <= flag00+1;
74.         Record00 <= count2(6 downto 0); --"00" marked
75.     end if;
76.     if INP ='1' and Regist(0) = '0' and Regist(1) = '0' and
77.         Regist(2) = '1' and flag00 = "01" then
78.         flag00 <= "11";
79.         Record00 <= count2(6 downto 0); -- Double assessment of "00"
80.     end if;
81.     if INP ='1' and Regist(0) = '0' and Regist(1) = '0' and
82.         Regist(2) = '0' and Regist(3) = '1' and flag000 = "00" then
83.         flag000 <= flag000+1;
84.         Record000 <= count2;           --"000" marked
85.     end if;
86.     if INP ='1' and Regist(0) = '0' and Regist(1) = '0' and
87.         Regist(2) = '0' and Regist(3) = '1' and flag000 = "01" then
88.         flag000 <= "11";
89.         Record000 <= count2;           -- Double assessment of "00"
90.     end if;
91. end if;
92. end if;
93. END PROCESS;
94.     Record1 <= Count1; --Measure delay duration
95. END behavior;

```

Appendix C

MATLAB FILES

The project applied the MATLAB simulation procedure to verify the experimental practicability, where the program codes include the three modules to achieve the

C.1 Sample collection – receives and records the induced response;

C.2 Data modification – adjusts and processes the digital data;

C.3 Decay Analysis – realizes mark points evaluation.

C.1 Sample Collection

Listing C.1: Sample Collection Module

```
1. %% To collect the signal sample
2. % The program records the signal sample of induced response
3. % draw the plot and store the data into files.
4. clear all;
5. filename1 = 'K:\matlab\Practical test\33.txt';
6. A = importdata(filename1);
7. temp=A(1:71,2);
8. h=1:71;
9. plot(h,temp) % Draw the induced response
10. h_3=1:0.01:71 % Define the sampling interval
11. t_3=interp1(h,temp,h_3,'cubic') % Refine the sample
12. hold on
13. subplot(1,2,1)
14. plot(h,temp,'--',h,temp,'+',h_3,t_3) % Draw the decay duration
15. hold off
16. %Transform data into array
17. n=[h_3',t_3']
18. m=n(1:7001,2)
19. l=0.45:0.00005:0.8
20. qq=[l',m]
21. % Output the result and store data into
22. % the excel and txt files respectively
23. outname = 'K:\matlab\Practical test\33.xlsx';
```

```

24. xlRange = 'A1';
25. xlswrite(outname,qq,1,xlRange)
26. xlswrite(outname,A,2,xlRange)
27. results=[l;t_3]
28. fid=fopen('practical33.txt','w');
29. fprintf(fid,'%1.7f %1.20f\r\n',results);
30. fclose(fid);

```

C.2 Date Modification

Listing C.2: Data adjustment and processing module

```

1. %% Data Modification
2. % The program adjusts the sampling data and at the same time,
3. % measures the delay and decay duration. Data is saved in the
4. % database for platform use.
5. clear all
6. a=xlsread('k:\matlab\Practical test\33.xlsx',1,'B4913:B7001')
7. aa=a*100 %Value magnification
8. b=find(aa>7) %Date adjustment
9. n033=length(b) %Delay duration measurement
10. save('DB1','n033','-append') %Save in database
11. %Decay duration measurement
12. a0=find(aa<7)
13. c=aa(a0)
14. l=length(c)
15. t=0
16. for i= 2:l %Comparison with prior data
17.     if c(i)< c(i-1)
18.         t=t+1
19.         d(t)= c(i-1)
20.     end
21. end
22. ll=length(d)/100
23. m=(0:0.01:ll-0.01) %Define the interval
24. data033=[m',d'] % Transform into array
25. save('DB1','data033','-append') %Save in database
26. %Store result in excel file
27. outname = 'K:\matlab\Practical test\inp33.xlsx';
28. xlRange = 'A1';
29. xlswrite(outname,m',1,xlRange)
30. xlswrite(outname,d',1,'B1')

```

C.3 Decay Analysis

Listing C.3: Data analysis at the decay duration

```

1. %% Decay Analysis
2. % The module is developed to analyse the date at the decay duration
3. % and evaluates the mark points. It finally displays the result.
4. clear all;
5. load DB1.mat %load the database
6. filename = 'K:\matlab\Practical test\data033.xlsx';

```

```

7.  xlRange = 'A1';
8.  xlswrite(filename,oup033.Data,2,xlRange) %Read the data
9.  a1=find(oup033.Data((2:1000),1)==0) %Find the decay duration
10. t0=0 --Reset the value
11. t01=0
12. l0=length(a1)
13. %Date comparison with prior result
14. for i0=3:l0
15.     if a1(i0-1)==a1(i0-2)+1 %Define the '0'
16.         t0=t0+1
17.         b1(t0)=a1(i0-2) %Define the "00"
18.         if a1(i0)==a1(i0-1)+1
19.             t01=t01+1
20.             c1(t01)=a1(i0-2) %Defien the "000"
21.         end
22.     end
23. end
24. %Output and display the result
25. f1 = figure('name','33 ') %Save data
26. cnames= {'Mark Piont','Time'};
27. tname=uitable('ColumnName',cnames);
28. table_data={
29.     'Delay',n036; %Interface display
30.     '1st 0',a1(1);'2nd 0',a1(2);'3nd 0',a1(3);
31.     '1st 00',b1(1)-1;'2nd 00',b1(2)-1;
32.     '1st 000',c1(1);'2nd 000',c1(2);};
33. set(tname,'data',table_data);

```

Appendix D

COMSOL SIMULATION

The induced response simulation establishes the target models by COMSOL to change the critical parameters for signature analysis. The simulated models involve the variable shape, size, distance and varying threat component with a sharp edge.

D.1 Shape model simulation

The simulated models are made of iron material and in the same volume, placed at the same distance to the coil, while the shape of the target is changed concerning knife, block, torus and sphere.

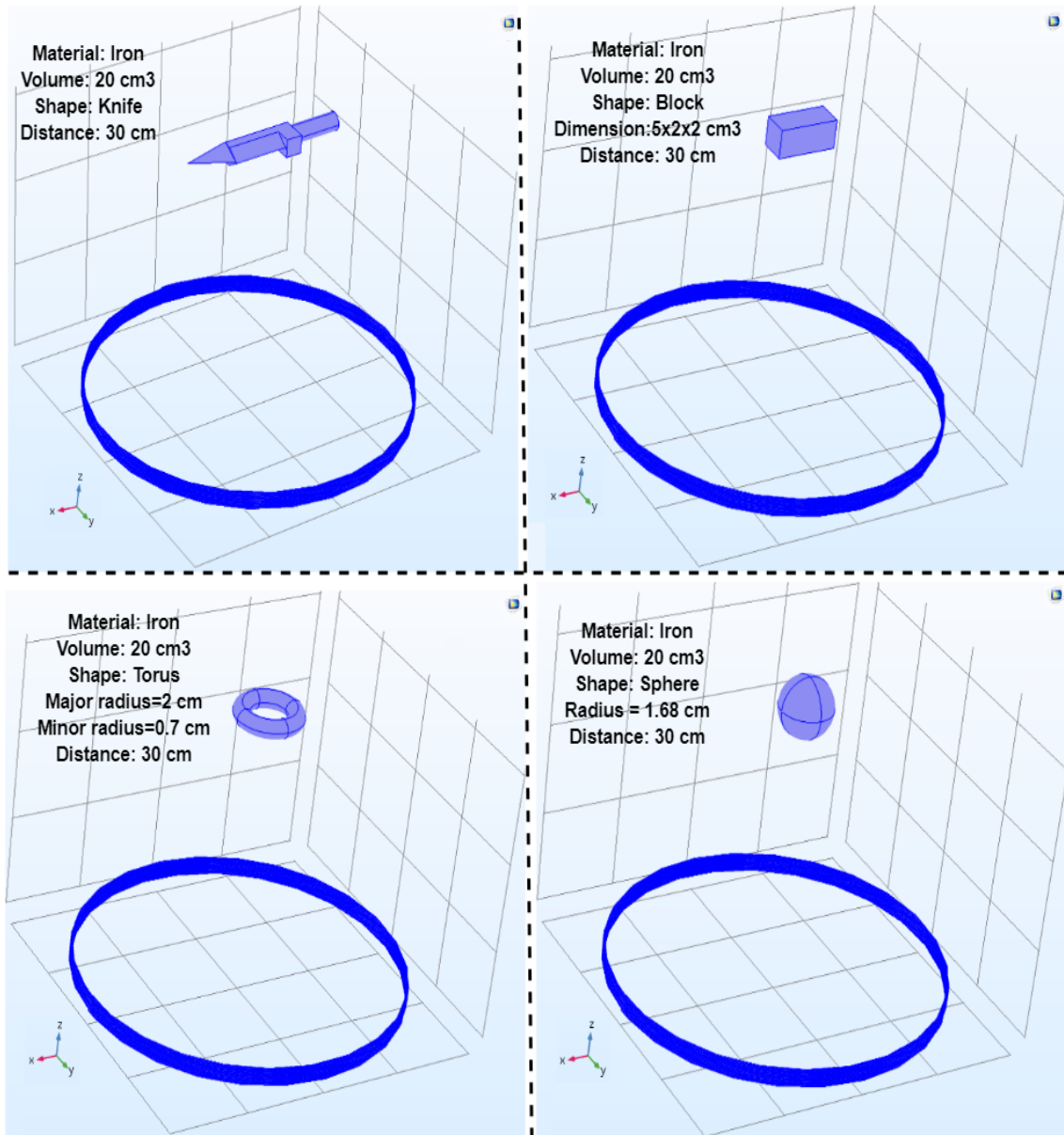


Figure D.1: Shape model simulation.

D.2 Size model simulation

The cubic size of target is changed for $2 \times 2 \times 2 = 8 \text{ cm}^3$, $3 \times 3 \times 3 = 27 \text{ cm}^3$, $4 \times 4 \times 4 = 64 \text{ cm}^3$ and $5 \times 5 \times 5 = 125 \text{ cm}^3$, while the material, shape and distance are identical.

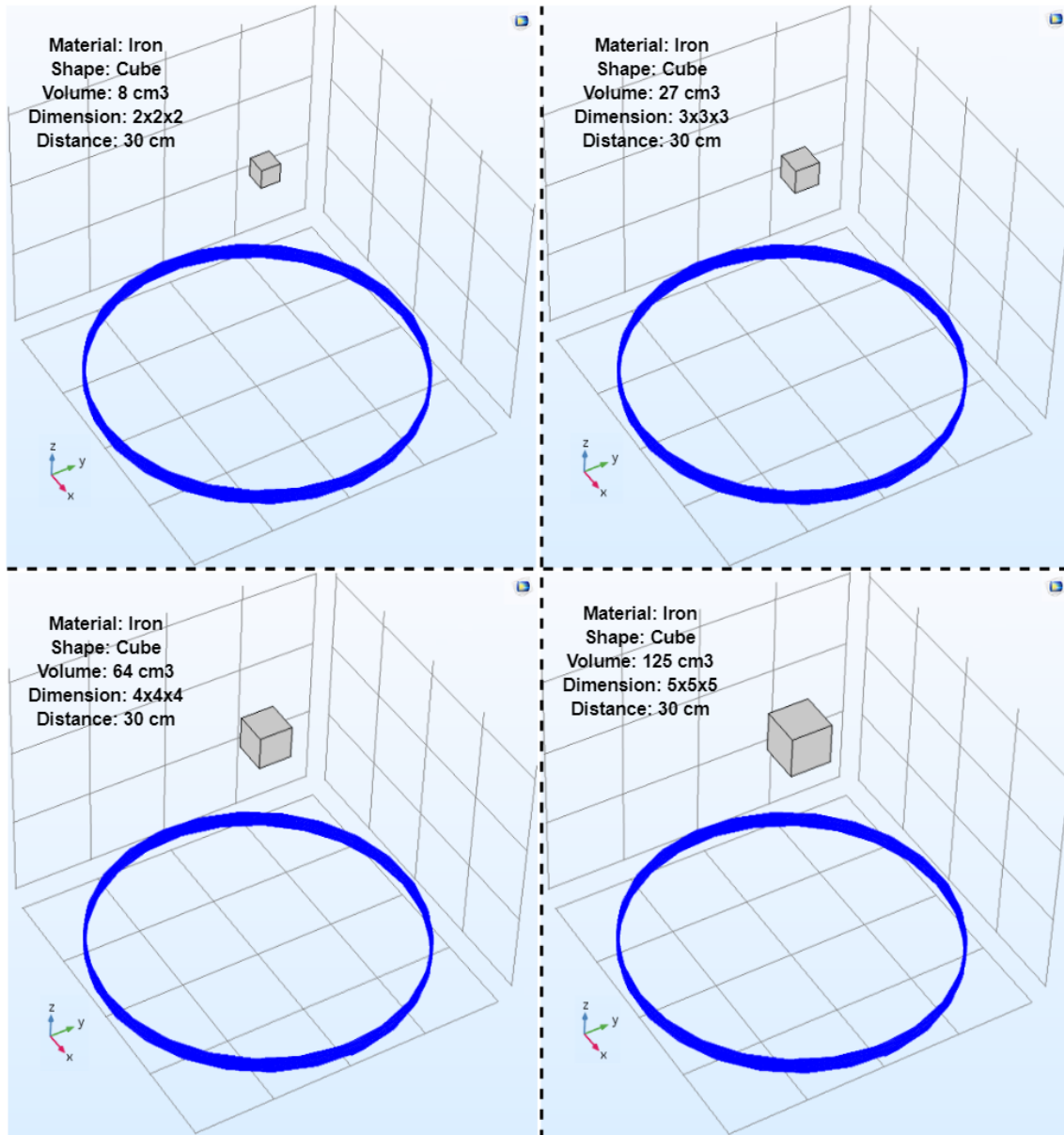


Figure D.2: Size model simulation.

D.3 Distance model simulation

The same target is placed at a different distance to the search coil (20 cm, 22 cm, 24 cm, 27cm and 30 cm).

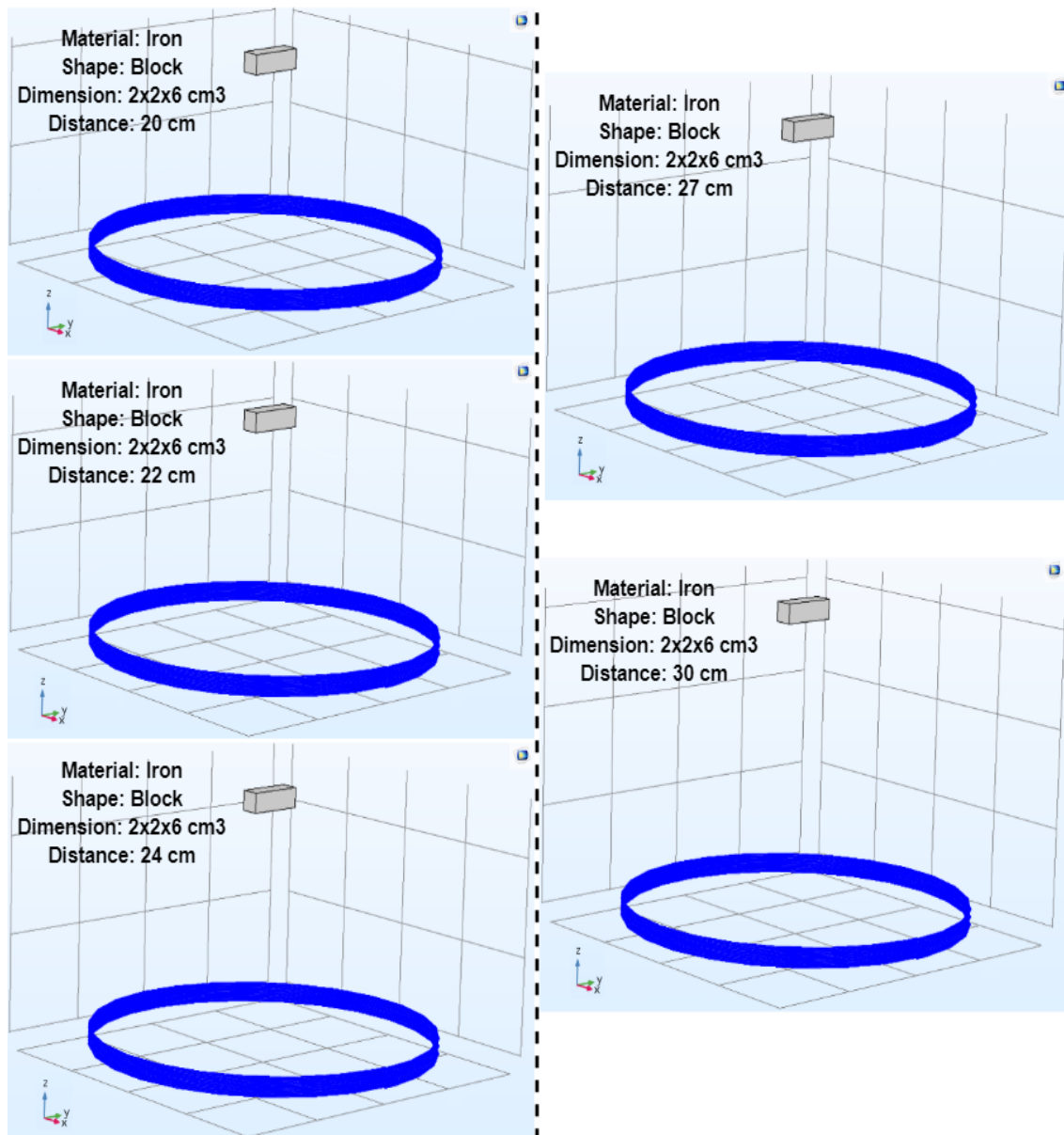


Figure D.3: Distance model simulation.

D.4 Sharp edge simulation

The threat component with a sharp edge in degree 5 is changed in the different volume of 10 cm³, 20 cm³, 30 cm³ and 40 cm³, while the material, shape and distance are identical.

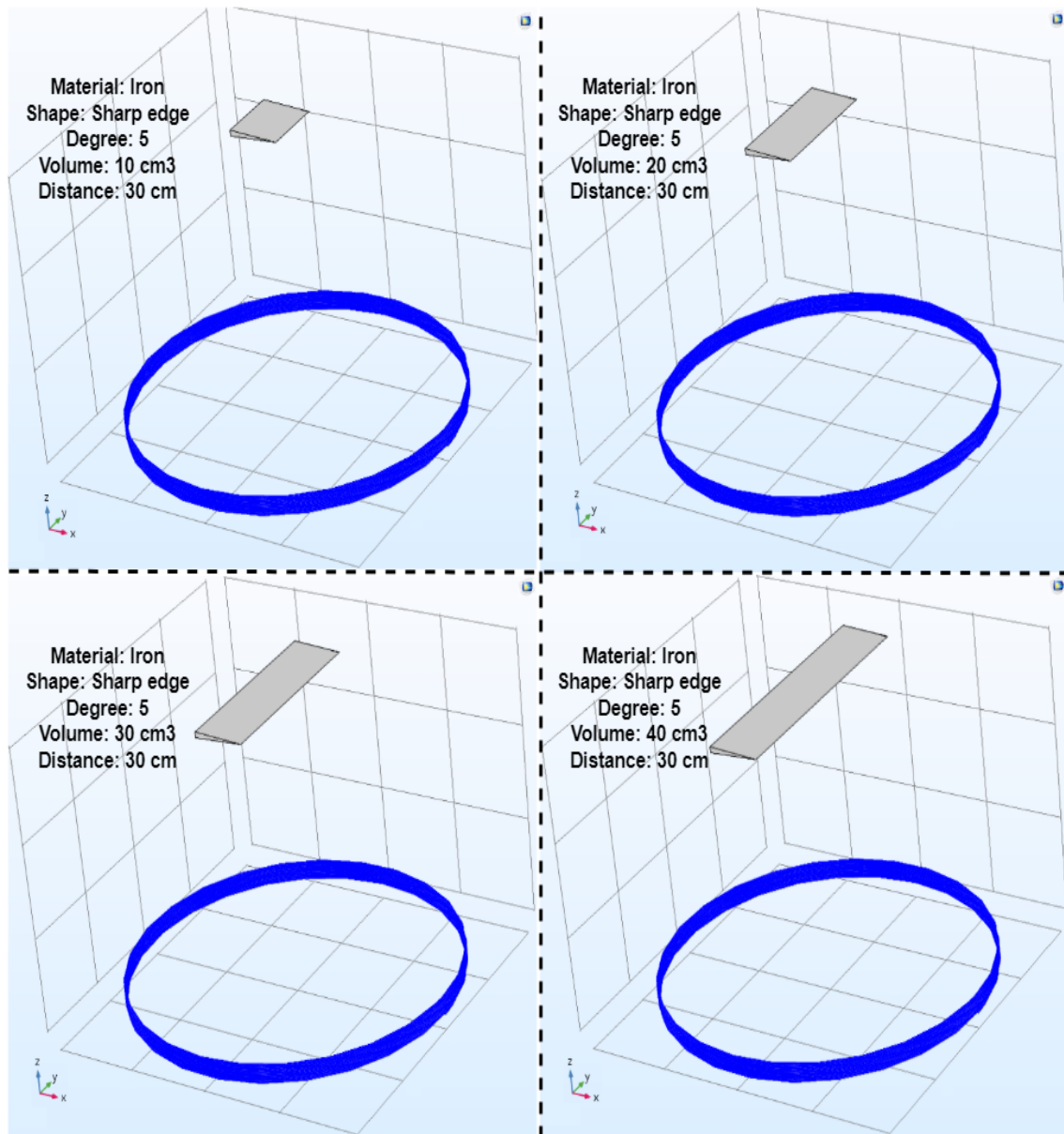


Figure D.4: Sharp edge model simulation.